Design and Synthesis of Intracellular MR Contrast Agents Targeting β-Galactosidase

Design und Synthese von intrazellulären MR Kontrastmitteln mit β-Galactosidase als Target

DISSERTATION

der Fakultät für Chemie und Pharmazie

der Eberhard Karls Universität Tübingen

zur Erlangung des Grades eines Doktors

der Naturwissenschaften

2009

vorgelegt von

Aneta Brud

Tag der mündlichen Prüfung:	4. November 2009
Dekan:	Prof. Dr. Lars Wesemann
1. Berichterstatter	Prof. Dr. Thomas Ziegler
2. Berichterstatter	Prof. Dr. Karl-Heinz Wiesmüller

This PhD thesis was prepared in collaboration between the High-Field Magnetic Resonance Center of the Max-Planck Institute for Biological Cybernetics, Tübingen, (supervisors: Dr. Joern Engelmann, Prof. Dr. Kamil Ugurbil) and the Institute for Organic Chemistry, Eberhard-Karls University of Tübingen, under the guidance of Prof. Dr. Thomas Ziegler.

Hereby I declare the fact that I am writing this work and no different than the indicated aids have been used.

Tübingen, September, 2009

To Georgios

Acknowledgments

The work described in this thesis would not have been possible without the contribution of many others who helped me through the years for completing this dissertation. Namely, I would like to particularly thank the following:

First and foremost, I would like to thank to my supervisors for the support and guidance during my PhD period in Tuebingen. Prof. Dr. Kamil Ugurbil provided space, funding and intellectual support during the time he was a Director at Max-Planck-Insitute for Biological Cybernetics.

My heartfelt thank goes to Prof. Dr. Thomas Ziegler, who taught me every aspect of carbohydrate chemistry and gave me innumerous valuable suggestions during our scientific discussions. He has also provided optimal facilities that helped the completion of my doctoral thesis.

I wish to express my deepest thanks to Dr. Joern Engelmann for his unrestricted support, valuable advices and guidance during my study and living in Tuebingen. Joern has been always supportive for my ideas and encourage me to purse various projects. Thank you for the patience and constant support you have given me during my PhD period.

I would like to thank to Prof. Dr. Karl-Heinz Wiesmuller, EMC microcollections GmbH, who critically evaluated the doctoral thesis and gave valuable suggestions, which have been incorporated in the thesis. We had also many insightful discussions about research work during the group meetings in the Max Planck Institute.

I would like thank to members of the committee: Prof. Dr. Hermann A. Mayer, Prof. Dr. Martin E. Maier and Prof. Dr. Stefan Laufer. It has been my honor to bring together such renowned group of scientists in the committee.

I am very thankful to our biology group: Dr. Joern Engelmann, Ms. Ritu Mishra and Ms. Hildegard Schulz for performing cell biological experiments. Special thanks to Joern and Hildegard for establishing the enzymatic assays.

I would also like to thank Dr. Rolf Pohmann for performing some MRI measurements and Dr. Guido Sauer for help in ESI-MS analyzing the samples after the enzymatic reaction. I thank Dr. Dorothee Witsuba for performing ESI-HRMS experiments.

I would like to thank Dr. Josef Pfeuffer for his suggestions and help at the beginning of my PhD project.

I owe a sincere thanks to Dr. Taduesz Lemek for his support.

Many thanks to the colleagues and friends of the bioconjugate group: Dr. Wu Su, Dr. Rajendra Joshi, Dr. Sven Gottschalk, Dr. Anurag Mishra, Dr. Goran Angelovski, Deepti Jha, Dr. Kirti Dhingra, Dr.Ilgar Mammadov for our scientific discussions, help and friendly working atmosphere.

I thank to the all members I worked with in the group of Prof. Dr Thomas Ziegler for their help.

Thanks to Ms. Tina Schröder and Mr. Rainer Hirt for all the help concerning administrative arrangements.

Finally, I thank the family and parents, for their love and support through the life. I especially thank my fiancé, Georgios, who is my best friend. His constant support, understanding, encouragement and unconditional love made difficult times easier and good times even better.

I also thank all who I did not mentioned by name but helped or enriched my academic and social life in Tuebingen.

Abbreviations

Abbreviation	Name
AA	Amino acid
Ac	Acetyl
Ag_2CO_3	Silver carbonate
AgOTf	Silver triflate
ArH	Aromatic
Boc	Tert-butoxycarbonyl
Bz	Benzoyl
Bn	Benzyl
CBz	Benzyloxycarbonyl
CA	Contrast agent
CPP	Cell penetrating peptide
cyclen	1,4,7,10-tetraazacyclododecane
cald	Calculated
δ	Chemical shift
$CDCl_3$	Chloroform deuterated
DCM	Dichloromethane
DDQ	2,3-dichloro-5,6-dicyanobenzoquinone
DIPEA	N,N'-diisopropylethylamine

DMF	Dimethylformamide
DOTA	1,4,7,10-tetraazacyclododecane-N,N',N'',N'''-tetraacetic acid
DOTA (tris-t-Bu ester)	1,4,7,10-tetraazacyclododecane-1,4,7-tris(acetic acid-tert-butyl ester)-10-acetic acid
D_2O	Deuteriumoxid
DTPA	Diethylenetriaminepentaacetic acid
EDC	1-Ethyl-3-(3'-dimethylaminopropyl) carbodiimide
ESI-MS	Electrospray ionization mass spectrometry
Eq	Equation
Et	Ethyl
EtOAc	Ethyl acetate
FITC	Fluorescein isothiocyanate
Fig	Figure
Fmoc	9-fluorenylmethoxycarbonyl
FmocOSu	9-flurenylmethyl-N-succinimidyl carbonate
$GdCl_3$	Gadolinium chloride
GFP	Green fluorescent protein
h	Hour(s)
H_2	Hydrogen
HATU	2-(1-H-7-azabenzotriazol-1-yl)-1,1,3,3-tetramethyluronium hexafluorophosphate

HBTU	2-(1H-benzotriazol-1-yl)-1,1,3,3-tetramethyluronium hexafluorophosphate
HBSS	Hanks' balanced salt solution
HCl	Hydrochloric acid
HIV	Human immunodeficiency virus
HOBt	1-hydroxybenzotriazole
HPLC	High performance liquid chromatography
HSA	Human serum albumin
J	Coupling constant
k (Lys)	Lysine
Me	Methyl
MeOH	Methanol
Me_3SiOTf	Trimethylsilyl trifluoromethanesulfonate
MR	Magnetic resonance
MRI	Magnetic resonance imaging
NBS	N-bromosuccinimide
NMR	Nuclear magnetic resonance
NMM	N-methylmorpholine
Pd-C	Palladium carbon
PMB	p-methoxybenzyl
Pbf	2,2,4,6,7-pentamethyldihydrobenzofuran-5-sulfonyl

PBS	Phosphate buffered saline
q (Gln)	Glutamine
r (Arg)	Arginine
RFP	Red fluorescent protein
R_f	Retention factor (TLC)
RP-HPLC	Reverse phase high performance liquid chromatography
TBDMS	Tert-butyldimethylsilyl
^{t}Bu	Tert-butyl
TFA	Trifluoroacetic acid
THF	Tetrahydrofurane
TIPS	Triisopropylsilane
Trt	Trityl
UV	Ultraviolet
rt	Room temperature

Chapter 1

Literature review

1.1 Introduction

"When we turn to look at the nature of biology itself we see stretching before us an almost unlimited number of important, interesting, and unsolved problems. This is partly due to the inherent complexity of biology and partly due to a passionate desire to understand the world around us and our own natures in particular"

Francis Crick

A living organism can be seen as a complex system, where precisely defined and hierarchically organized processes involve a countless number of distinct molecules. The understanding in what way molecules and cells develop into an individual as well as how constituent parts collaborate together to sustain a life would provide an essential knowledge concerning abnormal molecular and cellular processes leading to hereditary, but not only diseases[1]. The recognition of such aberrations at genetic or molecular level is a vital prerequisite to deliver the success of innovative therapies aiming for their early detection and correcting rather than only treating disease symptoms. Though in order to attain and study such vital biological targets, suitable methods are required that for years were only restricted to the invasive histology as well as molecular biological assays. Advances in imaging techniques provide a tool for the rapidly evolving fields of molecular and cellular imaging. Their expansion opened an avenue for noninvasive visualization of specific key molecules and their interactions in animals and humans over time using suitable imaging probes[2,3,4]. Among well established methods based on acquiring the biological targets using nuclear and optical imaging modalities the application of MRI was the latest. Even then, over recent years an impressive progress has been made in exploitation of MRI as powerful molecular imaging tool. This success has been driven through the combination of technological advances and the development of sophisticated MRI probes. The next sections will be devoted to the presentation of the importance of MRI in molecular and cellular imaging by highlighting the major achievements and challenges in this rapidly growing field of research.

1.2 Magnetic Resonance Imaging and imaging probes

Magnetic resonance imaging (MRI) has become over the years an invaluable tool of clinical diagnostic radiology[5,6,7]. The instantly growing popularity of this technology not only for clinical applications but also in experimental research derives from its capability to produce non-

invasively three-dimensional images of opaque organism with high spatial and temporal resolution without using ionizing radiation[8]. MR images are generated using NMR signal of water hydrogen nuclei, where the measured signal intensity depends on water density in a given volume, longitudinal T_1 (spin-lattice) and transverse T_2 (spin-spin) relaxation times[9]. The differences in relaxation times and the heterogeneous distribution of water inside the body lead to an intrinsic contrast between different examined tissues. That makes it possible to create anatomical maps of the organism. Nevertheless, in some cases the observed contrast between examined areas of interest e.g. healthy and damaged tissue is not sufficient for their delineation due to the small differences in observed relaxation times. This sensitivity barrier, faced at early years of MRI developments, was successfully overcome by designing and application of pharmacological compounds called MRI contrast agents (CAs)[10]. These molecules alter the signal intensity by accelerating the relaxation times of water protons in their surroundings thereby increasing the contrast in the examined regions of interest. Such MRI probes are generally classified as positive T_1-CAs (paramagnetic) and negative T_2-CAs (superparamagnetic) regarding to the relaxation process they predominantly affect. Accordingly, the investigated region containing CAs can be visible as brighter area in T_1-weighted images after administration of T_1-CA (positive contrast enhancement) or as a darker region in T_2-weighted images when T_2-CA was added (negative contrast enhancement). In general, the application of T_1-CAs is preferred[11] in MR examinations since the detection of positive contrast enhancement in the acquired image appears to be much easier as compared to the negative one. The majority of currently utilized T_1-CAs are complexes based on the paramagnetic gadolinium metal ion (Gd^{3+}). The popularity of this lanthanide ion originates from its excellent paramagnetic properties due to the high number of unpaired electrons (seven), the high magnetic moment and slow relaxation of electron spins[12,13]. However, the toxicity of free Gd^{3+} requires its complexation with a suitable chelate in order to render it biologically safe without impairing paramagnetic features[14]. The polydentante ligands such as acyclic DTPA (diethylenetriaminepentaacetic acid) and macrocyclic DOTA (1,4,7,10-tetracarboxymethyl-1,4,7,10-tetraazacyclododecane) are known to form kinetically inert and thermodynamically stable complexes of Gd^{3+}. Both complexes are clinically approved and routinely used in medical MR examinations[15]. Even though Gd-DTPA and Gd-DOTA are extremely valuable for obtaining anatomical information, non-specificity and restriction to the extracellular space abandon their use *per se* in assessing information about

biological targets. In response to the emerging need for noninvasive visualization of anomalous as well as normal processes at cellular and molecular level *in vivo* a new generation of more specific MRI CAs was required[16]. Thus, the development of targeted and responsive MR CAs became an emerging and rapidly evolving field over past decade. The design of optimal MR probes is, however, challenging as there are a number of parameters, which can determine its effectiveness. These factors will be briefly discussed in the following chapter.

1.3 Relaxivity

The efficiency of a given MR CA is measured in terms of its relaxivity r_i ($mM^{-1}s^{-1}$), which is defined as relaxation rate R_i ($1/T_i$) of water protons observed for a 1mM solution of contrast media, where subscript (i) stands for longitudinal ($1/T_1$) or transverse ($1/T_2$) rate. The theory of solvent nuclei relaxation in the presence of paramagnetic species has been described by Solomon[17], Bloembergen and Morgan[18]. The observed overall enhancement of water proton relaxation rate ($R_{i,obs}$) is the sum of diamagnetic ($R_{i,d}$) and paramagnetic contributions ($R_{i,p} = R_{i,p}^{IS} + R_{i,p}^{OS}$, where IS-inner sphere, OS-outer sphere) (Equation 1)[19]. The diamagnetic term corresponds to relaxation rate of solvent nuclei in the absence of CA (~ R_i of pure water), while the paramagnetic term is the relaxation rate enhancement in the presence of a paramagnetic substance, which is linearly proportional to the concentration of contrast media (Equation 2).

$$R_{i,obs} = R_{i,d} + R_{i,p}^{IS} + R_{i,p}^{OS} \quad i=1,2 \quad \text{(Eq 1)}$$

$$R_{i,obs} = R_{i,d} + r_i\,[Gd] \quad \text{(Eq 2)}$$

Paramagnetic contribution encompasses of inner sphere ($R_{i,p}^{IS}$) and outer sphere ($R_{i,p}^{OS}$) components (Equation 1). The inner-sphere relaxation mechanism derives from the chemical exchange of the water molecules bound to the first coordination sphere of metal and bulk water, whereas the outer-sphere contribution arises from random translational diffusion[20] of water molecules near the paramagnetic center. The inner-sphere term is easier influenced as compared to outer sphere component. Therefore, current design of CAs towards their relaxivity improvements focuses mainly on exploring and tuning the different parameters related to inner sphere relaxation. The longitudinal relaxation rate $(1/T_{1,p})^{IS}$ is given by Equation 3, where q is the number of bound water molecules per Gd, τ_m- the mean residence time of the metal bound

inner sphere water protons (equal to the reciprocal exchange rate $\tau_m=1/k_{ex}$), P_m- the mole fraction of bound water molecules, and T_{1m}- the relaxation time of the bound inner-sphere water. Further important component characteristic of relaxation processes is the correlation time, determined by Equation 4, where τ_r is the rotational correlation time and T_{1e} the electron spin relaxation time of the metal ion.

$$(1/T_{1,p})^{IS}=qP_m/T_{1m}+\tau_m \qquad \text{(Eq 3)}$$

$$1/\tau_c = 1/T_{1e}\ 1/\tau_m+1/\tau_r \qquad \text{(Eq 4)}$$

The equations shown in this chapter demonstrated, that total relaxivity depends on several parameters illustrated schematically in Fig.1. Amongst them q, τ_m and τ_r are generally used for the design of efficient CAs. Accordingly, a high relaxivity can be obtained by increasing q, optimizing τ_m and slowing down molecular tumbling (increasing τ_r)[21,22]. Although optimization of these parameters can dramatically increase r_1, the practice showed that attaining their favorable combination still remains a formidable challenge. For instance, most extracellular MRI CAs used in medical applications show r_1 in the range of 4-10 $mM^{-1}s^{-1}$ that is far away from maximum r_1~100 $mM^{-1}s^{-1}$ predicted for them by relaxivity theory[23]. Due to low r_1 such commercial MR probes are only efficient at high concentrations (≥ 1 mM), which is beyond detection limit of MR targeted imaging considering that biological targets are normally existing at low concentration (pico- and nanomolar range) and assuming one to one binding (Gd-chelate to targeted molecule) as pointed out by Caravan[24]. In order to overcome sensitivity limitations and to design a new generation of high relaxivity CAs for the detection of molecular targets by means of MRI, many valuable approaches where reported until now.

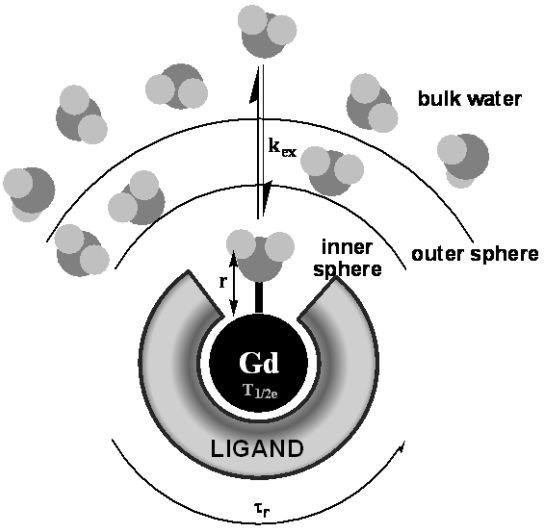

Figure 1. Schematic representation of model Gd-complex with one inner sphere coordinated water molecule in solution (bulk water) and parameters influencing relaxivity.
(r- metal/proton distance, k_{ex}- water/proton exchange rate {$k_{ex}=1/\tau_m$, τ_m- mean residence lifetime of bound water}, τ_r- rotational correlation time, $T_{1/2e}$- electron spin relaxation time).

1.4 Strategies for increasing the relaxivity of Gd-based MRI CAs

The augmentation of the sensitivity of MRI probes is a key prerequisite for the development of MR-based molecular and cellular imaging applications. In general, this task has been attempted either by optimization of the molecular parameters that govern relaxivity for a single MR reporter unit, or by developing suitable amplification strategies leading to the accumulation of a large number of MR reporter units at the targeted site. The following sections are devoted to present these approaches.

1.4.1 Gd-chelates with two coordinated water molecules

The relaxivity can be improved markedly by increasing *q* (see Equation 3), but the toxicity of gadolinium limits the possibility for increasing the number of water molecules in its first coordination sphere[25]. Typically, the stability of a Gd-complex, being of overwhelming importance under *in vivo* conditions, is decreasing with the more coordination sites open for interactions with water molecules. But the increase in *q* may also result in reduced r_1, if endogenous bicarbonates or phosphonates are able to replace the coordinated water. This behavior was observed e.g. in Gd-DO3A (q=2), which was not a proper ligand for achieving high

relaxivity as water molecules could be surrogated by various anions[26]. Thus, the alternation of q to increase r_1, requires suitable ligands, that have to form stable Gd-complexes, but also provide restricted access of endogenous anions. Two promising systems with q=2 shown in Fig.2 have been presented recently. Gd-AAZTA is a polyaminopolycarboxylate system as well but its relaxivity of 7.1 $mM^{-1}s^{-1}$ (20 MHz, 25ºC) was doubled in comparison to Gd-DOTA or Gd-DTPA (q=1, typical agents)[27]. This complex proved to be stable and inert towards bidentante anions as well as transmetallation with Zn^{2+}, Ca^{2+}. The hydroxypyridinone (HOPO) class of compounds reported first in 1995 by Raymond and coworkers[28] represents an innovative type of Gd-chelates, where metal ion is coordinated by six oxygen donor atoms. For that reason, two[29] or even three[30,31] water molecules can be coordinated to the lanthanide and importantly cannot be replaced by other anions due to the peculiar geometry of these complexes. Thus, with relaxivity in the range of 7-13 $mM^{-1}s^{-1}$, high stability and optimal water exchange such Gd-chelates are promising reporter units, where increase of MR probe sensitivity was achieved by optimizing molecular parameters. Moreover, both developed systems can be further utilized for amplification strategies with multiple complexes linked together.

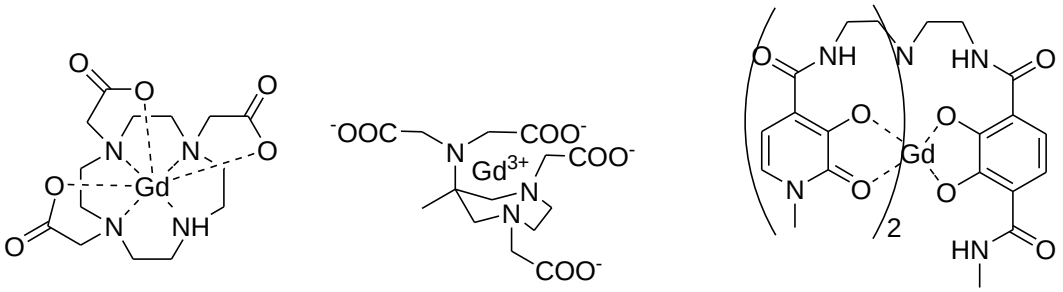

Figure 2. Structure of Gd-chelates with q=2.

1.4.2 Macromolecular systems as a way to increase r_1

The use of macromolecular systems with multiple Gd-complexes was widely explored as valuable amplification strategy to achieve effective MR CAs with the capacity to detect molecular targets. Common approaches in preparation of such constructs exploit either a covalent or noncovalent grafting of Gd-chelates to macromolecules or their encapsulation into

nanocarriers. The self-assembling[32] or hydrophobic aggregation by formation of micelles[33] represent methods to attain accumulation of a huge number of Gd-complexes. An interesting example of improving r_1 through an encapsulation approach was provided by the entrapment of several commercial Gd-HPDO3A complexes (between 8-10) inside the spherical cavity of apoferritin[34]. The relaxivity of this construct was very high as a r_1 value of $80\pm5 mM^{-1}s^{-1}$ was calculated per entrapped Gd-chelate. This was 20 times more than relaxivity obtained for free Gd-HPDO3A in water ($4.2\ mM^{-1}s^{-1}$). The authors elucidated that a large part of observed relaxation enhancement arises from multiple interactions between the paramagnetic complex, exchangeable protons and water molecules (freely moving in the interior cavity or bound to the inner sphere of protein). Liposomes have also been explored as nanocarriers for Gd-complexes. Sipkins et al.[35] reported on a Gd-containing polymerized liposome with an avidin moiety on its surface. It was demonstrated that endothelial integrin $\alpha_v\beta_3$ receptors on the tumor endothelium could be visualized by binding the liposome based MR probe to a biotinilated antibody against $\alpha_v\beta_3$. Several other examples with paramagnetic complexes located in the membrane[36,37,38] or encapsulated in the liposomal cavity[39,40] were reported.

As predicted by the relaxivity theory a large enhancement of relaxivity of Gd-chelate is expected by increasing the rotational correlation time. Therefore, in tandem with developments of encapsulation approaches several studies have been focused on setting up amplification strategies, which involve the grafting of small and fast-tumbling Gd-complex to large molecules leading to its slower molecular tumbling and thereby increasing τ_r. The noncovalent binding of Gd-chelates to human serum albumin (HSA), which is i.e. a valuable target for MRI angiography, represents an approach for attaining high relaxivity by increasing τ_r[41]. However, in order to achieve a sufficient increase of r_1 for HSA adducts a fast exchange of coordinated water is required. This dependence of observed r_1 from τ_m was investigated by Caravan[24]. A Gd-DTPA analog MS-325 (Fig 3), having a fast water exchange yielded in a much higher relaxivity upon binding to HSA as compared to its bis(N-methyl)amido derivative with a slower water exchange. Amongst several investigated systems with q=1 a high relaxivity of $65.8\ mM^{-1}s^{-1}$ was reported[42] for Gd-TTDA-BOM as adduct with HSA. Further enhancement of relaxivity can be also expected with increasing the hydration number. Indeed, Aime and coworkers reported[43] on Gd-AAZTAC17 with q=2 (Fig 3) which upon binding to defatted HSA showed a r_1 of $84\ mM^{-1}s^{-1}$,

which is so far the highest reported value for a Gd-based complex non-covalently bound to a slow-tumbling substrate.

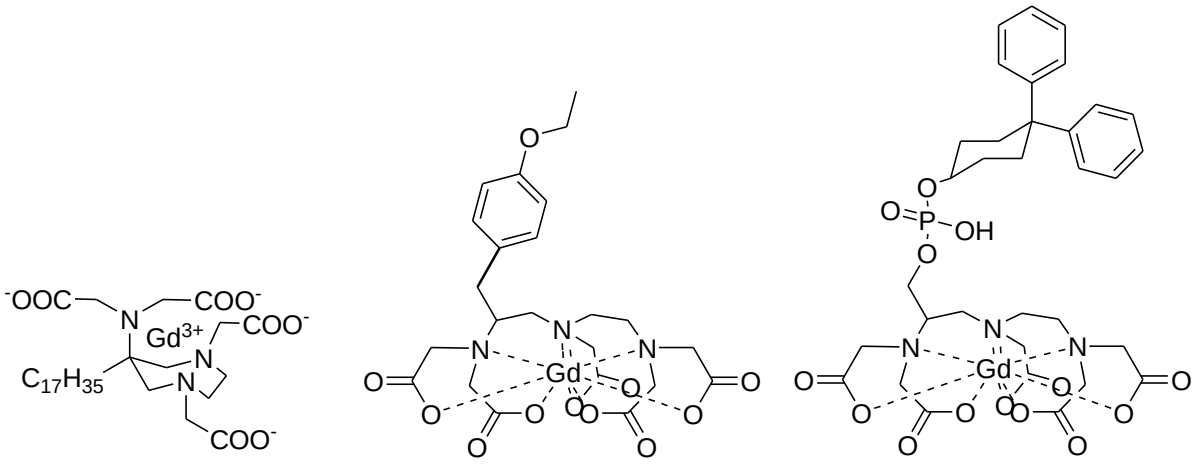

Gd-AAZTAC17 Gd-TTDABOM MS-325

Figure 3. Structures of Gd-complexes binding to HSA.

A further approach to increase sensitivity of MRI probes has been based on the construction of slow tumbling macromolecular system with covalently attached multiple Gd-chelates having a fast water exchange rate. The local rotational flexibility should be taken into account, while designing such constructs. In case of fast internal motion of Gd-complexes (attached by a flexible linker) the increase in τ_r associated with slow-moving macromolecules cannot be realized resulting in a meager change of observed r_1. Thus, connecting Gd-chelates in linear fashion gives an oligomer showing low r_1 enhancement due to anisotropic rotations despite an attained increase in molecular weight. Caseli et al.[44] demonstrated a modified dextran polymer with Gd-DO3A-monoamide complexes (52 kDA) with a relaxivity of 10.6 $mM^{-1}s^{-1}$ (0.47 T, 37ºC) per Gd. In comparison to linear polymers attachment of Gd-chelates to dendrimers provided constructs with higher r_1 as result of the more isotropic rotation due to the more globular structure but internal motion of Gd-chelates were still present. Gadomer-17 (17 kDA), showing r_1 of 16.5 per Gd (0.47 T, 40 ºC), represents such a polyamide dendrimer containing Gd-DO3A-monoamide chelates[45]. Recently virus capsids have been investigated as potential scaffolds for appending of multiple Gd-chelates[46,47,48]. In this fashion Reymond and coworkers obtained a system consisting of $Gd(hopo)_2(tam)$ chelates covalently attached to bacteriophage

MS2 capsids. The construct with tyrosine linkers showed a remarkably high relaxivity of 41.6 $mM^{-1}s^{-1}$ per Gd and 3900 $mM^{-1}s^{-1}$ per particle while much lower r_1 (30.7 $mM^{-1}s^{-1}$ per Gd and 2500 $mM^{-1}s^{-1}$ per particle, 30 MHz, 25ºC) was observed in case of lysine linker. It was concluded, that the rigidity of the spacer incorporating the Gd-chelates to the macromolecule clearly governs its final relaxivity[49]. The role of internal flexibility was also investigated[50] by Zhang et al. The authors reported on an attractive tetrameric agent, where a large increase in r_1 was induced due to the incorporation of two target binding sites that endow the system, which undergoes changes from a flexible to one with restricted molecular motion since it is rigidified at the targeted site (r_1=41.3 $mM^{-1}s^{-1}$, before binding r_1=10 $mM^{-1}s^{-1}$, 20 MHz, 37ºC). Another approach to restrict impact of motion on relaxivity can be achieved via placing the metal ion at the barycenter of the molecule. The Gubert group reported[51] on such efficient CAs (r_1=39 $mM^{-1}s^{-1}$, 0.47T, 37ºC) consisting of Gd-DOTA with bulky hydrophilic arms attached to each of the α-carbons of the acetate arms. Thus, the rigidity appears to be an influential parameter affecting relaxivity of slow-tumbling constructs.

The example presented in this chapter briefly illustrated how relaxivity and thus the sensitivity of Gd-based CAs can be improved through altering the rotational dynamics (τ_r, rigidity), water exchange rate, hydration number and/or accumulating multiple Gd-chelates. The strong influence of these parameters on relaxivity provides the basis not only for a solely steady increase in the sensitivity of CAs, but also through the attentive design, MR reporters can be obtained, where modulation of these parameters and a change in relaxivity would occur in the presence of specific targeted molecules. Various systems were investigated with purpose to achieve such CAs.

1.5. Biologically activated and responsive MRI Contrast Agents.

In the recent years the development of Gd^{3+}-based contrast agents, which specifically alter MR signal in the presence of biological targets has attracted a growing attention[52]. Several CAs were reported, that proved to be sensitive to diagnostically relevant parameters such as pH[53,54], temperature[55], enzymatic activity or ion concentrations (e.g. Ca^{2+}, Zn^{2+}). The illustrative examples of bioactivated or responsive MRI CAs with main focus on enzyme activated MR reporters will be presented in the following sections.

1.5.1 MRI reporters sensing on changes in their environment

The subtle changes of physico-chemical variables like pH or ion concentrations that signals the occurrence of biological process or pathological changes can be used to create environment-responsive Gd^{3+}-based contrast agents.

pH sensitive CAs

Tissue acidosis is characteristic for inflammation[56] and tumor processes[57,58]. The local changes in pH of the affected regions as compared to the normal tissues, even though small, can produce a measurable difference in relaxivity of suitably designed CA. In order to create pH-dependent MR reporters, the functionality attached to the Gd-complex should be able to alter its relaxivity along with pH variations due to the protonation/deprotonation state of appended groups. In the majority of the examples reported so far, alteration of *q* through binding/repulsion of chelating arms to the gadolinium center was used as driving force of pH dependent changes in r_1. The examples of pH responsive MR CA include Gd-DO3A derivative bearing a phenyl group linked via an acid/base sensitive sulphonamide linkage[59] or a Gd-chelate containing p-nitrophenolic pendant arm[60]. A basically different approach[61] was used by Aime to achieve pH-responsive polymeric CAs. The pH-dependency of relaxivity origninated from changes in rotational correlation time due to protonation of polyornithine under low pH (higher mobility, shorter τ_r) or its deprotonation with increasing pH (intramolecular association, longer τ_r).

Ion-responsive CAs

Various biological signal transduction events involve divalent cations i.e. Ca^{2+}, Zn^{2+} or Fe^{2+}. Excess or deficiency may cause several diseases. Therefore, a design of specific MRI CA, which report on fluctuations in the concentration of these cations by changes in r_1 is highly desirable. The pioneering work on ion-responsive MR probes was introduced by Meade and coworkers[62] by developing MRI probes sensing for Ca^{2+}, an essential metal ion in numerous biological processes[63]. The proposed agent consists of the well known Ca^{2+} chelator BAPTA (1,2-bis(o-aminophenoxy)ethane-N,N,N,N-tetraacetic acid) that bridges two Gd-DO3A complexes. The changes in r_1 are observed due to alternation of free coordination sites for water molecules in Gd-chelates. In the absence of Ca^{2+}, the complex shows low relaxivity of 3.3 $mM^{-1}s^{-1}$ (500 MHz, 25ºC) due to the binding of four aminoacetate arms of BAPTA domain to the Gd^{3+} ion thereby

giving a coordinatively saturated complex (q=0). The addition of Ca^{2+} leads to 75% increase in observed relaxivity as result of conformational changes caused by strong and selective binding of the aminoacetate arms to Ca^{2+}, thus allowing access of water to the paramagnetic metal ion. A further attempt was undertaken to synthesize Ca^{2+} responsive CAs by modifying Ca^{2+} binding part[64].

Zn^{2+} was also recognized as a metal ion with a critical role in cellular physiology being involved in catalytic activity and signal transduction pathways[65]. For instance it is known, that under anomalous stress conditions such as epileptic seizure or stroke a thousand-fold increase in concentration of the free Zn^{2+} is observed due to its release from synaptic nerves to the somatic tissue[66,67]. Examples of MRI probes, whose relaxivity is Zn^{2+} concentration dependent include Gd-DTPA with pyridyl Zn^{2+} binding groups[68] or recently published[69,70] Gd-daa3.

Comblin et al. used an innovative strategy based on self-assembling to obtain an iron-activated MRI CA[71].

1.5.2 Enzyme responsive MRI contrast agents

Enzymes being highly specific biochemical catalysts function by converting one molecule into another. They are essential for a countless number of biological transformations taking place inside the living organisms[72]. For instance signal transduction or cell regulation including metabolic pathways demand the action of enzymes. These catalysts can serve as indictors of disease processes[73,74,75] and have been used as important gene expression markers[76,77,78]. Therefore, development of enzyme targeting MRI CAs would provide an invaluable tool for mapping enzyme location or measuring their activity *in vivo* by means of MRI[79]. The formation or cleavage of specific bonds have been used to design such enzyme activable CAs. The clear advantage of applying enzymes as labeling tool is its regeneration after enzymatic reaction, thus a large signal amplification should occur. Despite clear relevance, the enzyme-based approach remains still in its infancy as design of such systems proved to be challenging. Attempts have been made to design a suitable MR probe to monitor gene expression. The bacterial *LacZ* gene encoding for the enzyme β-galactosidase is most commonly used as reporter gene[80,81] when introduced together with the gene of interest to confirm transfection and monitor regulation processes. Meade and co-workers demonstrated the first time an enzyme activated MRI CA, EgadMe[82] and its analogs[83,84,85], designed to report on β-galactosidase activity to visualize LacZ

gene expression *in vivo*. This system based on blocking the access of water molecules to the first coordination sphere of the gadolinium metal by incorporation of a galactose moiety into a Gd-DO3A chelate (q=0). In the presence of *β*-galactosidase, the masking sugar unit was cleaved from the Gd-complex, thus allowing water molecules to interact with gadolinium (q=1 or 2) leading to a significant increase of relaxivity (Scheme 1). The *in vivo* detection of *LacZ* gene expression in *Xenopus laevis* embryos with EgadMe was of great importance as prove of principle that MRI can be applied to image a reporter enzyme even if it is present at low concentrations. It should be mentioned that this CAs had to be introduced by microinjection due to the lack of transmembrane permeability. Recently, the same group demonstrated an approach based also on the modulation of q for the detection of *β*-glucoronidase[86].

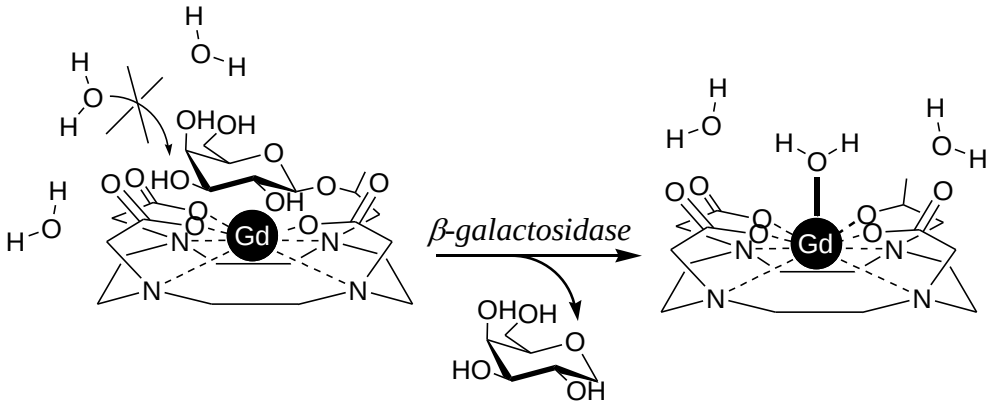

Scheme 1. Activation of EgadMe by *β*-galactosidase.

A different approach to obtain the enzyme responsive MRI CAs explores changes of the rotational correlation time through a modulation of the imaging probe affinity towards proteins (e.g. HSA). In this scenario, the enzymatically cleavable moiety is introduced into a protein binding unit in order to prevent its strong interaction with protein in the absence of enzyme. The activation of such a CA occurs upon enzymatic reaction *via* cleavage of the masking group with subsequent binding of the fast tumbling Gd-complex to proteins to form a slowly tumbling macromolecular adduct (increase in τ_r) with higher relaxivity. Lauffer and coworkers first reported[87] on such a CA, which was based on a hydrophobic 1,1'-dixydroxybiphenyl unit attached to Gd-DTPA with the masked binding affinity towards HSA by introducing of

hydrophilic phosphonate ester. In the presence of alkaline-phosphatase this ester was cleaved and concomitant an increase of r_1 was observed. Recently, a *β*-galactosidase-activated MRI CA was obtained with the similar biphenyl unit and a suitable galactose residue as masking enzyme cleavable moiety (Scheme 2)[88]. In another example, the aromatic linker was replaced by a short peptide sequence showing high HSA binding affinity, which was temporarily concealed by the attachment of a short tri-lysine peptide. Upon enzymatic cleavage of the masking unit by thrombin activatable fibrinolysis inhibitor (TAFI) the Gd-DTPA linked positively charged peptide with poor HSA affinity was successfully converted into the strongly binding sequence[89]. A further interesting approach was used to detect stearase activity in macrophages[90]. In this case the solubility of CA was used as driving force for observed relaxivity enhancement in the presence of enzyme. Here, an insoluble MR probe with long aliphatic chains attached via ester spacers to a Gd-DTPA derivative was converted into a soluble and active form of CA by stearase due to the hydrolysis of ester linkages after internalization into the cells.

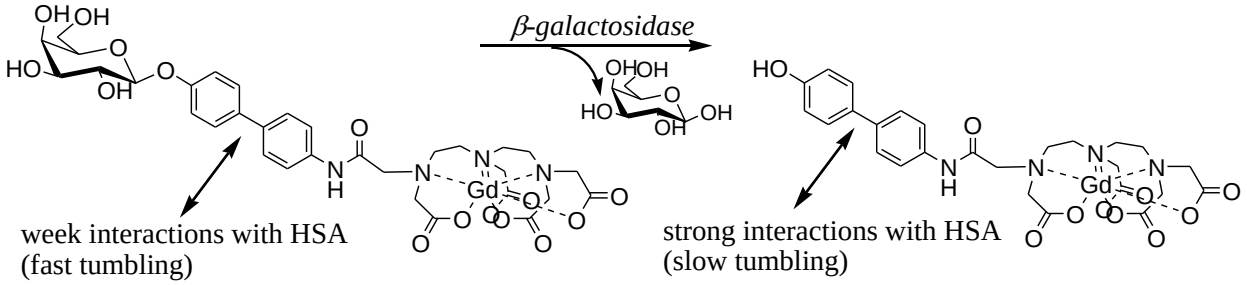

Scheme 2. *β*-galactosidase mediated activation of Gd-DTPA derivative interacting with HSA.

The so far presented strategies were based on specific breaking of chemical bonds by enzymes leading to structure modifications of the CAs and its relaxivity enhancement. Along with developments towards enzyme hydrolysable MRI CA, the opposite activation mechanism was explored based on chemical bond formation specifically mediated by enzymes (e.g. polymerases and oxidoreductases). In this case a paramagnetic substrate can be oxidized by a certain enzyme to generate reactive products that subsequently oligomerizes *in situ* to produce larger molecules with a reduced tumbling rate, thus higher relaxivity. This strategy was initially demonstrated for a model Gd-DOTA derivative bearing a hydroxytyramide moiety, which proved to be a substrate

of horseradish peroxidase (HRP)[91]. An analog of this model compound was synthesized by the replacement of hydroxytyramide with 5-hydroxytryptamide (serotonin moiety) and used to image myeloperoxidase (MPO) activity[92]. This enzyme is secreted by leukocytes at the inflammation site and for instance MPO was found to reside in vulnerable atherosclerotic plaques at high local concentration[93]. In an attempt to further improve the enzyme-mediated relaxivity enhancement two oligomerizable moieties (tyramide or 5-hydroxytryptamide groups) were linked onto a Gd-DTPA derivative[94,95]. Such design facilitated cross-linking of enzyme genetrated reactive species and finally higher rigidity of polymeric product thereby leading to an increase in r_1. The authors proposed that the observed relaxivity change was due to increase in the degree of oligomerization as well as to covalent interactions of CAs with proteins present in the MPO-rich area. Further applications of such enzyme-mediated MR amplification strategies were presented for targeted imaging in tumor models[96].

The detection of matrix metalloproteinase-2 using solubilility-switchable CA was recently presented by Jastrzębska et al.[97] The presented biologically activated MR contrast agents although showing stunning properties are generally restricted to the extracellular environment thereby cell membrane impermeable. Actually most of physiological processes of interest take place inside the cell. Therefore, a design of suitable intracellular delivery strategies represents a vital prerequisite for the employment of such CAs in the imaging of biological targets at molecular and cellular level.

1.6 Cell labeling strategies

The persistently growing number of approaches (i.e. gene/cellular therapy, molecular/cellular imaging) aiming for cellular and molecular targets emerged a design of efficient delivery vectors able to transgress therapeutic or diagnostic cargo molecules across semi-permeable cell membranes[98]. Physical methods like microinjection or electroporation[99] were used to load different molecules into the cells (e.g. DNA), but both methods possess several limitations as invasive techniques associated with potential cell damage. Thus, effective carriers that deliver cargo molecules specifically at desired locations *in vivo* at high levels and without inducing toxicity/immunogenic reactions are needed. Nevertheless, achieving such optimal carriers that would fulfill all efficiency criteria, proved to be difficult. Viral-mediated delivery was broadly applied to transfer genetic material into cells[100]. Although normally high levels of transduction

are obtained, the potential risk of random insertion of viral vector genomes into the host chromosome and immune responses are some of the main concerns for their widespread application. In contrast, currently used non-viral carriers like liposomes proved to be safe and non-immunogenic vectors for several cargo types, but their delivery efficacy have still to be improved[101,102,103].

A relatively new but rapidly evolving group of delivery vectors is represented by cell penetrating peptides (CPPs)[104]. This is due to the great ability of CPPs to facilitate efficient internalization of cells a wide range of molecular cargos (e.g. small molecules, large particles, proteins or plasmid DNA into cells). Cargo molecules can be associated to the peptides via non-covalent interaction[105] or linked covalently by various spacers[106]. CPPs are typically short sequences of amino acids containing either a high number of positively charged amino acids residue (polycationic peptide) or otherwise linked together in an alternating fashion hydrophobic (nonpolar) and charged (polar) amino acids (amphiphatic peptide). Most CPPs were designed based on the sequence of proteins called protein transduction domains (PTD) or on the amphipathic character of the entire proteins. Examples of such CPPs include Tat peptides[107], VP22 derived peptides[108], CYLOP-1[109], penetratin[110], and proline-rich peptides[111]. Several CPPs including polyarginine and polylysine[112,113] were developed considering the critical role of positive charges for translocation abilities. CPPs hold a great potential for the intracellular delivery of various therapeutic molecules, but their widespread application is limited by the lack of cell specificity, which can be further improved by vast understanding of the translocation mechanism.

1.7. Aim of the work

The emerging need for suitable MR imaging probes that have an ability to translocate across the cell membrane and report on a biological process or signal the presence of a targeted molecule was an inspiration for the presented work. The particular aim of this project was to develop novel cell permeable MRI contrast agents targeting the intracellular localized enzyme *β*-galactosidase. Such a MR probe able of crossing cell membrane in both directions (influx and efflux into/from the cell) would be selectively entrapped only in *β*-galactosidase containing cells by its enzymatic conversion into form with increased cellular retention time due to cleavage of delivery vector. This thesis includes three major parts of completed work:

Chapter 2 presents the affords made towards design and synthesis of the intracellular MR probes based on a galactose moiety targeting *β*-galactosidase. A sugar core has to be synthesized containing modifications on C6 as well as on the glycosidic C1 to include the imaging reporters and to maintain the enzymatic activity to cleave off the delivery vector. The bimodality of these probes was achieved by incorporation of the suitable reporters FITC and Gd-DOTA detectable by optical imaging modalities and MRI. This allows the biological and MR evaluation of the synthesized MR probes in a transgenic cell line expressing *β*-galactosidase (C6/LacZ) in comparison to the parent cells (C6) without enzyme in order to reveal their ability for specific accumulation in enzyme containing cells. In search for parameters that govern the ability of these probes to enhance contrast in MR images, the relationship between the molecular structure and the relaxivity r_1 was also investigated.

Chapter 3 focused on the evaluation of the enzymatic activity of *β*-galactosidase on the intracellular MR contrast agent. In an attempt to understand the factors, which govern the interaction of these bulky conjugates with the enzyme, and thereby the enzymatic activity, a series of model molecules with particular structural variations were synthesized. Their enzymatic evaluation as well as the establishment of several enzymatic assays for the different types of substrates will be discussed in this section.

In Chapter 4 a method for efficient labeling of macromolecules with MR and optical imaging reporters was established. This approach took advantage of combining bimodality and pre-loading in the design of a suitable precursor, which can be appended to bulky molecules using a mild bioconjugation protocol. The synthesis and applicability of this precursor was shown.

Chapter 2

Bimodal intracellular MR contrast agents targeting *β*-galactosidase as prospective tools for the evaluation of cellular therapies

2.1 Introduction

Cell based therapies endow modern medicine with an invaluable tool for the treatment or complete averting many of the most severe diseases such as cancer[114,115], neurodegenerative disorders[116,117] as well as cardiovascular or inflammatory malfunctions[118,119]. The basic idea of this novel approach is that selected cells should act as a therapeutic drug after they are transferred into the patient. Theoretically such cells reach any side inside of the body and therefore can be used to restore the damaged tissues, recognize inflammation sites, fight diseases or take over the function of defective genes[120]. Despite the vast therapeutic potential and growing interest for numerous human applications the success of therapeutic approaches has been rarely seen. The major hindrance for improving these innovative methods is the insufficient understanding of the mechanisms, which determine the *in vivo* fate of the cells after their transplantation. In order to acquire such essential knowledge, the noninvasive monitoring of transplanted cells migration, biodistribution, survival and differentiation in the living organism over time becomes a vital necessity[121].In the last two decades, many remarkable approaches for cell tracking using nuclear or optical techniques, but also more recently MRI were developed Such noninvasive imaging methods require efficient cell labeling protocols and suitable imaging probes in order to create "marked-cells" detectable by the corresponding imaging modality. The first clinically applied approach for noninvasive cell tracking was the leukocytes scintigraphy[122]. This technique is using the accumulation of externally radiolabeled leukocytes (^{111}In-oxine[123,124] and ^{111}In-tropolonate[124, 125] or ^{99}Tc-HMPAO[126,127]) to detect inflammation *loci* in patients using nuclear medicine modalities. Over the years, several interesting cell tracking strategies by means of optical techniques were developed. Shortly, cells can be tagged with fluorescent dyes[128,129], quantum dots[130] or "permanent marker"-genes expressing either fluorescent proteins (e.g. GFP[131,132], RFP[133])
or enzymes (e.g. *β*-galactosidase[134,135], luciferase[136,137]). Although application of optical methods for cell tracking in preclinical animal models is very useful, the transfer in human settings is limited due to light scattering and absorption in tissues. In addition, the usage of nuclear imaging methods for long-term evaluation of cell therapies in patients introduces health and safety concerns[138]. This is due to the compulsory repetitive use of ionizing radiation and thus administration of radioactive tracers in order to assess transplanted cell migration *in vivo*.

In contrast to optical and nuclear medicine techniques, MRI allows the repetitive and noninvasive acquisition of whole body images of intact, opaque organisms without exposure to ionizing radiation. These features situate MRI as a very powerful modality that meets all needs of monitoring cellular therapies as efficient and safe diagnostic method allowing repetitive imaging of transplanted cells in humans. Cellular imaging using MRI requires the incorporation of MRI contrast agents into the targeted cells. Thus, *in vitro* pre-labeling of therapeutic cells with MRI probes is mostly applied *prior* to their reintroduction into the living organism[139]. To date, several prospective applications utilizing this approach were presented. These include organogenesis studies by embryonic stem cell tracking[140,141] or stem cell migration to lesions of cerebral ischemia[142,143,144] and tumor[145]. However, the gradual diminution of CA over time as consequence of cell division and differentiation narrows the applicability of the pre-labeling approach for long term monitoring of cell trafficking.

Keeping in mind these limitations, the goal of this project was to design novel MR contrast agents, which can be repetitively given to an individual after cell transplantation and would then selectively accumulate within the transferred cell populations. This approach would allow the long term monitoring of cell trafficking *in vivo* since such MR probe could be administrated multiple times, in contrast to only single time possible for *in vitro* cells pre-labeling. However, in order to utilize such a strategy, transplanted cells must possess distinctive "features" (e.g. receptor, enzyme), which set them as targets for the MR probe and allow their selective detection amongst millions of other cells in the body. In an established preclinical animal model (in collaboration with the Hannover Medical School Transplantation Research Center) the intracellular enzyme *β*-galactosidase (expressed by the bacterial *LacZ* gene in the transplanted cells) was chosen as unique cell "feature" targeted by the MR contrast agent. This paradigm was designed as a proof of principle to monitor the *fate* of hematopoietic stem cells from mice producing *β*-galactosidase (donor) after their transplantation into wild type mice (recipient) lacking this enzyme. In addition, there are many examples in clinical reality, where enzymes can be used as therapeutic drug but at the same time serve as target for tracking the transplanted cells. The Hurler syndrome (Mucopolysaccharidosis I) represents such a case, where the deficiency of an enzyme (α- L-iduronidase), leading ultimately to brain retardation and death, can be potentially corrected by transplanting hematopoietic stem cells containing α-L-iduronidase from a healthy donor[146].This enzyme could also used to follow the transplanted cells.

Thus, development of highly specific and biocompatible MR contrast agents which should accumulate inside the targeted cell by a specific interaction with a cytoplasmic enzyme is an intricate but vital prerequisite to achieve such cellular imaging *in vivo*. In this chapter the design, synthesis and biological evaluation of model intracellular MR contrast agents targeting *β*-galactosidase will be presented, which consist of four functional domains: MRI/FR reporter, enzyme sensor and delivery vector (Fig 4).

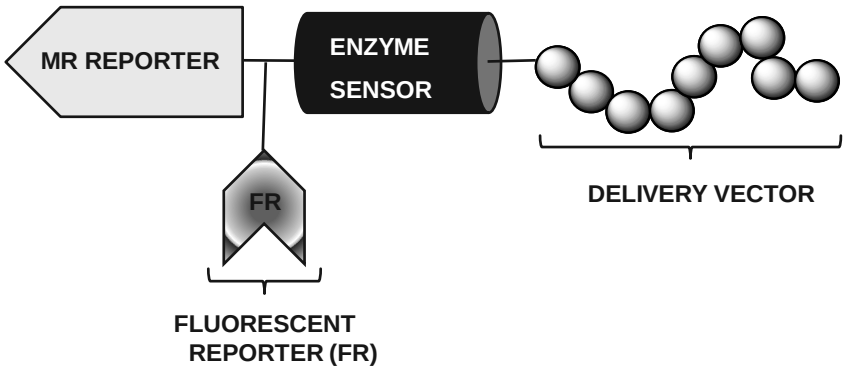

Figure 4. Schematic structure of enzyme targeting dual-labeled intracellular contrast agents

2.2 Results and Discussion

2.2.1 Design of bimodal CAs targeting *β*-galactosidase

The design of **CA-1** and **CA-2** (Fig 5) was based on an enzyme activated trapping approach, where the targeted MR imaging probe with capacity for fast and effective penetration in both directions of the cell membrane is entrapped only inside cells expressing *β*-galatosidase by the cleavage of cell permeable delivery vector (peptide) upon *β*-galactosidase catalyzed reaction. This should lead to a reduction of the outflow of the MR imaging moiety, thus promoting its accumulation in the *β*-galatosidase expressing cells as illustrated on the Scheme 3 (*in vitro* experiment). The final goal is to use the same compounds to track transplanted stem cells *in vivo* (Scheme 3, *in vivo* experiments). An example showing an effect of cellular retention on the observed MRI contrast enhancement was presented for a polyarginine conjugated to Gd-DOTA through a disulfide bond that is non-specifically cleaved inside any given cell due the reductive intracellular environment[147].

In order to obtain specifically accumulating **CA-1** and **CA-2** the peptide was attached via a linker at the position C-1 of galactose moiety, where enzymatic action takes place. Thus, the galactose moiety served as specifically cleavable spacer between both MR/FR reporters and the delivery vector. The hydroxyl groups at C-2, C-3 and C-4 are essential for the binding of the galactose derivative to the active site of the enzyme and their substitution will prevent the enzymatic reaction at anomeric center (detailed discussion in Chapter 3). Therefore position C-6 of the galactose moiety was selected to attach the MR/FR reporters to fulfill the criteria of maintaining enzyme activity and specificity.

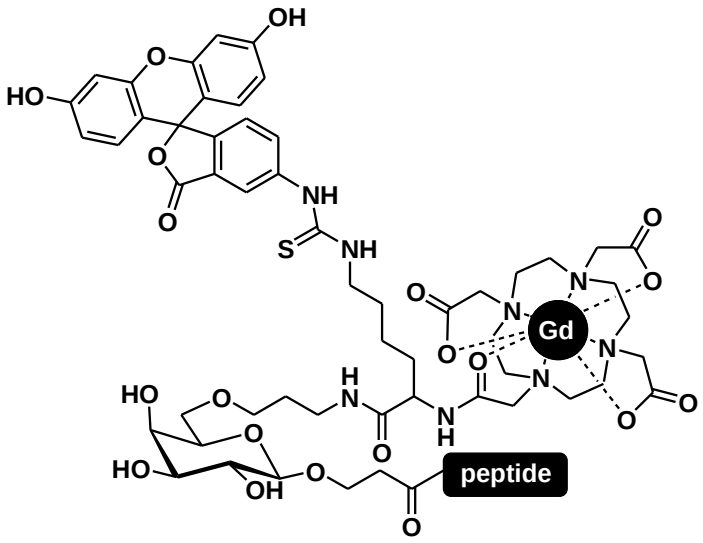

peptide = Arg−Lys−Lys−Arg−Arg−Gln−Arg−Arg−Arg CA-1 (Tat_{49-57})

Arg−Arg−Arg−Gln−Arg−Arg−Lys−Lys−Arg CA-2 (Tat_{57-49})

Figure 5. Synthesized Contrast Agents **CA-1** and **CA-2**

The peptides D-Tat_{49-57} and D-Tat_{57-49} were chosen as delivery vectors and compared for their translocating ability of **CA-1** and **CA-2**. Moreover, the CPPs synthesized with D-amino acids were selected to ensure that observed cellular retention of MR reporter is due to enzymatic reaction and not due to peptidases mediated peptide degradation. The fluorescent dye fluoresceine isothiocyanate (FITC) was introduced into the molecular structure of these CAs in

order to create dual-modality probe detectable using MRI and optical imaging techniques. This allows combining of advantages of both technologies discussed in details in Chapter 4.

In this chapter the synthesis, MR and biological examination of **CA-1** and **CA-2** will be presented to reveal their ability to act as intracellular *β*-galactosidase targeting MR contrast agents.

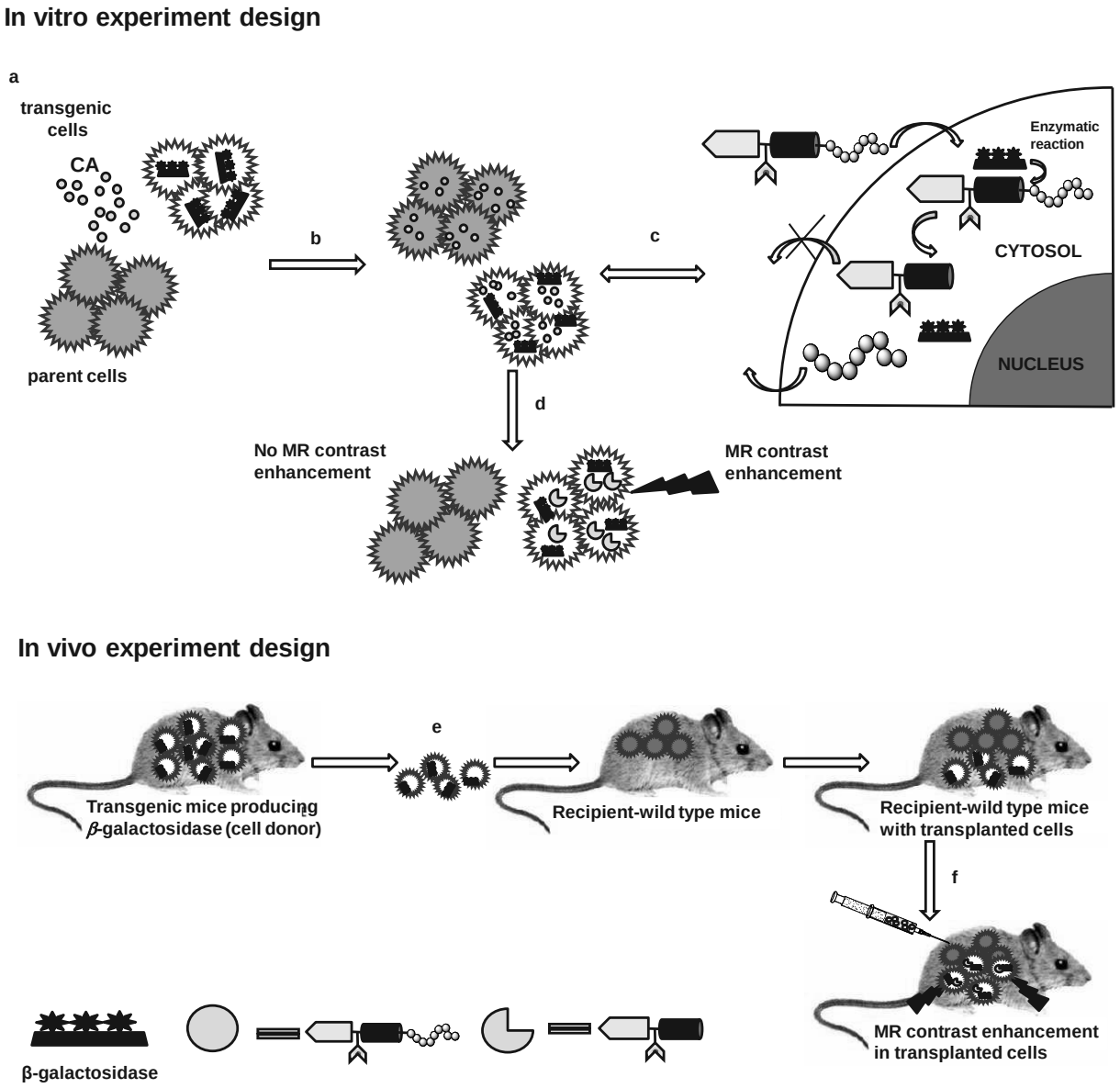

Scheme 3. Proposed mode of action for intracellular β-galactosidase targeting MR contrast agents; a) Incubation of transgenic and parent cell lines with CA; b) Cells were labeled with CA;

c) Enzymatic reaction inside transgenic cells; d) Accumulation of MR/FITC reporters only in transgenic cells; e) Transplantation of β-gal expressing cells from donor into recipient f) Injection of CA to recipient mouse with transplanted cells expressing *β*-galactosidase and MR signal enhancement only in these cells.

2.2.2 Synthesis of CA-1 and CA-2 conjugates

Solid phase synthesis (SPS) was a major breakthrough in chemical multistep synthesis of biopolymers (peptides, oligosaccharides, peptide nucleic acids etc.)[148] and became an essential tool used in drug development as well as in combinatorial chemistry[149]. In principle, SPS is based on repeated cycles of sequential deprotection-conjugation of protected building blocks resulting in the formation of the target molecule that is covalently attached via a linker to the insoluble polymeric support (resin). The main advantage of utilizing SPS in multistep synthesis over solution phase procedures is the easy purification during the synthesis. The excess of reagents as well as by-products of the synthesis can be washed from the growing product that is retained on the resin during a simple filtration/washing process after every reaction step. However, the prerequisite for highly efficient SPS is a nearly quantitative yield of the single coupling reaction. Thus, the suitable side-chain protecting groups of the building blocks, coupling reagents and resin have to be chosen carefully in order to facilitate the formation of the target compound in high yield[150].The bimodal conjugates **CA-1** and **CA-2** (Fig 5) were synthesized manually on preloaded Wang resin by continuous SPS utilizing the Fmoc-N^{α} /tBu strategy. The main advantages of this protocol over Boc-N^{α}/benzyl chemistry are the mild condition used for Fmoc-N^{α} group deprotection, elimination of hydrofluoric acid for cleavage of the final product and high specificity of removing Fmoc-N^{α} in the presence of side chain protecting groups[151]. In order to utilize the continuous Fmoc based scheme for the synthesis of **CA-1** and **CA-2** an appropriate Fmoc-protected β-galactose derivative **16** was required serving as the enzymatically cleavable linker.

2.2.2.1 Synthesis of building block 16

The main part of the proposed CAs was the monosaccharide building block **16** based on a galactose moiety, which was designed on the way to enable its conjugation to the Tat peptide (at the anomeric centre) and to the imaging moieties DOTA ligand /lysine-FITC (at C-6 position) on resin. The carboxylate and temporarily protected amino group (Fmoc carbamate) were selected

as orthogonal functions introduced to the final structure of the galactose unit. This would make compound **16** fully compatible with the Fmoc mediated SPS scheme. Hence, a substrate specificity of the enzyme β-D-galactosidase, as discussed already in the introduction part, demanded, that only position C-6 and C-1 of the galactose derivative can be used as attachment points for imaging and transduction moieties. In order to ensure, that a modification of the galactose part by substitution of hydroxy group at C-6 position would not prohibit an enzymatic hydrolysis, model compounds were synthesized. Their enzymatic activity was compared with a standard substrate p-nitrophenyl-β-D-galactopyranose (PNPG) (detailed discussion presented in the Chapter 3). Taking into account all structural requirements of the carbohydrate core **16** an efficient synthetic strategy had to be planned. Two feasible approaches for introducing the selected orthogonal functional groups (COOH and NH-Fmoc) into the sugar moiety were considered (Fig 6).

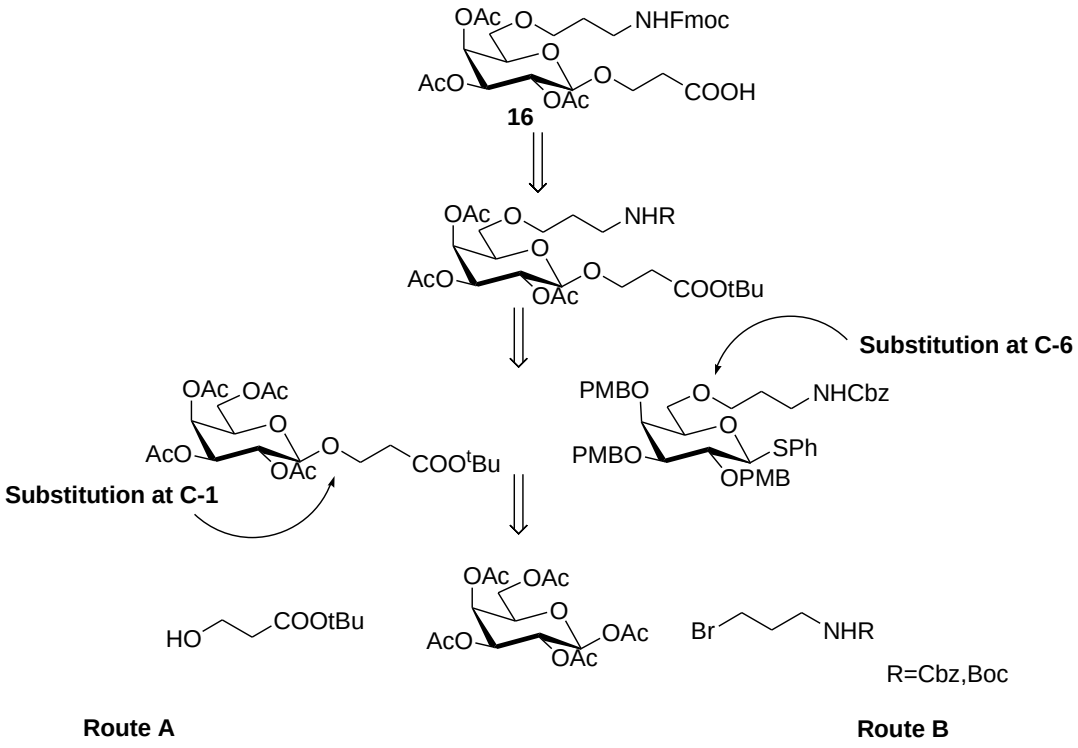

Figure 6. Retrosynthetic analysis for carbohydrate building block **16**

Their assembly could be achieved *via* initial formation of the *O*-glycosidic bond at the C-1 carbon (route A) or substitution at the C-6 position of galactose unit (route B). A numerous O-glycosylation methods have been established until now[152]. Nonetheless, control of high stereoselectivity in the nucleophilic substitution at the anomeric center towards a desired α- or β-anomeric product still remains a formidable challenge to the synthetic chemist. The broad scope of factors, which can play a critical role in the ratio between α/β anomers includes the activating method, neighboring group participation, kind of protecting groups on glycosyl donor and acceptor (steric and electronic effects), the anomeric effect, temperature and solvent[153].

Taking into consideration the complexity of the *O*-glycosylation reaction at the anomeric center, route **A** was primarily chosen to obtain the desired *β*-anomer **16**. A key advantage of this approach could be ascribed to an early formation of the *O*-glycosidic bond. Hence, such strategy would offer the flexibility intended for the modification of activating method/glycosyl donors, in the case of poor α/β selectivity or low reaction yields, at the very beginning of the multistep synthetic route. Accordingly, a synthesis of **2** was initially attempted by Konigs-Knorr procedure based on acetobromogalactose **1** as glycosyl donor (Scheme 4). The treatment of commercially available galactose peracetate with 33% HBr/CH_3COOH in DCM yielded **1** (95%), which was further reacted with tert-butyl 3-hydroxypropionate in the presence of the insoluble promoter Ag_2CO_3. However, a poor reaction yield demanded further modifications of glycosylation protocol as **2** was obtained in only 30%. The replacement of Ag_2CO_3 with AgOTf catalyst resulted in formation of **2** in a moderate 47% yield. The further increase of conversion towards **2** was achieved by employing the thiogalactose donor **3**, which was synthesized in 70% using a previously described procedure[154]. In its subsequent reaction with *tert*-butyl 3-hydroxypropionate in the presence of NBS-Me_3SiOTf by adopting a method described by Qin et al.[155], the resulting *β*-anomer **2** was efficiently obtained in 65% yield. Next, acetyl protecting groups were quantitatively removed prior to silylation of **4** with TBDMSCl in DMF in the presence of imidazole used as base. The compound **5** was obtained only in 35% yield but a further use of a mixture of Et_3N and pyridine as solvent improved the yield of silylated product to 50%. In order to facilitate later on the formation of an ether bond at the C-6 position of the sugar moiety, suitable hydroxyl protecting groups (benzyl or its derivative), chemically stable as well as resistant to migration under the strong basic conditions had to be used. Nonetheless, formation of **6** *via* benzylation of **5** with benzyl bromide and NaH used as base (DMF as solvent) could not be

accomplished due to the elimination of the 3-tert-butyl propionate linker under the applied reaction conditions. A complex mixture of side-products such as eliminated product (major), partially benzylated **5** and desired **6** (minor) were observed in LC-MS spectra in addition to TLC. Further optimizations of the reaction conditions like temperature and reagent ratio failed to provide feasible formation of intermediate **6**.

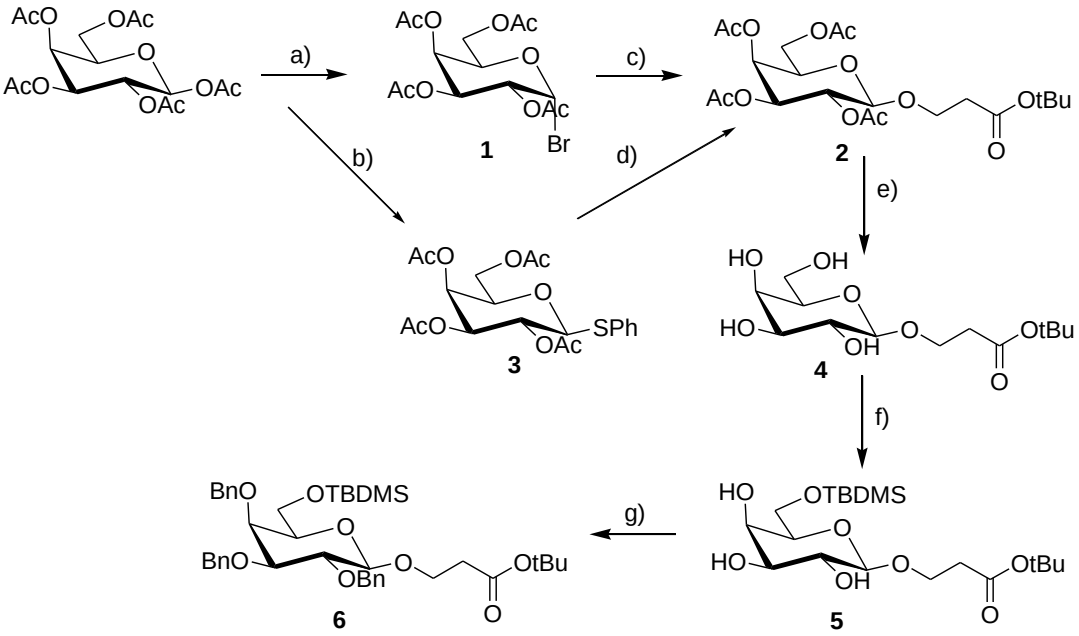

Scheme 4. Synthesis of sugar core **16** (pathway A)

Reagents and conditions: a) HBr/CH_3COOH, DCM, rt, 2 h; b) thiophenol, BF_3xEt_2O, DCM, 0°C, 4 h; c) Ag2CO3, DCM, -40°C or AgOTf, -20 °C-rt, DCM d) $HO(CH_2)_2COO^tBu$, NBS/TMSOTf, DCM, -50 °C e) $NaOH_{cat.}$, MeOH f) pyridine, Et_3N, TBDMSCl, 0°C-rt g) NaH, BnBr, DMF, 0°C-rt.

Due to several synthetic problems encountered while proceeding through pathway **A**, an alternative synthetic strategy **B** (Fig 6) was executed effectively leading to the formation of desired carbohydrate core **16** (Scheme 5). This approach was based on the transformations involving a thioglycoside renowned as versatile and robust glycosyl donor in carbohydrate chemistry. Consequently, the thiogalactose donor **3** was quantitatively deacetylated to give **7**.

The selective silylation of primary 6-OH with TBDMSCl in pyridine/Et_3N yielded **8** (80%). At this point, like it was mentioned before for derivative **5**, introducing protecting groups, robust and migration resistant under strong basic conditions, was the requisite for efficient formation of **11**. Thus, *p*-methoxybenzyl (PMB) ethers were implemented as temporal protection for the free hydroxyl groups of **8**. Moreover, this choice was dictated by a wide spectrum of mild cleavage conditions available for PMB ethers (oxidation, hydrogenation, acidolysis). At first, the synthesis of **9** was approached *via* benzylation of **8** with *p*-methoxybenzyl chloride (PMBCl) in DMF. However, the product was obtained in low yield (35%). Further optimization involving a longer reaction time (an increase from 12 to 24 h), heating and addition of more PMBCl after a certain reaction time did not improve the yield. In contrast, replacement of PMBCl with *p*-methoxybenzyl bromide (PMBBr) resulted in an efficient formation of **9** (70%). Profitably, a much shorter reaction time (4 h) was required to complete the benzylation of **8**. This enabled to eliminate the side-products observed during reaction with PMBCl, thus improve the overall yield of **9**. Subsequent removal of TBDMS ether by treatment with a solution of TBAF in THF yielded compound **10** (69%). The following transformation involved the incorporation of a Cbz-aminopropyl linker *via* an ether bond created at the primary hydroxyl group of carbohydrate **10**. So far, there are hardly any reports on formations of tether alkylethers at the C-6 position of galactose moieties[156,157]. In general, a popular in organic chemistry approach towards ether synthesis is based on the reaction of *in situ* generated alkoxide (using base or metal hydride) with a sterically unhindered substrate possessing a good leaving group. Accordingly, the monosaccharide **11** was produced in 45% yield in a reaction carried out at room temperature between benzyl 3-bromopropylcarbamate[158] and derivative **10** pre-activated with an excess of NaH (4 eq). Given that an incomplete conversion of **10** was observed, in an attempt to further improve the yield, the reaction temperature was increased to 55°C. However, this resulted in side-product formation (not detectable at room temperature) with apparently no significant shift in conversion towards **11** since the remaining starting material **10** was still detected on TLC and in ESI-MS spectra. Given that elimination of bromine might compete with formation of ether bond more alkylating agent (2 and 4 eq) was added after a certain reaction time at room temperature. Though, conversion of **10** was still not improved. Hence, the initially established protocol proved to be the best under the tested conditions to give derivative **11**.

At this point, *p*-methoxybenzyl ethers at 2,3,4-hydroxyls of **11** were exchanged with acetyl protecting groups in order to: I) facilitate a subsequent formation of the required *β*-anomer (neighboring group participation effect) and II) stabilize an ordinarily quite labile glycosidic bond towards later applied acidic conditions[159]. Though a catalytic hydrogenolysis is the mildest and most convenient deprotection method of PMB ethers, the presence of the thiophenyl group excluded its application owing to catalyst poisoning as reported by Izumi et al.[157] The attempts to remove PMB groups with 5% TFA/DCM (v/v) further increased to 10% TFA/DCM according to the procedure described by Yan et al.[160] resulted in a mixture of completely and partially deprotected **11** as well as by-products, that could not be separated by column chromatography. Ultimately, the PMB groups were removed by oxidative cleavage with DDQ as oxidant in a DCM-water mixture (30:1) to give derivative **12** as brownish oil (60%). Initially applied proportions of DCM-water such as 18:1[161] resulted in incomplete deprotection of **11**. The ratio between dichloromethane and water had an important impact on the reaction rate, which increased significantly with decreasing amount of water. The obtained product **12** was acetylated with acetic anhydride in pyridine to give **13** (85%), which was afterwards reacted with tert-butyl 3-hydroxypropionate in the presence of NBS-Me_3SiOTf and activated molecular sieves by adopting a method described by Qin et al.[155] The resulting β-anomer of **14** was formed at a 50% yield. The removal of the tert-butyl protecting group with a TFA-DCM mixture (1:1) occurred with the partial acidolysis of the Cbz group, followed by the catalytic hydrogenation (Pd/C) to give crude **15**. The next reaction with Fmoc-OSu yielded the desired building block **16** (65%).

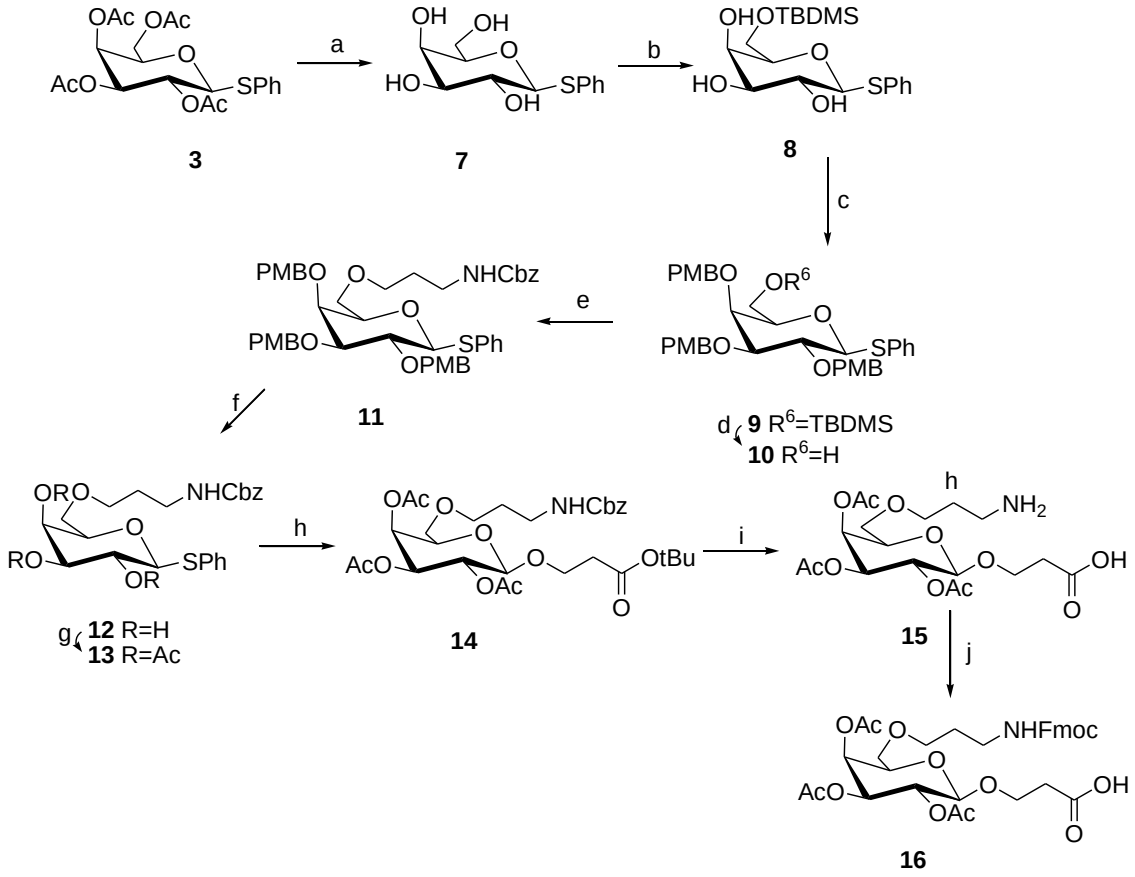

Scheme 5. Synthesis of building block **16** (pathway B)

Reagents and conditions: a) $NaOH_{cat.}$, MeOH ; b) pyridine, Et_3N, TBDMSCl, 0°C-rt; c) NaH, PMBBr, DMF, 0°C-rt; d) 1M TBAF/THF, THF; e) $Br(CH_2)_3NHCbz$, NaH, DMF, 0°C-rt; f) DDQ, H2O/DCM (1:30), rt; g) Ac_2O, pyridine; h) $Br(CH_2)_2COO^tBu$, NBS, TMSOTf, DCM, -50°C; i) 1): DCM/TFA 1:1, 2): H_2/Pd , EtOH; j) FmocOSu, Na_2CO_3, DCM, water.

2.2.2.2 Solid phase synthesis of the ligands 24a and 24b

SPS of ligands **24a** and **24b** was carried out manually by the Fmoc mediated strategy as illustrated in Scheme 6. Arginine pre-loaded Wang resin with a low level of substitution (0.4 mmol/g) was chosen as a solid support in order to prevent an aggregation of growing product[162,163]. First, permeation peptides D-Tat$_{49-57}$ and its inverse isomer D-Tat$_{57-49}$ derived from the truncated basic domain sequence of the entire HIV-1 Tat protein were synthesized. The standard SPPS protocol based on sequential cycles of Fmoc deprotection with 20% piperidine/DMF solution and coupling of amino acid (4 eq) activated with HBTU/HOBt (3.6 eq) was employed. Initially applied conjugation time of 30 min was insufficient to complete the reaction of the amino acid, as analyzed by the Kaiser test[164], and therefore it was further extended to 1 h. Subsequently, the carbohydrate core **16** was conjugated to the free N-amino terminal of the peptides. A longer coupling time (3 h) of **16** (3 eq) activated with HATU (3 eq)/DIPEA (6 eq) in DMF was applied to ensure, that the reaction went to completion. A four times excess of reagents over the resin attached product is usually applied per coupling step in SPPS. Taking into consideration the intricate multistep synthesis of **16**, a method with less amount of this carbohydrate used in a single conjugation step would be valuable. Thus, protocols with only one or two equivalents of carbohydrate **16** were examined by analyzing the sample aliquots by Kaiser test and ESI–MS at definite time points. It was found, that in case of two times excess of **16** the coupling time had to be further extended to 6 h. When an equivalent amount of **16** was used no complete coupling was observed even after 12 h reaction time. Hence, the protocol utilizing 2 eq of derivative **16** per synthesis cycle was optimal for the formation of intermediate **19** as it required less of **16** in combination with an still acceptable increase of reaction time. At this point, the Fmoc-D-Lys(Dde)-OH linker was conjugated to the free amino residue of **19** (at the sugar moiety) followed by selective Fmoc deprotection of **20**. Next step involved a coupling of DOTA tris(tert-butyl) ester **28** to the α-amino group of lysine for 24 h (**21**).

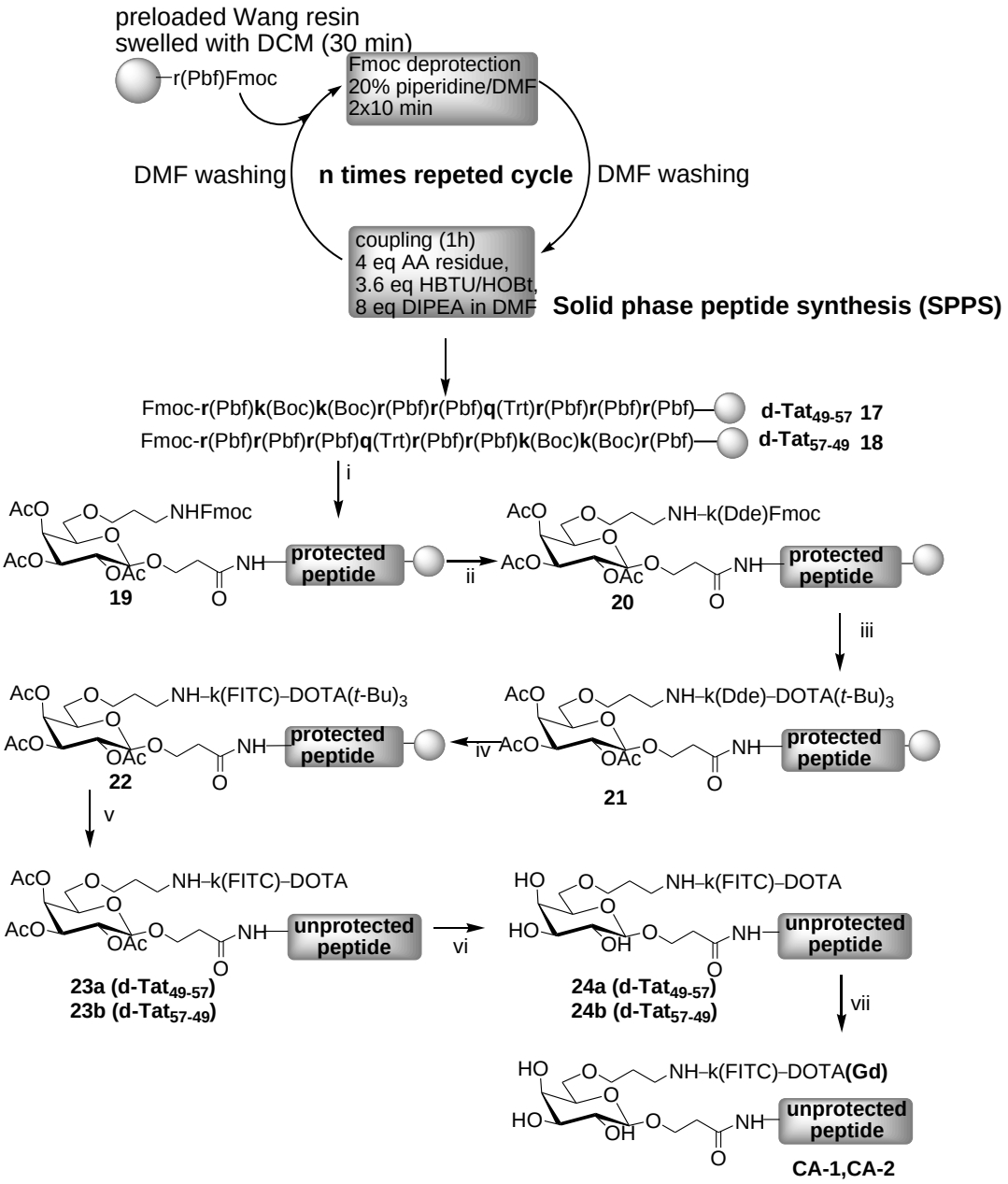

Scheme 6. Synthesis of **CA-1** and **CA-2** conjugates

Reagents and conditions: i) SPPS: single coupling: Amino acid (AA), HBTU/HOBt, DIEA, DMF, 1 h; ii) **16,** HATU, DIPEA, DMF; iii) Fmoc-Lys(Dde)-OH, HATU, DIPEA, DMF; iv) DOTA-(t-Bu)$_3$, HATU, DMF; v) a: 2% hydrazine hydrate, DMF; b: FITC, DIPEA; vi) TFA:m-crezol:TIPS-H_2O (90:5:2.5:2.5) vii) hydrazine hydrate/MeOH; viii) $GdCl_3x6H_2O$, 40ºC/12 h, rt 2 days

The ligand **28** was synthesized as illustrated in the Scheme 7 using a modified procedure to that reported by Mizukami et al.[165]

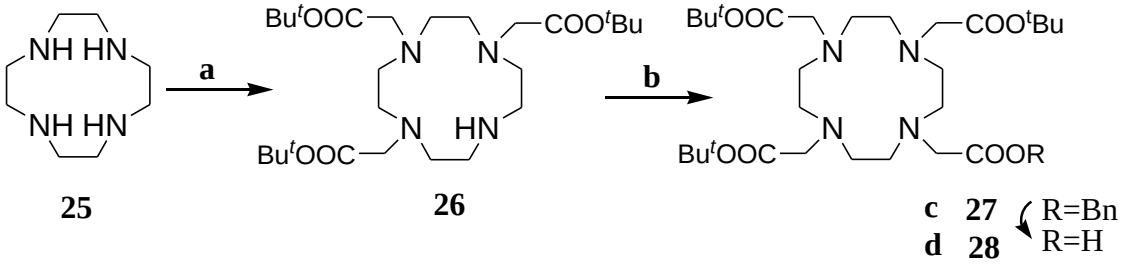

Scheme 7. Reagents and conditions: a) $BrCH_2COO^tBu$, K_2CO_3, CH_3CN; b) $BrCH_2COOCH_2Ph$, K_2CO_3, CH_3CN c) H_2/Pd,

Afterwards, the Dde group was removed from **21** by treatment with 2% hydrazine hydrate in DMF, and FITC was coupled on the designated ε-amino group of lysine for 18 h (**22**). Ultimately, the complete molecules were cleaved off the resin using TFA/TIPS/m-cresol/water (90: 2.5: 5: 2.5), simultaneously deprotecting the acid-labile amino acid side chains as well as tert-butyl esters on the DOTA ligand. This cleavage cocktail containing m-cresol improved the solubility of obtained product as compared to the initially used mixture of TFA/TIPS /water (95: 2.5: 2.5). The released *O*-acetylated products (**23a**, **23b)** were purified by RP-HPLC and characterized by ESI-MS. Mass spectra of these conjugates showed the same molecular ion peaks as consequence of the identical molecular weight and composition (both peptides consists of the same amino acids). Due to this fact only the mass spectra of one conjugate with D-Tat_{49-57} will be presented further on (both conjugates will be fully characterized in the experimental part). The detected molecular ions for **23a** and ligand **23 b** were consistent with the calculated mass of desired products (2659.34).

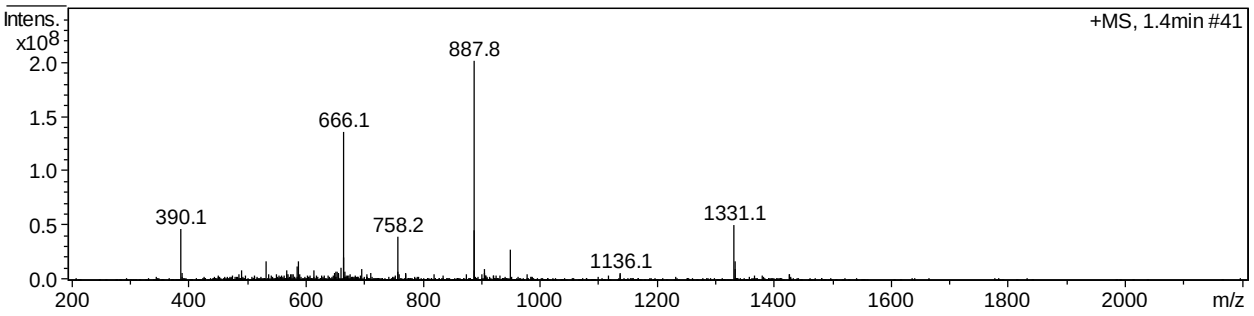

Figure 7. ESI-MS Spectrum of **23a**.

Detected molecular ions m/z = 1331.1 ($(M+2H)^{2+}$), 1136.1($(M\text{-}FITC)+2H)^{2+}$), 887.8 ($(M+3H)^{3+}$), 758.2 ($(M\text{-}FITC)+3H)^{2+}$) 666.1 ($(M+4H)^{4+}$), 390 (FITC) were consistent with the calculated mass of product (2659.34).

The *O*-deacetylation of the obtained conjugates **23a** and **23b** was difficult. Initial attempts to remove the carbohydrate protecting groups by hydrazinolysis, prior to release of molecules from the resin[166,167] resulted in decomposition of the β-glycosidic linkage under the required acidic cleavage conditions. Therefore, deprotection of acetate groups, which are known to stabilize indirectly the ordinarily acid labile bonds, was performed after detachment of conjugates from the solid support. The commonly used deacetylation procedures like Zemplen deprotection[168], saturated methanolic ammonia[169,170], treatment with aqueous sodium hydroxide or diethylmethylamine/water[159] resulted in incomplete deprotection of **23a** and **23b** with one remaining acetyl group most likely at 4-OH of the galactose unit. It was also described by Kunz and co-workers that due to the steric hindrance a removal of acetyl-*O*-4 might prove to be difficult[171,172]. Finally, the use of hydrazine hydrate in methanol (1:6)[173] and 12 h reaction time with careful monitoring of the progress of reaction by analytical HPLC allowed obtaining the desired ligands **24a** and **24b**. The crude products were purified by semi-preparative RP HPLC and characterized by ESI-MS. The substantial decrease in the estimated quantity of the final ligands **24a** and **24b** was observed as result of this acetyl deprotection step (in average only 1/4 of the initially calculated amount was obtained). The detected molecular ions for ligand **24a** and ligand **24b** were consistent with the calculated mass of the desired products (2533.31).

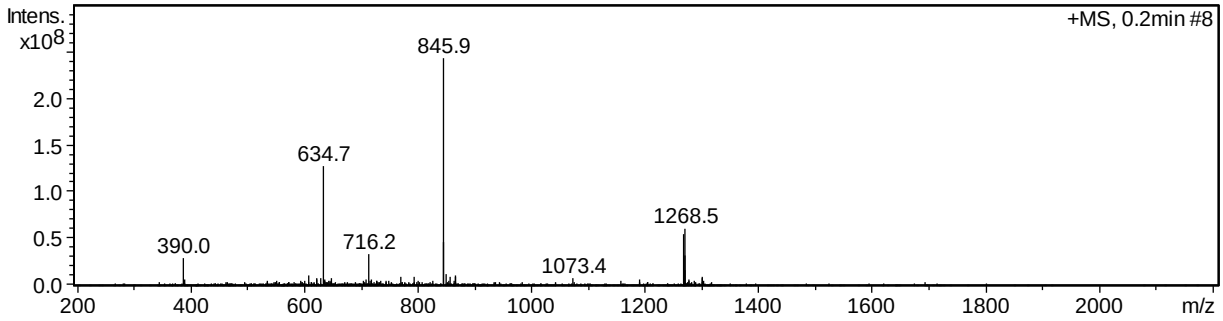

Figure 8. ESI-MS Spectrum of **24a.**

Detected molecular ions m/z = 1268.5 ($(M+2H)^{2+}$), 1073.4 $(M\text{-}FITC)+2H)^{2+}$), 845.9 5 ($(M+3H)^{3+}$), 716.2 $(M\text{-}FITC)+3H)^{3+}$), 634.7 ($(M+4H)^{4+}$), 390 (FITC) were consistent with the calculated mass of the product (2533.31).

2.2.2.3 Preparation of Gd^{3+} complexes of 24a and 24b

The cell-permeable contrast agents **CA-1** and **CA-2** were obtained by adding a titrated solution of $GdCl_3$ (0.9 eq) in ultrapure water to the solutions of **24a** and **24b** (1 eq). The ratio between ligand and metal was essential in order to avoid an excess of free gadolinium and its non-specific binding outside the ligand after loading. Initially, the applied standard chelation protocol[174]with heating at 60 ºC for 12 h resulted in the formation of side-products and only minor amounts of Gd^{3+}-complexes. This was most likely due to the low stability of the sugar based conjugates at higher temperature. Hence, the loading conditions had to be optimized. In an experiment with heating at 40 ºC for 24 h similar, but less impurities were observed (based on the analytical HPLC and ESI-MS analysis). Ultimately, successful complexation with gadolinium was performed using a protocol with heating at 40 ºC for 12 h followed by stirring for 2 days at room temperature in order to ensure complete insertion of the lanthanide ion into the ligand cavity (monitored by analytical HPLC). Despite structural resemblance, ligand **24b** was degrading faster as compared to **24a**, when exposed to the higher temperature. The reasons for that inexplicable lower stability have still to be examined. The absence of free Gd^{3+} ions in solution was verified by performing the xylenol orange indicator test[175]. The crude **CA-1** and **CA-2** were purified before performing biological and MR experiments. At first, RP-HPLC purification was performed to separate small impurities formed during the complexation. After lyophilization, the obtained CAs were dialyzed to remove inorganic salts. In addition, a competitive assay with DTPA confirmed the absence of free Gd^{3+} in the sample. The formation of the complexes was

verified by ESI-MS mass spectrometry in the negative and positive mode. The detected molecular ion peaks were consistent with the calculated mass of **CA-1** and **CA-2** (2688.20 g/mol). The molecular ion peak in mass spectra of **CA-1** at 1343.5 ($(M-2H)^{2-}$) showed the characteristic isotopic pattern for Gd-containing molecules.

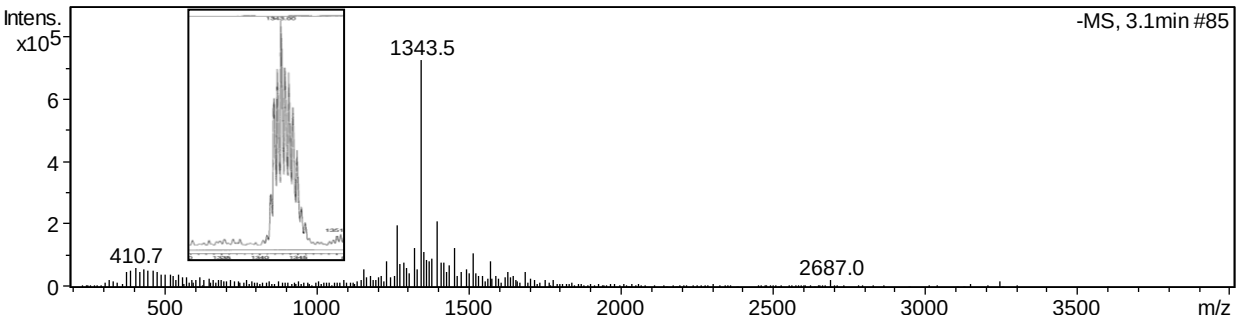

Figure 9. ESI-MS spectra of **CA-1** recorded at negative polarity at the extended range of mass. Detected molecular ion at m/z = 2687 ($(M-1H)^{1-}$), 1343.5 ($(M-2H)^{2-}$) were consistent with the calculated mass of **CA-1** (2688.20 g/mol). The inset shows the expanded region for the molecular ion peak detected at 1343.0 ($(M-2H)^{2-}$) with the characteristic isotopic pattern for Gd-containing molecules (for spectra recorded in the range of 100-2200).

In general, a multistep synthetic strategy as a combination of solution phase (monosaccharide **16** and MR chelate **28**) and solid phase approach (*O*-acetylated ligands **23a** and **23b**) was established leading successfully to the formation of the desired conjugates **CA-1** and **CA-2**. The preparation of the galactopyranose derivative **16**, which fulfills criteria of enzymatic specificity, being at the same time compatible with Fmoc mediated SPS to incorporate MR/FITC and transduction moieties, proved to be challenging. Ultimately, the approach **B** based on a thiogalactoside led to an efficient formation of **16**, in contrast to initially explored strategy **A**. The SPS of *O*-acetylated derivatives **23a** and **23b** was efficiently accomplished, but a subsequent acetyl group deprotection appeared to be difficult. Despite several explored deacetylation protocols, only small quantities of the final ligands **24a** and **24b** could be obtained (about 1/4 of calculated amount). The complexation protocol of these conjugates with $GdCl_3$ required optimization. This was due to observed degradation of **24b** than **24a** under generally used conditions (60°C). In addition, despite structural resemblance, ligand **24b** was degrading faster

as compared to **24a**, when exposed to higher temperature. Nevertheless, even though many chemical problems were encountered during the synthetic course, both conjugates were ultimately obtained and could be explored for their ability to act as specific intracellular CA.

2.2.3 *In vitro* biological studies on the intracellular delivery of CPP conjugated MR CAs

The dual-labeled **CA-1** and **CA-2** containing D-Tat_{49-57} and D-Tat_{57-49} peptides, respectively, were compared for their translocation ability across the cell membrane. Fluorescence spectroscopy and microscopy were used to evaluate cellular uptake and subcellular localization in the transgenic C6/LacZ cell line (containing the target enzyme *β*-galactosidase) and its parent C6 glioma cell line (without target). The preliminary fluorescent studies were performed in order to select the more efficient conjugate for further detailed biological evaluation. These studies showed that both synthesized CAs could efficiently enter into the cells in a concentration dependent manner from 5 to 20 µM after incubating the cells for 18 h with contrast media (Fig 10a and 10b). Only negligible toxicity was observed (data not shown). **CA-1** showed significantly higher tendency for intracellular accumulation in C6/LacZ as compared to parent C6 glioma cells over the whole range of measured concentrations (Fig 10a). In contrary, no significant difference in the cellular uptake of **CA-2** between both cell lines was observed at wide range of labeling concentrations (5, 10, 15 µM) with the exception of 20 µM applied concentration, where a significant distinction in the cellular accumulation between C6/LacZ and C6 glioma cells was detected (Fig 10 b).

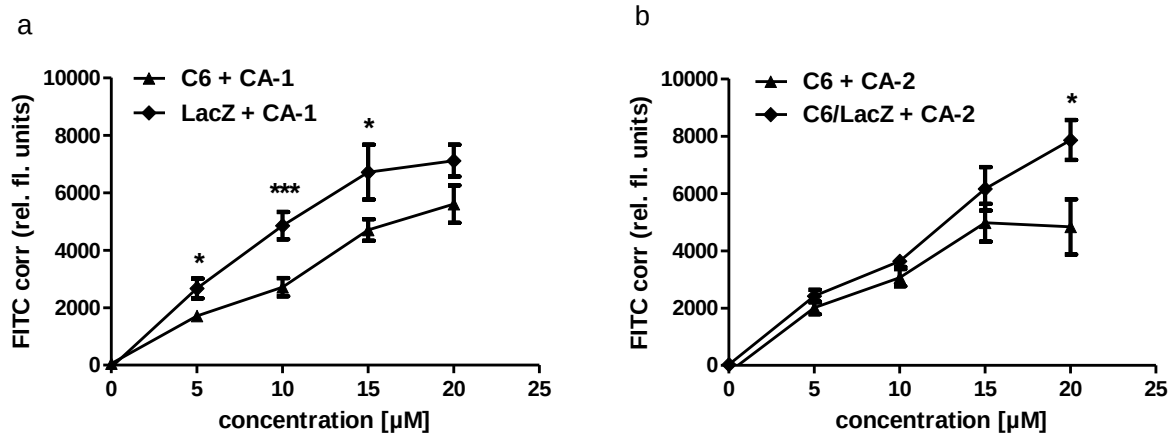

Figure 10. Cell uptake of CAs into C6 and C6/LacZ cells measured by fluorescent spectroscopy. a) Cell internalization of **CA- 1** means are ±SEM (n=2-4 with six replicates).
b) Preliminary cell internalization studies with **CA-2,** means are ±SEM (n=2 with six replicates); Cells were incubated with CAs at various concentrations in complete serum containing medium for 18 h at 37°C. External fluorescence was quenched with trypan blue and successive washings with HBSS. *p<0.05, ***p<0.001, statistically significant different compared to control (Student's *t*- test);

Overall, the conjugate with D-Tat$_{49-57}$ (**CA-1**) as compared to **CA-2** showed substantially higher accumulation levels in the target containing cells over the complete range of tested concentrations. Taking into consideration the preliminary cellular uptake screening studies **CA-1** was selected for detailed biological studies. The statistically significantly higher accumulation of **CA-1** in *β*-galactosidase containing cells was reproducibly detected as illustrated on Fig 10a. Although D-Tat$_{57-49}$ (**18**) was reported to be a more efficient carrier than D-Tat$_{49-57}$ (**17**) for other molecules[176], the second peptide proved to be a better vector for intracellular delivery of our covalently attached cargo as shown on Fig 10a and 10b. The observed difference can be probably explained by the influence of the transported cargo on the transduction efficiency of the evaluated peptides. This conclusion was supported by a recent study reported by El-Andaloussi et al.[177] The authors demonstrated that delivery efficacy and cytotoxicity of CPPs strongly depends on the nature and size of cargo but also its attachment position within the peptide. Moreover, as highlighted by Simon et al.[178], a large differences in cellular uptake of Tat peptides

can be observed amongst various cell types and also for the same cells under different culture and treatment conditions. In view of these findings, one should keep in mind while comparing existing results in the literature with those obtained for **CA-1** and **CA-2**, that different cell lines and serum containing culture medium (closer to *in vivo* conditions) were used to evaluate the efficacy of their cellular uptake and specificity, in contrast to the pre-existing literature reported conditions.

An incubation time of 18 h was selected to facilitate a sufficient level of the intracellular accumulation of the imaging probe, thus achieving a significant MR contrast enhancement. However, the chosen duration for cellular labeling, certainly beneficial for MRI due to its intrinsic insensitivity, might influence cell metabolism and cause cytotoxicity. In order to confront these concerns an additional experiment with a short incubation time point (2 h) and two different concentrations of **CA-1** was performed (Fig 11).

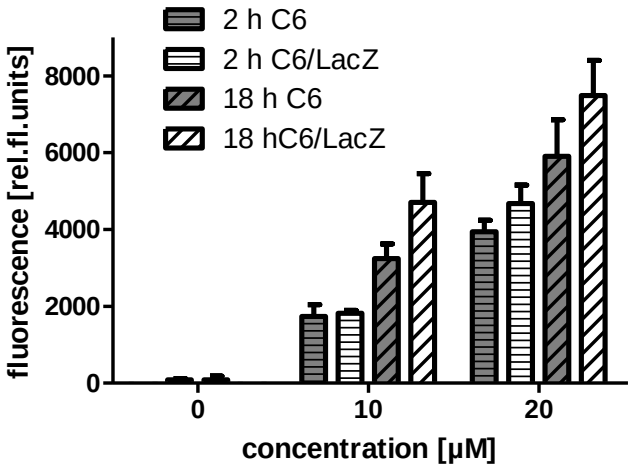

Figure 11. Cell internalization of **CA-1** into C6/LacZ and C6 cells measured by fluorescent spectroscopy.

Cells were incubated with contrast agents at various concentrations in complete medium for 2 and 18 h. External fluorescence was quenched with trypan blue and subsequent washing with HBSS;

The obtained preliminary results were compared with the 18 h incubation time and clearly demonstrated no influence of longer incubation on the observed cytotoxicity. As expected, much higher intracellular accumulation of **CA-1** was observed at the longer incubation time, although

2 h were enough to detect a significant uptake into the cells in relation to control by the means of fluorescent spectroscopy.

Further, the information about the subcellular localization of synthesized conjugates was assessed by fluorescence microscopy. The microscopic images showed a predominantly vesicular localization of **CA-1** and **CA-2** conjugates displayed as bright green punctuate dots in the peri-nuclear area of the cells (Fig 12).

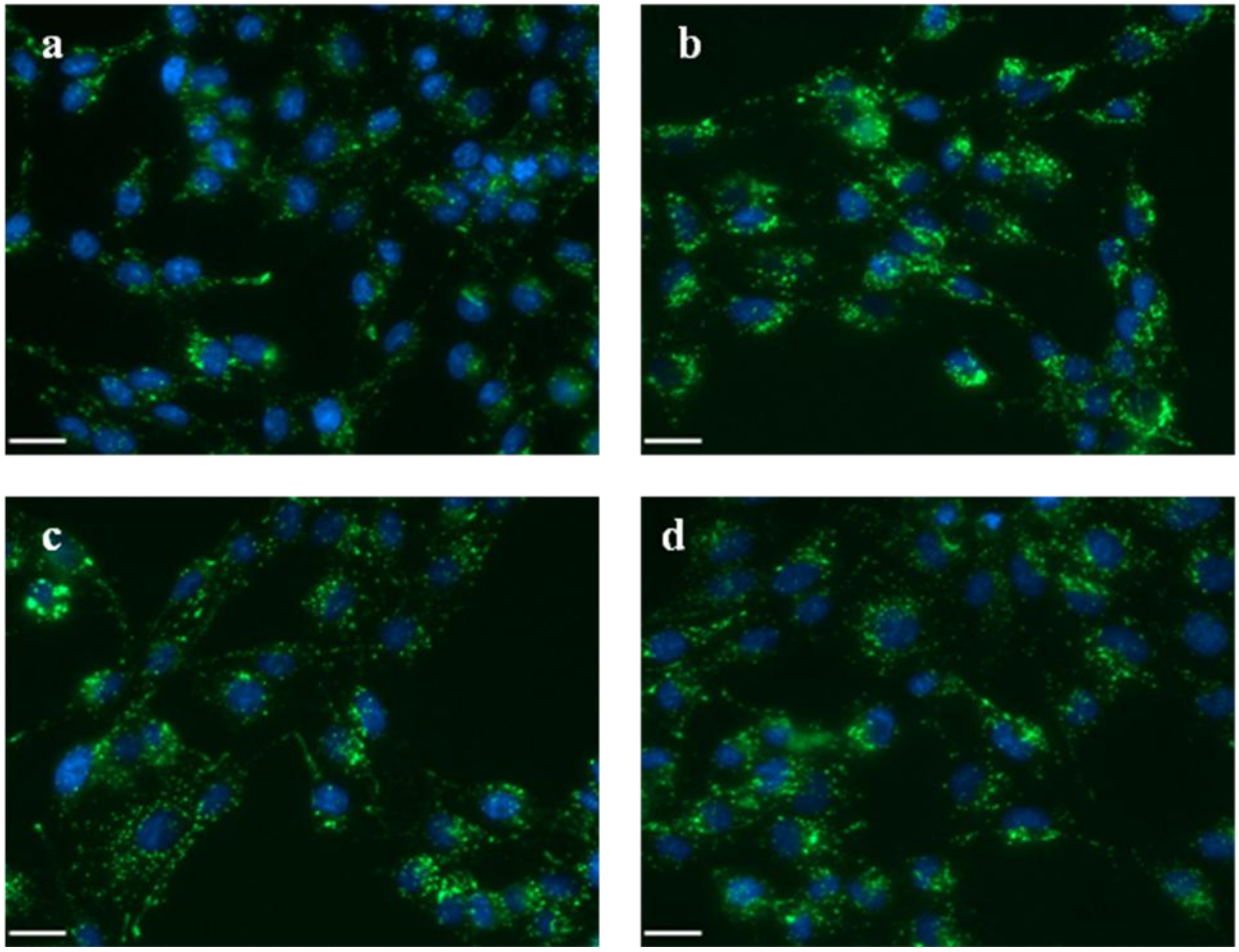

Figure 12. Fluorescence microscopic images displaying the intracellular localization of CA-1 (a, b) and CA-2 (c, d). in C6/LacZ (a, c) or C6 (b, d) cells were incubated with CAs at 20 µM in complete medium for 18 h. Cell nuclei were counterstained with Hoechst 33342 and external fluorescence was quenched with trypan blue, followed by subsequent washing with HBSS. Nuclei: blue (Hoechst 33342), CA: green (FITC fluorescence). The bar represents 20 µm.

This indicated to endocytosis as the main route of cell entry by **CA-1** and **CA-2**. Little or no release into the cytosol was observed. The encapsulation of therapeutic or diagnostic agents in intracellular vesicles represents a bottle neck for several research areas aiming to target at cellular level[179]. Despite that, **CA-1** and **CA-2** could very efficiently label cells as revealed by fluorescence spectroscopy, their vesicular entrapment appears to be the major obstacle for specific interactions with the mainly cytosolic localized *β*-galactosidase. Therefore, further modifications of the conjugates are under progress in order to achieve a release of contrast media from the endosomes or a direct uptake to the cytosolic compartments of the cell.

2.2.4 *In vitro* MR studies of CPP conjugated Gd-DOTA based MR contrast agents

Among various small size Gd-chelates developed until now, gadotetrate (Gd-DOTA) exhibits advantageous high stability thanks to its macrocylic structure and eight strongly binding "attachments points" to the toxic Gd^{3+} metal ion. Consequently, Gd-DOTA functionalized on various ways proved to be a valuable synthon utilized in the preparation of CAs for *in vivo* application. In this section MR examination of the Gd-DOTA based conjugates will be discussed to assess their applicability as intracellular MR probes.

2.2.4.1 Determining concentration and relaxivity of CPP conjugated MR contrast agents CA-1 and CA-2 in aqueous solution

The ability of **CA-1** and **CA-2** to shorten water proton relaxation times T_1, expressed by means of their relaxivity (r_1), was studied at a proton Larmor frequency of 128 MHz (3T) at room temperature. In order to calculate r_1, defined as increment of longitudinal T_1 of water protons induced by a 1mM concentration of CA, the exact concentration of the studied metal chelate has to be known. The determination of accurate content of compound in the sample is an essential matter for molecules like peptides or proteins as they are obtained in the form of TFA salts after HPLC purification with buffers[178,179]. Relative purities of **CA-1** and **CA-2** conjugates were higher than 95% (analytical HPLC), however, an accurate quantity and nature of the counter-ions paired to the positively charged amino acid residues cannot be determined based on the HPLC profiles. Thus, the concentration values calculated by weight had to be corrected for the total mass of salts present in the sample (in average 70% for **CA-1** and **CA-2**). Since each conjugate consist of single FITC molecule and Gd^{3+} chelate, an exact concentration of the probes was

determined by UV-Vis absorption measurements of the fluoresceine at 485nm. The concentration of the stock solutions were calculated according to Lambert-Beer equation assuming $\boldsymbol{\varepsilon}_{\text{fluorescein 485 nm}}$ as 81,000 l/(mol·cm) (evaluated with a standard compound Gd-DO3A-FITC) and further dilutions were made according to this calculated concentration of contrast media. Hence, UV-Vis absorption enabled the evaluation of the mM concentration without knowing the exact character of the counter-anions.

Relaxivity of **CA-1** and **CA-2** was calculated by taking the slope of a plot of the relaxation rates R_1 ($1/T_1$) *versus* various concentrations (mM) of corresponding Gd^{3+} complexes as shown in the Figure 13. **CA-1** and **CA-2** showed relaxivity of 16.8±0.6 and 17.7±0.9 $mM^{-1}s^{-1}$ (means ± SEM, n=4), respectively.

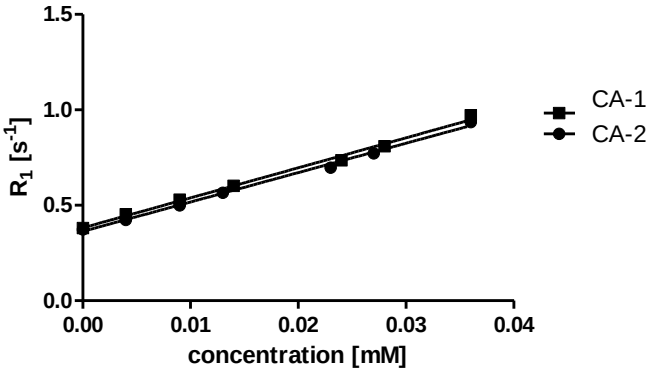

Figure 13. Relaxation rates R_1 *versus* different concentrations of **CA-1** and **CA-2** in aqueous solution. The mean $1/T_1$ of selected exemplary experiment is shown. Relaxivity ($mM^{-1}s^{-1}$) was determined by linear regression.

No statistically significant difference between both complexes was found (Student's *t* test) indicating, that the nature of the peptide had no influence on r_1. The investigated Gd^{3+}-complexes showed a remarkable increase of relaxivity as compared to the commercial Gd-DOTA chelate (Dotarem®) r_1= 4.0±0.12 $mM^{-1}s^{-1}$ (measured under same conditions in our lab). The exact estimation of salts in the peptide and thus the real concentration of CA in the samples was critical to correctly determine the relaxivity as highlighted by Piwnica-Worms and coworkers[180]. Accordingly, if the concentration calculated by weight would be used to evaluate r_1 of **CA-1** (real concentration corresponded only to ~ 30% of weighted amount) the relaxivity would have been

incorrectly calculated as 5.04 mM^{-1} s^{-1}, which is the range of typical values of small sized macrocyclic Gd chelates in the literature[181]. Even though relaxivities of Gd-DOTA-peptides were mostly published[180,182] in the range of 6.8-8.5 mM^{-1} s^{-1}, some conjugates showed a larger r_1 enhancement like demonstrated by Keelara et al.[183] for Gd^{3+} DOTA-based chelators attached covalently to bombesin analogues (r_1=9.3-19.2 $mM^{-1}s^{-1}$). In order to broaden the understanding of the high relaxivity phenomenon of **CA-1** and **CA-2,** a relation between r_1 and the molecular structure of conjugates was further explored in the following chapter.

2.2.4.2 Influence of the structure on relaxivity of dual-labeled targeted MR contrast agents

The relaxivity of Gd^{3+}-based complexes is governed by several influential factors (presented in the section 1.3). Amongst them, an increase in τ_r by slowing the tumbling rate with increasing the molecular weight of paramagnetic species is expected to radically escalate r_1 values (discussed in section 1.4.2). Importantly, rigidity of these bulky constructs has to be taken into account while optimizing τ_r owing to its dependency on not only global but also local rotational dynamics (discussed in section 1.4.2).

Taking into consideration the molecular structures of **CA-1** and **CA-2** the incorporation of lysine spacer with FITC introduced rigidity in close vicinity to the Gd^{3+}-chelate, which might decelerated its internal mobility. In view of that, higher relaxivities of **CA-1** and **CA-2** could be apparently explained by their rotational dynamics due to the slow tumbling of the covalently attached metal ligand, reflecting the increase in molecular weight and its slow internal motion as consequence of created rigidity[184]. In order to understand the effect of internal motion, and rigidity on r_1 values of **CA-1** and **CA-2**, the model conjugate **CA-3 (**Fig 14) with a more flexible linker was synthesized as described in the subsequent chapter **2.2.4.2.1.** In addition, the influence of molecular weight on the relaxivity was assessed by comparison with a middle sized complex **CA-4** (synthesis and detailed characterization in Chapter 4).

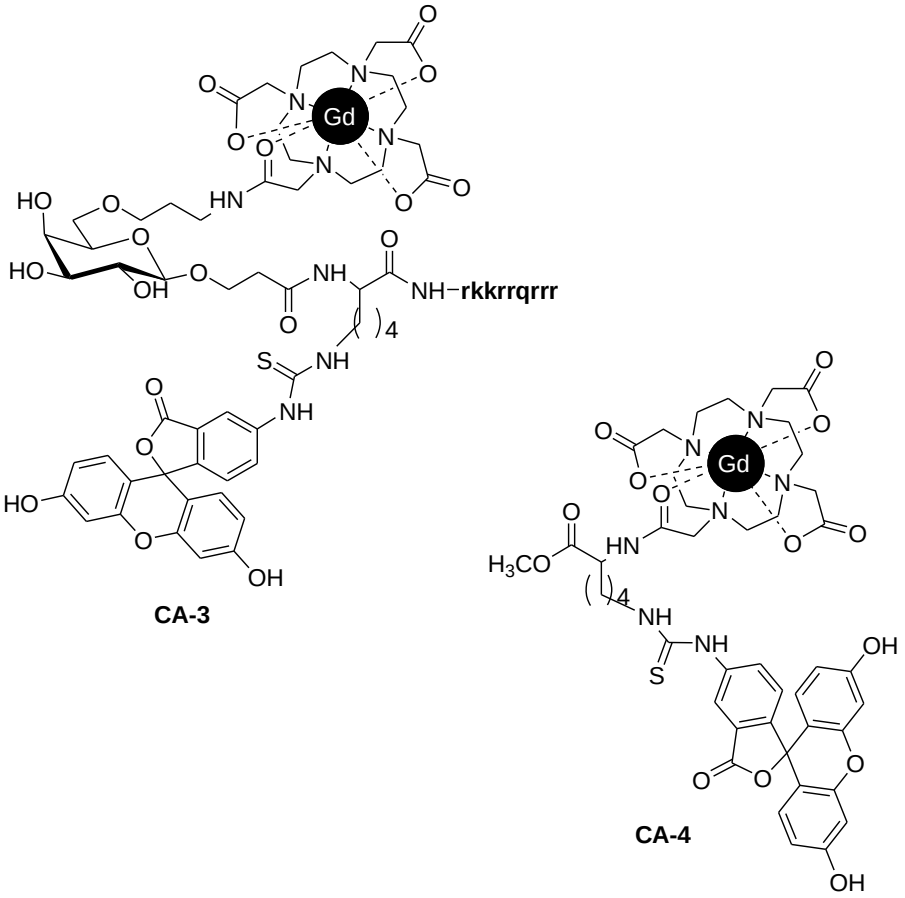

Figure 14. Model conjugates **CA-3** and **CA-4**

2.2.4.2.1 Synthesis of the bimodal intracellular CA-3 with flexible linker

CA-3 was obtained by continuous Fmoc mediated SPS strategy as demonstrated in Scheme 8. First, D-Tat$_{47\text{-}59}$ (**17**) was synthesized on pre-loaded Wang resin as described in section **2.2.1.1**. The Fmoc-Lys(Dde)-OH residue was further introduced as spacer unit bridging FITC and carbohydrate-DOTA building block. Subsequently, the free α-amino terminal of Lys(Dde) was reacted with the sugar moiety **16** (3 eq) activated with HATU (3 eq)/DIPEA (6 eq) in DMF for 3h to result in intermediate **30**. Selective Fmoc deprotection was followed by coupling of DOTA tris(tert-butyl) ester **28** on the α-amino group of sugar moiety for 24 h (**31**). Afterwards, the Dde group was removed by treatment with 2% hydrazine hydrate in DMF, and FITC was coupled to the designated ε-amino group of lysine for 18 h (**32**). Ultimately, complete molecules were cleaved off the resin using TFA/TIPS/m-cresol/water (90:2.5:5:2.5) simultaneously deprotecting the acid-labile amino acid side chains as well as tert-butyl esters on the DOTA ligand. The released O-acetylated product **33** was purified by RP-HPLC and characterized by ESI-MS. The

O-deacetylation of **33** was accomplished with hydrazine hydrate/methanol (1:6) with careful monitoring of the progress of reaction by HPLC and ESI-MS. The crude product **34** was purified by semi-preparative RP HPLC and characterized by ESI-MS. The detected molecular ions were consistent with the calculated mass of **34** (2533g/mol). Subsequently, ligand **34** was chelated with gadolinium using an analogous protocol like for **CA-1** and **CA-2** with heating at 40 ºC for 12 h followed by the stirring at room temperature for 2 days. The crude product, after confirming a complete loading, was purified by semi-preparative RP-HPLC, dialyzed for 48 h and lyophilized. The detected molecular ions in ESI-MS spectra were consistent with the calculated mass of desired product **CA-3** (2688.20g/mol). The MR measurements were acquired as described before and r_1 was calculated as 10.8 $mM^{-1}s^{-1}$.

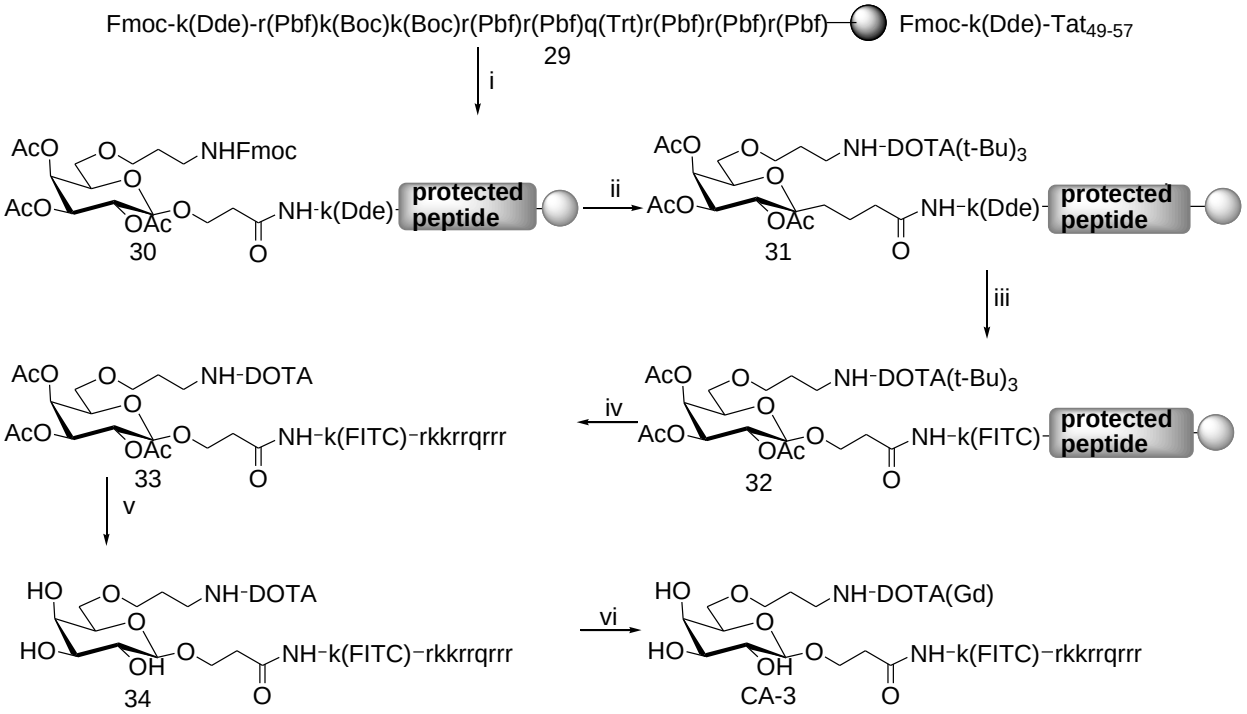

Scheme 8. Synthesis of **CA-3**

Reagents and conditions: i) SPPS: single coupling: Aa, HBTU/HOBt, DIPEA, DMF, 1h; ii) **16,** HATU, DIPEA, DMF; iii) DOTA-$(t\text{-}Bu)_3$, HATU, DMF; v) a: 2% hydrazine hydrate, DMF; b:

FITC, DIEA; vi) TFA:m-crezol:TIPS-H_2O (90:5:2.5:2.5) vii) hydrazine hydrate/MeOH; viii) $GdCl_3x6H_2O$, 40ºC/12h, rt 2 days

2.2.4.2.2 Relaxivity as function of molecular structure and rotational dynamics: comparison of CA-1, CA-2 with CA-3 and CA-4

In an attempt to elucidate the effect of molecular parameters such as internal motions as well as increase in molecular weight on the relaxivity of **CA-1** and **CA-2**, a comparison of r_1 values with those acquired for the model conjugates **CA-3** and **CA-4** was assessed (Fig 15).

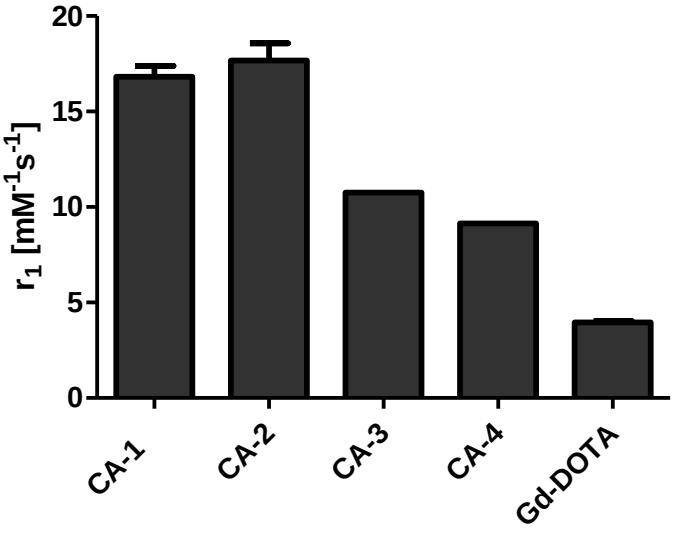

Figure 15. Comparison of r_1 values acquired at 3T for **CA-1, CA-2**, **CA-3, CA-4, Gd-DOTA**.

Taking into consideration the molecular structures of **CA-1** and **CA-2** it was hypothesized that the measured r_1 values were obtained as result of effective increase in global rotational correlation time, being a consequence of the internal rigidity introduced by neighboring effect of FITC to the Gd-chelate and higher molecular weight, as compared to the small fast tumbling Gd-DOTA itself. As pointed out by Caravan[185] a significant increase of relaxivity for slow tumbling constructs can be observed in case of slow or no internal motion of the attached metal chelates. Hence, fast internal motion of the the Gd-based complex would result in overall poor relaxivity despite a sluggish tumbling associated with the large size molecule as discussed in Chapter 1. In **CA-1** and **CA-2**, the Gd-DOTA chelate was covalently attached to the α-amino group of lysine

spacer and FITC was introduced at its ε-amino position. Such an arrangement created sterical rigidity in close vicinity to the metal chelate and restricted its free rotation. This apparently resulted in slower internal motions leading in combination with the slow global tumbling induced by molecular size to the effective increase of observed r_1 values (Fig 15). To investigate the impact of internal motion on the measured relaxivity **CA-3** (Fig 14) was designed to introduce more rotational flexibility into the molecular structure nearby the metal chelate by moving the FITC to the peptide part of the molecule. Accordingly, Gd-DOTA chelate was attached onto the sugar moiety and a lysine spacer with FITC at N^{ε}-position was incorporated between galactose moiety and D-Tat_{49-57} (Scheme 8). The measured relaxivity of **CA-3** (r_1=10.8 $mM^{-1}s^{-1}$) was inferior compared to **CA-1** and **CA-2** (Fig 15) as result of the free rotation of the attached Gd-chelate *via* the flexible linker. Given that all three conjugates had the same molecular weight, it was clearly demonstrated, that the structural rigidity introduced near the Gd-chelate has a large influence on the ability of CAs to increase relaxation rates of water protons in their surroundings.

Furthermore, a possible relationship between molecular weight and relaxivity of **CA-1** and **CA-2** was explored by comparing the obtained r_1 values with that of the dual-labeled contrast agent **CA-4** (Fig 14). In **CA-4**, metal chelate and FITC were linked together *via* a lysine spacer in the same fashion like in **CA-1** and **CA-2** but its molecular weight is considerably lower. The measured relaxivity r_1=9.2 $mM^{-1}s^{-1}$ of **CA-4** was substantially lower as those obtained for **CA-1** and **CA-2** (r_1=16.8 and 17.7 $mM^{-1}s^{-1}$ respectively). This difference could be associated with the increase in molecular size a well known phenomenon reported in the literature (discussed in Chapter 1). On the other hand, relaxivity of **CA-3** (r_1=10.8 $mM^{-1}s^{-1}$) though higher than that of Gd-DOTA itself (4.0 $mM^{-1}s^{-1}$), was only slightly different from r_1 of **CA-4**, but still lower as compared to **CA-1** and **CA-2**.

It seems that both factors, the interaction of the neighboring FITC and Gd-chelate introducing higher rigidity as well as increase in molecular weight had an additive influence on the relaxivity of **CA-1** and **CA-2**. Thus, these results clearly demonstrated, that not only increase in molecular weight, but also surroundings and interactions in close vicinity to the Gd-chelate should be considered while designing bulky contrast agents with amplification of r_1 by slowing down the tumbling rate.

2.2.4.3 In vitro MR studies on transgenic C6/LacZ cells and its parent cell line C6

The ability of **CA-1** and **CA-2** to increase the cellular relaxation rate $R_{1,cell}$ was assessed. Transgenic cells containing *β*-galactosidase (C6/LacZ) as well as the parent C6 glioma cells, not expressing the targeted enzyme, were incubated for 18 h with 20 µM of respective Gd^{3+}-complex. The long incubation time of 18 h was chosen to facilitate a higher intracellular accumulation of CA (discussed in the chapter **2.3.2**). Subsequently, MR imaging of cell pellets was performed at a 3T (128 MHz) human MR scanner at room temperature (details in Experimental section). Cells incubated identically without CAs were used as controls. The obtained MR results clearly demonstrated the ability of **CA-1** and **CA-2** to significantly increase the apparent cellular relaxation rate $R_{1,cell}$ in comparison to control cells without CA as summarized in Fig1. The contrast enhancement in T_1-weighted MR images of controls and cells with CAs was satisfactorily observed as well (Fig 16).

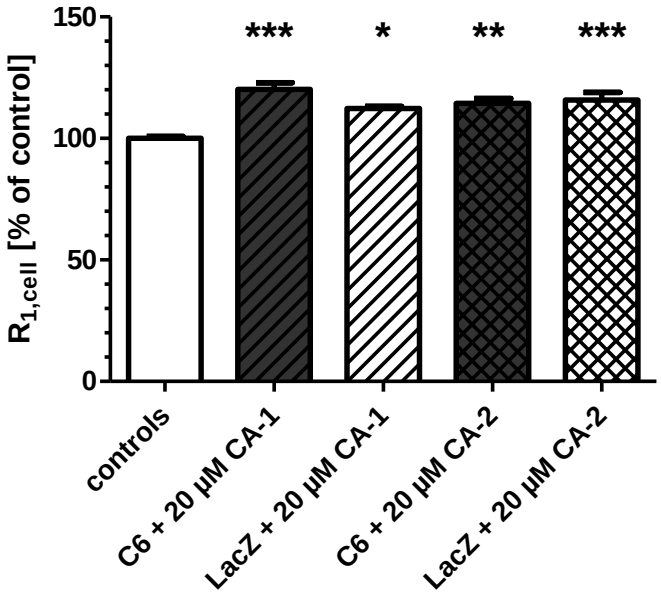

Figure 16. Relaxation rate $R_{1,cell}$ in C6 and C6/LacZ cells after loading with **CA-1** and **CA-2.** Cells incubated for 18 h with 20 µM of CAs. Afterwards the cells were trypsinized, centrifuged and re-suspended in 1.5 mL Eppendorf tubes at 2×10^7 cells/500 µL in complete DMEM for MR studies. Control: cells incubated identically with culture medium without CA. *$p<0.05$, **$p<0.01$, ***$p<0.001$, statistically significant different compared to control (ANOVA, Tukey's post test);

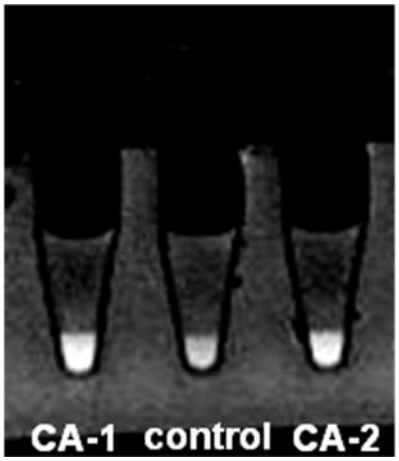

Figure 17. T_1-weighted MR images of LacZ/C6 cells after loading with CA-1 and CA-2 for 18 h. All experiments scanned 256^2 voxels in a field-of-view of 110 mm in both directions resulting in a voxel volume of 0.43 × 0.43 × 1 mm^3. Control: cells incubated identically with culture medium without CAs.

No statistically significant difference in $R_{1,cell}$ values between both complexes as well as cell lines was found (ANOVA, Tukey's post test), although in the fluorescent measurements a significantly higher accumulation of **CA-2** was observed for C6/LacZ compared to C6 cells at 20 µM labeling concentration (Fig 10b). On the other hand a statistically significant higher level of fluorescence was detected in the transgenic cells as compared to C6 cells at various labeling concentrations (5, 10 and 15 µM) of **CA-1** (details see chapter 2.3.2.). The largest difference was observed at 10 µM labeling concentration of **CA-1** (Fig 10a). In order to examine, if this behavior would be also reflected in MR images, both cell lines were incubated with 10 µM of **CA-1** for 18 h and measured at 3T (Fig18). The applied concentration was sufficient to induce an statistically significant increase of $R_{1,cell}$ values for C6/LacZ cells in comparison to the controls, whereas no difference was detected for C6 cells. Though a tendency for a larger increase of $R_{1,cell}$ in enzyme containing C6/LacZ cells as compared to C6 cells was observed at 10 µM, this change was not sufficient to be a statistical significant. Nevertheless, a similar trend in intracellular accumulation of **CA-1** has been detected using optical and MR modalities, with larger difference observed by fluorescence spectroscopy. This variation might be related to the sensitivity gap between both methods, because imaging by means of MRI requires much higher concentration of contrast media[186] and due to large "unspecific" MR signal contribution from vesicular entrapped

probes, it is likely that changes already observed by optical method were beyond the level of MRI detectability. It was reported by Aime et al.[187], that vesicular entrapment of contrast media is responsible for "quenching" of intracellular relaxation rates $R_{1,cell}$. The authors demonstrated a vast increase in measured longitudinal relaxation rates for cell labeled with CA by electroporation (diffused in cytosol) *versus* those labeled with contrast media by pinocytosis (endosomal entrapment). Thus, a structural modification of synthesized CAs is required to achieve their escape from endosomes to allow interactions with enzyme, but also to avoid "quenching effect" of $R_{1,cell}$.

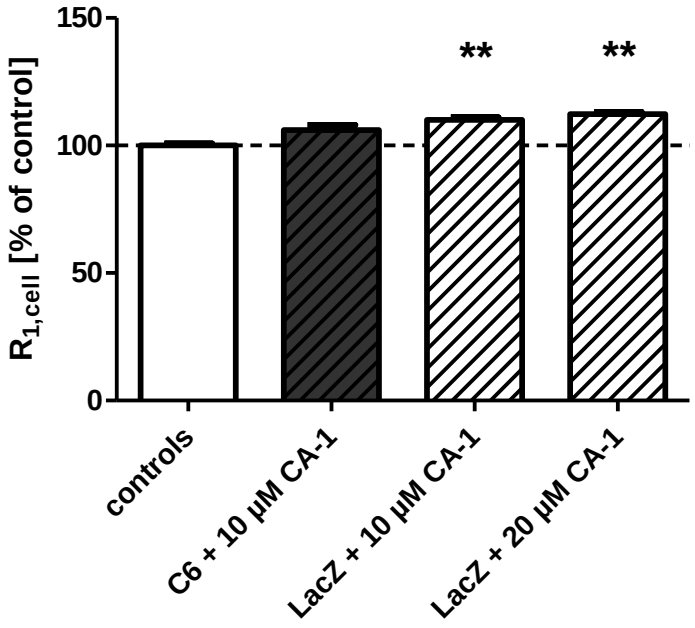

Figure 18. Relaxation rate $R_{1,cell}$ in C6/LacZ and C6 cells after loading with 10 µM of **CA-1** for 18 h.

Cells trypsinized, centrifuged and re-suspended in 1.5 mL Eppendorf tubes at 2×10^7 cells /500 µL in complete DMEM for MR studies. Control: cells incubated identically with culture medium without CA. **p<0.01 statistically significant different compared to control (ANOVA, Tukey's post test);

2.3 Summary & Conclusions

The multistep synthesis was established leading successfully to the formation of the desired bimodal conjugates **CA-1** and **CA-2** based on the galactose derivative targeting β-galactosidase. The synthesis of the galactose spacer 16 based on thiogalactoside proved to be more efficient as compared to that utilizing *O*-glycosyl donor as starting building block (route A). This can be explained by versatility and robustness of thiogalactoside donor allowing a variety of reaction conditions and chemical transformation in its presence. The O-deacetylation of conjugates **23a**, **23b** and **33** was difficult leading to significant reduction of expected product quantity. Probably steric hindrance around sugar moiety created by different functional domains of bulky conjugate was disturbing an efficient removal of all acetyl groups.

CA-1 and **CA-2** showed high relaxivities (16.8 and 17.7 $mM^{-1}s^{-1}$ respectively) as compared to the small, fast tumbling Gd-DOTA (4.0 $mM^{-1}s^{-1}$). This phenomenon can be explained by increase in molecular weight in combination with neighboring effect of FITC incorporated in close vicinity to Gd-chelate that created a more rigid system with restricted local motions leading to higher relaxivity. The attachment position of FITC had an important effect on acquired relaxivity since conjugate **CA-3** with flexible linker allowing fast local motions of Gd^{3+}-chelate showed lower r_1 (10.8 $mM^{-1}s^{-1}$) as compared to **CA-1** and **CA-2** even though all three molecules had the same molecular weight. Thus, it was concluded, that high relaxivity can be acquired by increase in molecular weight but this can be further significantly amplified by creating rigidity near the Gd^{3+}-chelate e.g. as in the described molecules by the positioning of the FITC. Although **CA-1** and **CA-2** were both very efficiently internalized into the cells as revealed by fluorescence spectroscopy, a conjugate with D-Tat_{49-57} (**CA-1**) showed substantially higher accumulation level in *β*-galactosidase expressing cells as compared to C6 cells (without enzyme) over the complete range of tested concentrations (5-20 µM). Whereas no significant difference between both cell lines was observed for **CA-2** except for the highest labeling concentration. The studies at shorter (2 h) and longer incubation time (18 h) showed that there was no influence of incubation time on the observed cell toxicity, however, much higher levels of intracellular accumulation were observed after 18 h incubation. Thus, longer incubation time proved to be better as yielding a higher quantity of MR/FR reporters inside the cell without affecting their viability. The MR studies of cells incubated with **CA-1** and **CA-2** showed that both conjugates could efficiently enhance cellular relaxation rate $R_{1,cell}$ of water. Nevertheless, at high concentration (20 µM) no

difference was observed between both cell lines. Similarly like in case of fluorescence studies **CA-1** showed a slight tendency for higher MR signal enhancement in enzyme containing cells indicating to an enzyme induced specific accumulation. However, no substantial increase in cellular retention of the MR probe in target expressing cells due to the selective cleavage of cell permeable peptide from **CA-1** and **CA-2** was detected, despite a very efficient intracellular uptake of conjugates. This can be most likely explained by the predominantly endosomal localization of CAs inside the cells as revealed by fluorescent microscopy. The vesicular entrapment of targeted CAs prevents their specific interactions with the β-galactosidase present in the cytosol. There seems to be an observable tendency for specific accumulation of **CA-1**, but owing to the mainly unspecific vesicular accumulation of probe, these changes were probably beyond the levels detectable by MRI. In addition, the vesicular entrapment will reduce a fast efflux of uncleaved probe from non-targeted cells, what would contribute significantly to a high unspecific "background label" masking potential specific accumulation. Hence, the endosomal escape of CAs or a direct uptake into the cytosol is critical if binding and/or reaction between molecular probes and cytosolic targets should lead to a significant increase in MR signal. Thus, further modifications involving the attachment of MR(Gd)/FITC-sugar building blocks to peptides showing endosomolytic activity are required to permit the proper interaction of the targeted β-galactosidase with such dual-labeled probes.

Chapter 3

Enzymatic activity of *β*-galactosidase as function of substrate structure

3.1 Introduction

The *β*-galactosidase from *Eschericha coli* catalyzes the breakdown of the *β*-glycosidic bond at the anomeric center of the galactosyl moiety while retaining the same stereochemistry of the substrate in the product[188,189]. The enzyme is a homotetramer (MW 464 kDa) and comprises of four identical units. Each is built up by a polypeptide chain with 1023 amino acids folded into five sequential domains with an extended fragment at the amino terminus[190,191]. *β*-galactosidase has four active sites[192] and Na^+ and Mg^{2+} cations are needed for maximal catalytic activity of the enzyme[193,194]. *β*-galactosidase exhibits fairly strict specificity towards the sugar residue[195,196], but shows wide permissiveness for various aglycons (functionality attached at the C-1 position) including alkyl, aryl or another sugar residue[197]. A change in conformation at the C-1 position to the α-anomer induced complete loss of enzymatic activity[198]. Studies with a series of methyl *β*-lactoside derivatives reported by Bock and Adelhorst[199] showed that alternation of hydroxyl groups at the positions 2, 3 and 4 of the galactose resulted in an inhibition of enzymatic activity for these substrates. Thus, only the changes at the C-6 position are compatible with enzymatic hydrolysis, but also dependent on the type of the introduced modifications[200,201]. Accordingly, substrates with a $-CH_2$-OH group replaced by substituents like hydrogen[202], methyl[203] or methylene[204] were hydrolyzed at a slower rate. This indicates that although the hydroxyl at C-6 is important for the binding to the enzyme its absence does not cause a total loss of enzymatic activity[195]. On the other hand substrate, in which 6-OH was substituted by tosyl[204] was not hydrolyzed. Hence, an alternation of the C-6 position could maintain *β*-galactosidase activity if cautiously done. Taking into account these enzyme specificity requirements, MR/FR reporters in **CA-1** were introduced at the C-6 position of galactose moiety via an alkyl linker to avoid steric hindrance, which would be created in case of direct attachment of these units to position C-6.

To date numerous studies about enzymatic specificity and catalytic mechanism of *β*-galactosidase were mainly performed for low molecular weight compounds such as p-nitrophenyl-β-galactopyranoside (PNPG), o-nitrophenyl-β-galactopyranoside (ONPG) and other derivatives[205,206,207]. In contrast, the molecular structure of **CA-1** is complex and as discussed above many factors like substitution at the C-6 position, introduced moiety (FITC, MR reporter), attachment of a peptide as aglycon and molecular size can notably influence its interactions with the *β*-galactosidase. Therefore, in order to understand the relationship between molecular structure and enzymatic reactivity for **CA-1**, the effect of modifications at the galactose and the

aglycon part was explored individually. Model conjugates **CA-5** and **CA-6** being C-6 modified analogs of PNPG were synthesized and used to evaluate the influence of this type of alteration on *β*-galactosidase activity. To further investigate the influence of peptide or peptide/FITC attachment at the anomeric center on the catalytic activity the model galactose-peptide conjugates **54**, **56** and **61** were synthesized and evaluated. Like **CA-1** these conjugates do not contain a chromogenic moiety, which will be released upon enzymatic reaction and could be measured by optical techniques. Thus, other assays allowing the detection of enzymatic hydrolysis had to be established for such conjugates. In this chapter, the synthesis and biological studies of these model molecules as well as evaluation of interactions involving **CA-1** and *β*-galactosidase will be presented.

3.2 Influence of modifications at the C-6 position of the galactose moiety

3.2.1 Synthesis of CA-5 and CA-6

The synthesis of **CA-5** and **CA-6** presented in Scheme 9 started from acetobromogalactose **1**, which was obtained as described in chapter 2. Subsequent coupling with *p*-nitrophenol in the presence of benzyltrimethylammonium bromide gave **35** in a 65% yield, followed by a quantitative Zemplen deprotection of acetyl groups (**36**). In order to obtain the monosaccharide **39**, a trityl (Tr) group was introduced as temporal protection of the primary 6-OH in *p*-nitrophenyl-β-D-galactopyranose (PNPG). Initially, the protection of 6-OH was attempted by reaction of **36** with triphenylmethyl chloride in DMF in the presence of DMAP by adopting procedure described by Chaudhary et al. [208], but not complete conversion of **36** was observed. A further tritylation of **36** in pyridine, followed by *in situ* benzoylation using procedure described by Ekborg et al.[209] was more efficient yielding **38** in 85% after 2 steps[209]. Although the authors reported the efficient detritylation of crude **38** within 30 min on a steam bath using 90% CH_3COOH/H_2O, similar results could not be achieved with this method. A longer deprotection time (up to 4h) and more solvent as compared to reported volume were required instead to completely deprotect the trityl derivative **38**. Thus, the original procedure was modified accordingly and finally **39** was obtained in 65% yield. This derivative has been further used as a building block for the synthesis of **CA-5** and **CA-6** containing alkyl spacer of variable length connecting MR chelate and sugar unit.

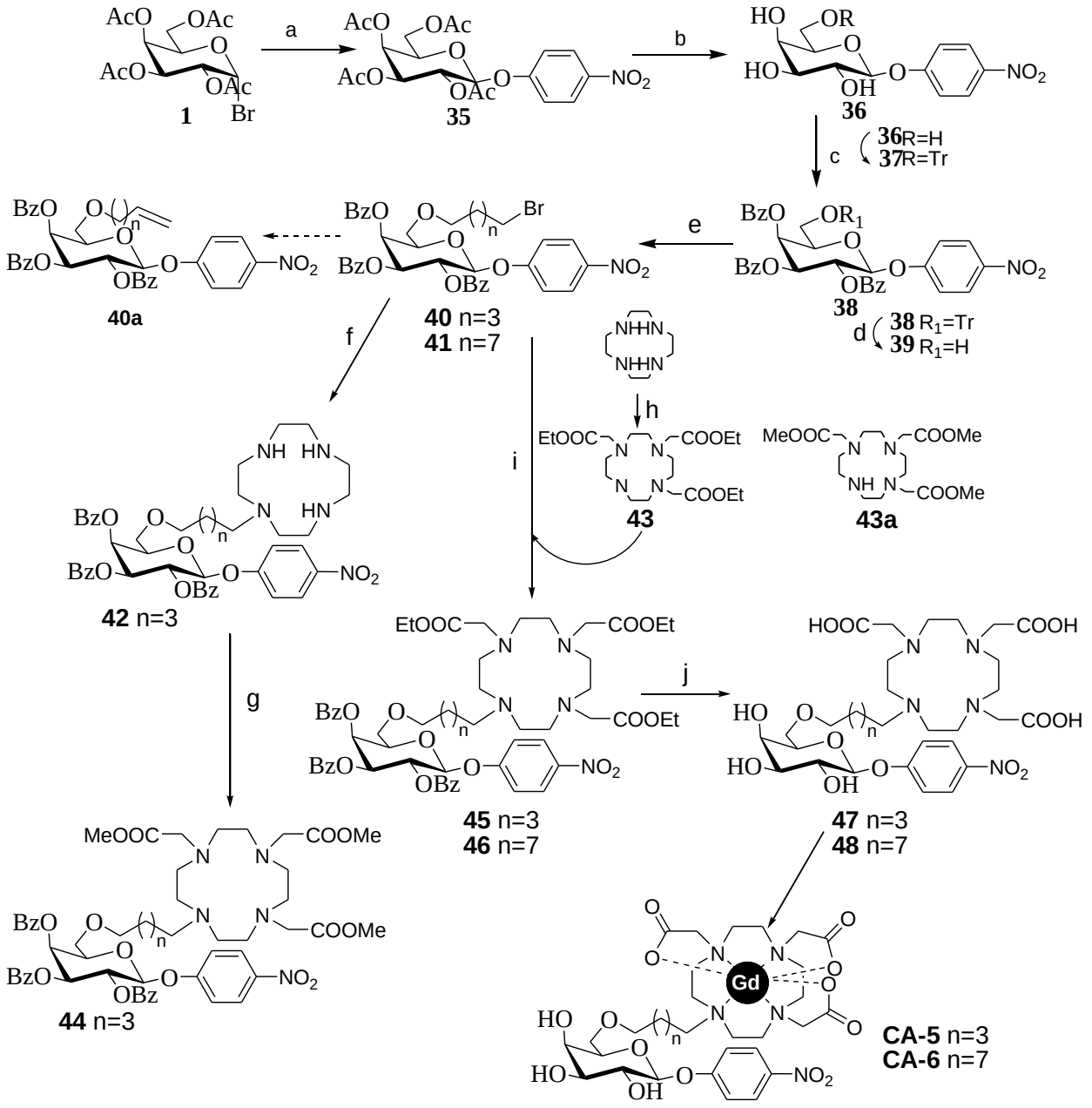

Scheme 9. a) Benzyltrimethylammonium bromide, K_2CO_3, $CHCl_3$, 48 h; b) 1) Ph_3Cl, DMAP, DMF, 24 h; 2) Ph_3Cl, pyridine, 3 days; c) BzCl, pyridine 24 h; d) 90 % H_2O/CH_3COOH, 60°C, 4-5 h; e) 1,5-dibromopentan or 1,9-dibromononane, NaH, DMF, conditions see Table 1; f) cyclen, $CHCl_3$, rt-60°C, g) $BrCH_2COOMe$ or $BrCH_2COOEt$, K_2CO_3, DMF, 55°C; h) cyclen, $BrCH_2COOEt$, $CHCl_3$, Na_2CO_3; i) K_2CO_3, DMF, 55°C; j) 1)NaOMe, pH=10-11 2) 1M NaOH aq k) $GdCl_3xH_2O$, 3 days, rt.

A compromise had to be found, in exploring reaction conditions and protecting groups, which will facilitate an ether formation, but at the same time can be removed without affecting the *β*-glycosidic bond and *p*-nitrophenyl group (PNP). The favored benzyls or *O,O*-acetyls as protecting groups of 3,4-hydroxyls of galactose assisting the formation of ether bond at C-6 position under basic condition (i.e. NaH) could not be used, as their removal will affect *β*-glycosidic bond or PNP. Therefore, benzoyl groups were selected since they should be sufficiently stable to enable the alkylation at C-6 position of PNPG under carefully applied basic conditions. Subsequently, pentyl and nonyl linkers were introduced *via* an ether bond formed at the primary hydroxyl group of the monosaccharide **39**. Up to now, only few reports on the formation of tether alkylethers at the C-6 position of a galactose moiety can be found in the literature[157,158]. Commonly used approaches involve the reaction of an *in situ* generated alkoxide with a sterically unhindered substrate possessing a good leaving group (e.g. halides or sulfonate esters). The synthesis of **40** and **41** proved to be difficult and both derivatives were obtained only at modest yields of 35% and 14%, respectively. The problems associated with the synthesis of **40** and **41** will be described below. A wide spectrum of reaction conditions, summarized in Table 1 was tested in order to facilitate the formation of **40**. In general, 1,5-dibromopentan was reacted with **39** in the presence of NaH using different reagent ratios, temperatures and reaction times.

Entry	NaH (eq)	Br-CH_5-Br (eq)	Solvent	Temp [°C]	Time [h]	Product [%]
1	1.2	5	DMF	0-rt	3	-
2	2	5	DMF	0-rt	6	-
3	2	5	THF	0-50	6	-
4	10	21	DMF	-15-rt	0.5	-
5	2	21	DMF	0-rt	0.5	-
6	1.7	1.7/$TBAI_{cat}$	DMF	0-rt	24	traces
7	2	10	DMF	-10-rt	0.5	traces
8	3	21	DMF	-15-rt	0.5	14
9	3	21	DMF	-30-rt	25 min	35

Table 1. Optimization of reaction conditions carried out for the formation of **40**.

Initially only one or two equivalents of base were applied (Entry 1 and 2), but the product **7** could not be obtained as monitored by LC-MS and TLC. When the solvent was changed to THF and temperature was increased (Entry 3), the color of reaction mixture turned to dark brown similarly like in case of long reaction time indicating to a degradation of the starting material. Mariner et al. [210] reported on an efficient formation of an ether bond at the 2-OH position of a thiogalactoside derivative in a reaction using a large excess of 1,4-dibromobutane and NaH. This procedure was adopted for the synthesis of **40**. However, a very rapid decomposition of starting material **6** occurred under these conditions. It was assumed, that at lower temperature **6** should be more stable in the presence of a strong base. Subsequently, sodium alkoxide of **40** was generated at -15ºC and reacted with 1,5-dibromopentan at room temperature (Entry 4). This attempt gave insufficient result similarly like for the next reaction carried out with a little excess of NaH (Entry 5), where **40** was also not formed. Further on, as presented in Entry 6, TBAI was added as catalyst, which is known to increase the solubility of alkoxides. Nevertheless, only traces of **40** were observed with a large amount of remaining starting material **39**. Considering, that a better stability of **39** was observed at low temperature, its conversion towards **40** was approached by generating an alkoxide with 2 eq of base at -10°C and followed by adding the alkylating agent with a subsequent increase in temperature (Entry 7). With this approach only traces of **40** were isolated, but **6** was still present. Therefore, the excess of NaH was slightly elevated and the temperature was further decreased. Thus, the synthesis of **40** was ultimately accomplished by activating **6** with NaH (3 eq) at -15 and -30ºC leading to 14% and 35% of isolated product, respectively. The potential product of bromine elimination **7a** (assumed due to the corresponding ion mass peak in ESI-MS) was observed increasing in amount at extended reaction time (1 h). In summary, the formation of an ether bond at the primary hydroxyl group of **6** appeared to be difficult. This problem had already been explored in Ziegler's group, where a number of methods were examined towards O-alkylation at the C-6 position of monosaccharides with despondent results[211]. The low yield of **40** can be attributed to many factors. An excess of NaH was required to facilitate the formation of an ether bond, but at the same time caused competitive elimination of bromine from **40**. In addition, although heating and long reaction times should help in the conversion of **39** towards **40**, both factors induced decomposition of **39** under the applied conditions. The optimized procedure established for the synthesis of **40** was further used to obtain **41** (longer linker) with a yield of 14%.

The following incorporation of the MR chelate in **40** or **41** could be approached *via* the primary formation of mono-substituted cyclen and afterwards introduction of protected carboxymethyls into the macrocycle (Scheme 9, f and g) or alternatively, a pre-synthesized tri-substituted DO3A derivative could be coupled (Scheme 9, i). The latter strategy was initially selected for the synthesis of **44**. Selective and high yield alkylation of cyclen is a vital prerequisite to obtain its pure derivatives in order to avoid the difficult separation of the side-products, mainly tetra-substituted cyclen in case of DO3A. The methyl ester was initially selected as protection for the carboxylate groups of DO3A since the ester can be easily cleaved under mild base-catalyzed conditions. However, an attempt to alkylate the cyclen with methyl bromoacetate to obtain DO3A (tris-methyl ester) **43a** resulted in the mixture of **43a** and tetra-substituted cyclen, which could not be separated by a column chromatography (traces of the side product seen in ^{1}H-NMR and ESI-MS spectra). This was probably due to the low steric hindrance introduced by methyl esters and a fast alkylation rate leading to a poor selectivity as compared to the formation of DO3A(tris-tert-butyl ester) using tert-butyl bromoacetate. As consequence, the synthetic strategy was changed. **40** (1eq) was reacted with an excess of cyclen (8 eq) in chloroform for 8 h at room temperature (to avoid formation of disubstituted by-product), followed by heating to 60ºC in order to increase its conversion to **42**. Next**,** the excess of cyclen was removed by extraction with water/DCM and the crude intermediate **42** was further alkylated with methyl bromoacetate in the presence of sodium carbonate yielding **44** in 40% in two steps. Thus, it was concluded, that even the preliminary chosen methyl groups are optimal due to their easy deprotection, the synthesis of methyl protected MR chelate appeared to be difficult. In an attempt to the further increase the reaction yield, ethyl esters were introduced since a synthesis of DO3A (tris-ethyl ester) **43** was already described in the literature[212]. Thus, **43** was obtained in 60% by reacting of cyclen with ethyl bromoacetate in the presence of sodium bicarbonate in chloroform at -10°C with slow increase to room temperature to facilitate the formation of tree-substituted DO3A. Afterwards, **43** was reacted with **40** to give **45** in 85% yield. Thus, a significant increase in the overall yield was observed in comparison to the methyl ester protected derivative **43a**. Since this procedure proved to be optimal, **46** was synthesized in the same way. Accordingly, **41** was reacted with **43** in the presence of potassium carbonate with heating for 24 h at 55ºC giving **46** in 70% yield. Subsequently, the benzyol groups were removed by stirring of **45** or **46** with sodium methoxide in methanol at pH 10-11. Next, the ethyl esters were deprotected by dissolving the crude

intermediate in ultrapure water and slowly adding 1N NaOH (pH ~10-11). The progress of the reaction was monitored by ESI-MS and after the ethyl esters deprotection was completed, pH adjusted to 7, the samples were concentrated and purified by RP-HPLC using MeOH/water and lyophilized to yield 55% and 40% of **47** and **48**, respectively.

The complexation with $GdCl_3$ (ligand: metal ratio 1:0.9) was carried out in ultrapure water with stirring at room temperature for 3 days. The pH of the solution had to be maintained in the range of 6.5-7 since at lower pH precipitation of **47** and **48** was observed. Crude **CA-5** and **CA-6** were purified by RP-HPLC using acetonitrile/water as mobile phase and characterized by ESI-MS. The molecular ion peaks measured in the positive mode with the characteristic isotopic pattern of gadolinium containing compounds were consistent with the molecular weight of **CA-5** and **CA-6**. The obtained conjugates were further evaluated for their relaxometric properties and as substrates for *β*-galactosidase.

3.2.2 In vitro relaxometry studies of CA-5 and CA-6

Relaxivity studies of **CA-5** and **CA-6** were performed at 128 MHz (3T) and room temperature. The longitudinal relaxation times T_1 were measured for six different concentrations of contrast media in the range of 5-40 µM. The relaxivity was found to be 9.01 $mM^{-1}s^{-1}$ for **CA-5** and unexpectedly only 1.68 $mM^{-1}s^{-1}$ for **CA-6**. This result could be explained by the precipitation of **CA-6** observed in the samples after the measurements leading to an error in acquired r_1 values. Thus, it was not possible to measure r_1 of **CA-6** correctly. The lower solubility of **CA-6** in water associated with long hydrophobic nonyl linker was probably responsible for observed precipitation.

3.2.3 Evaluation of enzymatic activity of *β*-galactosidase on CA-5 and CA-6

In order to investigate the influence of the modification at the C-6 position of the PNPG substrate, its analogs **CA-5** and **CA-6** were examined as substrates for *β*-galactosidase. Enzymatic activity on **CA-5** and **CA-6** was measured by monitoring the formation of the released *p*-nitrophenoxide anion at 405 nm at 37ºC with unmodified PNPG as reference. The obtained results (Fig 19) demonstrated that a substitution of the hydroxyl group at C-6 position of the galactose moiety caused a decrease of catalytic rate for **CA-5** and **CA-6** as compared to PNPG.

Nevertheless, such modifications still allowed enzymatic hydrolysis of **CA-5** and **CA-6** although at a slower rate as compared to PNPG. The relative enzymatic activity for **CA-5** and **CA-6** were determined to be 20±2% and 10±2% (means ±SEM, n=4) of *β*-galactosidase activity on PNPG (Fig 1b). The more rigid **CA-5** derivative with a pentyl linker proved to be a better substrate for the enzyme as compared to **CA-6**. Thus, not only substitution but also the length of the linker incorporated between the MR chelate and the C-6 hydroxyl group had an influence on the enzymatic activity. Incorporation of the Gd-DO3A complex *via* an alkyl linker still allowed binding of these substrates to the active site of *β*-galactosidase.

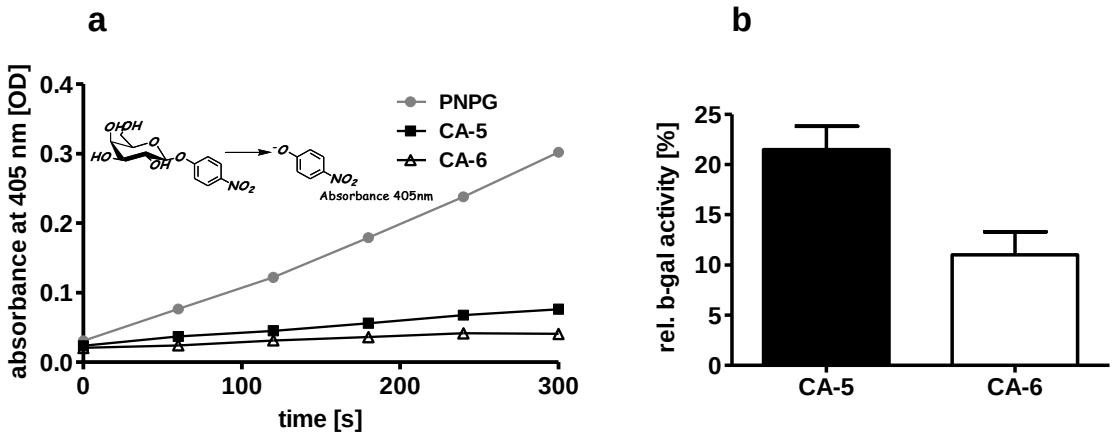

Figure 19. *β*-galactosidase activity on **CA-5, CA-6** and PNPG**.**

a) Exemplary kinetic curves of PNPG, **CA-5** and **CA-6** b) Relative activity of *β*-galactosidase on **CA-5** and **CA-6** calculated by setting enzyme activity for PNPG to 100%. Values are means ±SEM. β-galactosidase activity was measured in 96well plates in phosphate buffer containing $MgCl_2$, mercaptoethanol, and 553 μM of **CA-5**, **CA-6** or PNPG as reference, at pH = 7.3 and

37°C. The release of the yellow p-nitrophenolate was detected in a multiplate reader at 405 nm in kinetic mode for 15 min.

3.3 Influence of the aglycon moiety on enzymatic activity

The broad tolerance of *β*-galactosidase regarding the aglycon moiety allows the attachment of various types of residues such as alkyl, aryl or another sugar (see introduction) into the galactose moiety at its anomeric center. However, the nature of the appended molecule has a strong influence on the catalytic rate of enzymatic reaction and enzyme-substrate binding affinity. Until now, the majority of the examined substrates for *β*-galactosidase were low molecular weight molecules[213,214]. As pointed out by Skold et al.[215] many factors such as molecular weight and positive charge of substrate as well as ionic strength of the solution can significantly affect kinetics of the enzymatic hydrolysis for macromolecular substrates. In case of **CA-1** and **CA-2** positively charged Tat peptides were attached at the anomeric center of the galactose moiety to be cleaved off leading to cellular retention of the MR/FR reporters. In order to investigate the effect of the peptide on the enzymatic activity, the model conjugate **54** was synthesized with Tat attached *via* the same spacer like in **CA-1** but keeping the C6 position of the sugar unsubstituted. To evaluate the influence of the type of spacer between glycon and peptide as well as of the incorporation of FITC into peptide on the hydrolysis rate conjugates **54, 56** and **61** were synthesized and further examined as substrates for *β*-galactosidase.

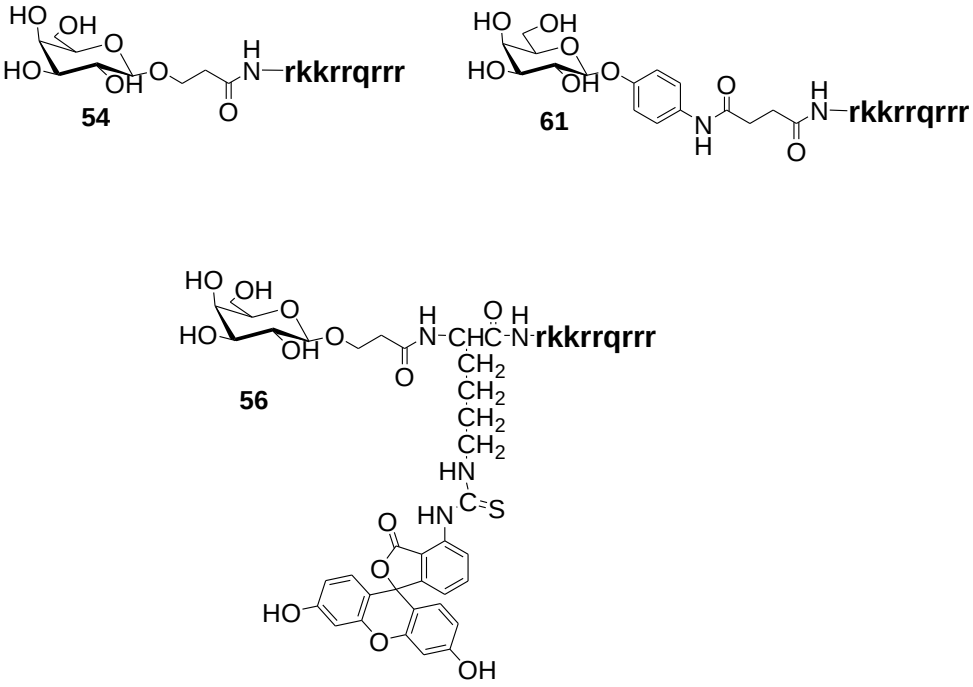

Figure 20 . Galactose-linker-Tat$_{49-57}$ conjugates.

3.3.1 Synthesis of 54 and 56

The galactose conjugates **54** and **56** were obtained by utilizing Fmoc mediated SPS strategy as shown in Scheme 10. First, side-chain protected D-Tat$_{47-59}$ (**17**) and lysine linker containing **29** were synthesized on the pre-loaded Wang resin as described in the chapters **2.2.2.2** and **2.2.4.2.1** respectively. The galactose moiety **49** was obtained in 60% through deprotection of tert-butyl protecting group of **3**. The Fmoc group was removed from the N-amino terminal of peptides **17** and **29** (20% piperdine /DMF) followed by coupling of **49** (3 eq) activated using HATU (3 eq)/DIPEA (6 eq) in DMF to a free amino function of peptide **17** for 3 h, to give the intermediates **50** and **51**. Afterwards, the Dde group was removed from **51** by treatment with 2% hydrazine hydrate in DMF (2x), and FITC was coupled on the designated ε-amino group of lysine for 12 h (**53**). The complete molecules were cleaved off the resin using TFA/TIPS/m-cresol/water (90: 2.5: 5: 2.5) simultaneously deprotecting the acid-labile amino acid side chains protecting groups of peptides.

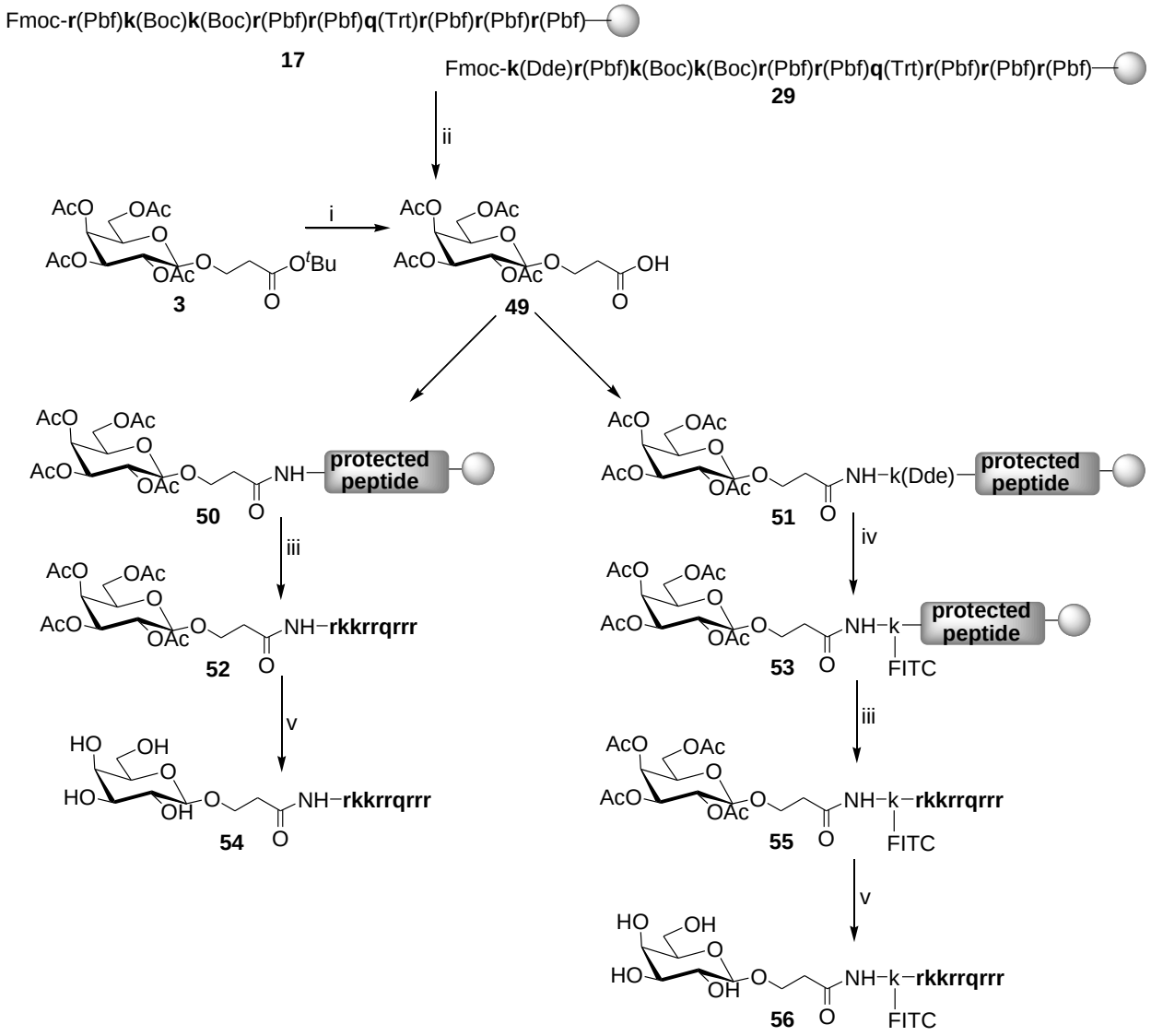

Scheme 10. Synthesis of conjugates **54** and **56.**

Reagents and conditions: i) TFA/DCM (1:1 v/v); ii) **16,** HATU, DIPEA, DMF, 3h; iii) TFA:m-crezol:TIPS-H_2O (90:5:2.5:2.5) iv) FITC, DIPEA, DMF; v) NH_3/MeOH (7N).

The released *O*-acetylated product **52** and **55** were preliminary purified by RP-HPLC and characterized by ESI-MS. Their O-deacetylation was carried out in saturated methanolic ammonia with monitoring the progress of reaction by LC-MS. The crude products **54** and **56** were purified by RP-HPLC and characterized by ESI-MS (Fig 21 and 22). The detected

molecular ions were consistent with the calculated mass of desired product (1573.81 g/mol and 2091.36 g/mol for **54** and **56** respectively).

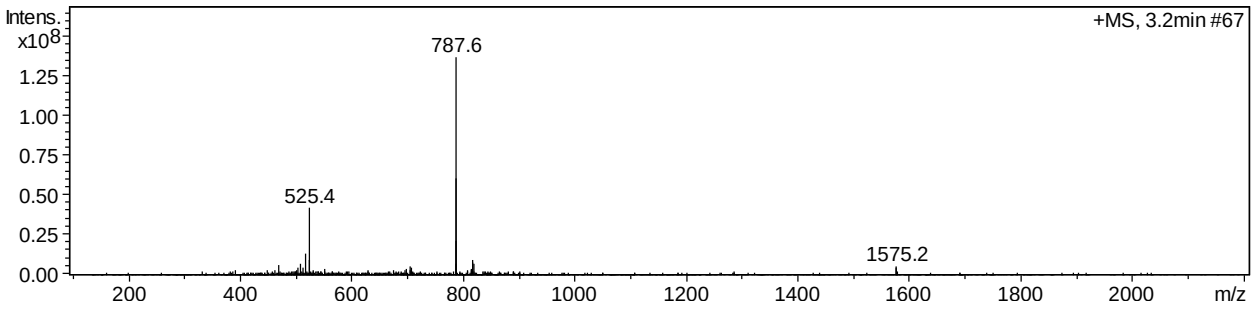

Figure 21. ESI-MS spectrum of **54 (**positive mode)**.**

Detected molecular ions m/z = 1575.2 ($(M+1H)^{1+}$), 787.6 ($(M+2H)^{2+}$), 525.4 ($(M+3H)^{3+}$) were consistent with the calculated mass of the product (1573.81 g/mol).

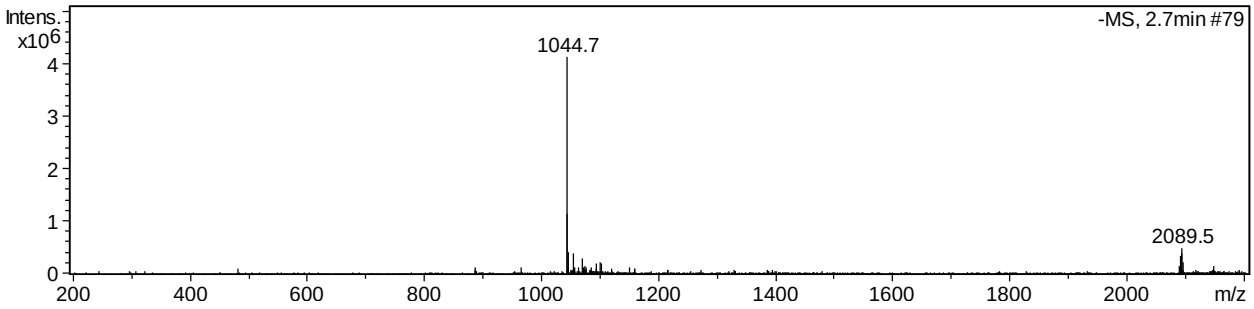

Figure 22 . ESI-MS spectrum of **56** (negative mode).

Detected molecular ions m/z = 2089.5 ($(M-1H)^{1-}$), 1044.7 ($(M-2H)^{2-}$), were consistent with the calculated mass of the product (2091.36 g/mol).

3.3.2 Synthesis of 61 with an aryl linker

Synthesis of **61** began with the galactose moiety **58** bearing an aryl linker for the attachment of peptide. In order to obtain such a carbohydrate building block first the nitrophenyl group of **35** was reduced to amino function in a mixture of ethyl acetate/ethanol to give **25** in 70% yield. In the next reaction of **57** with succinic anhydride **58** was formed in 55% yield. Peptide **17** was synthesized on pre-loaded Wang resin as described in chapter **2.2.1.1** and the Fmoc group was removed with 20 % piperidine/DMF. The following conjugation of **58** (3 eq) activated with HATU (3 eq)/DIPEA (6 eq) in DMF to the free α-amino terminal of peptide gave the intermediate **59**, which was further cleaved off the resin with a mixture of TFA/TIPS/m-cresol/water (90:2.5:5:2.5). The acid-labile protecting groups of the amino acid side chains in the peptides were simultaneously removed in this step.

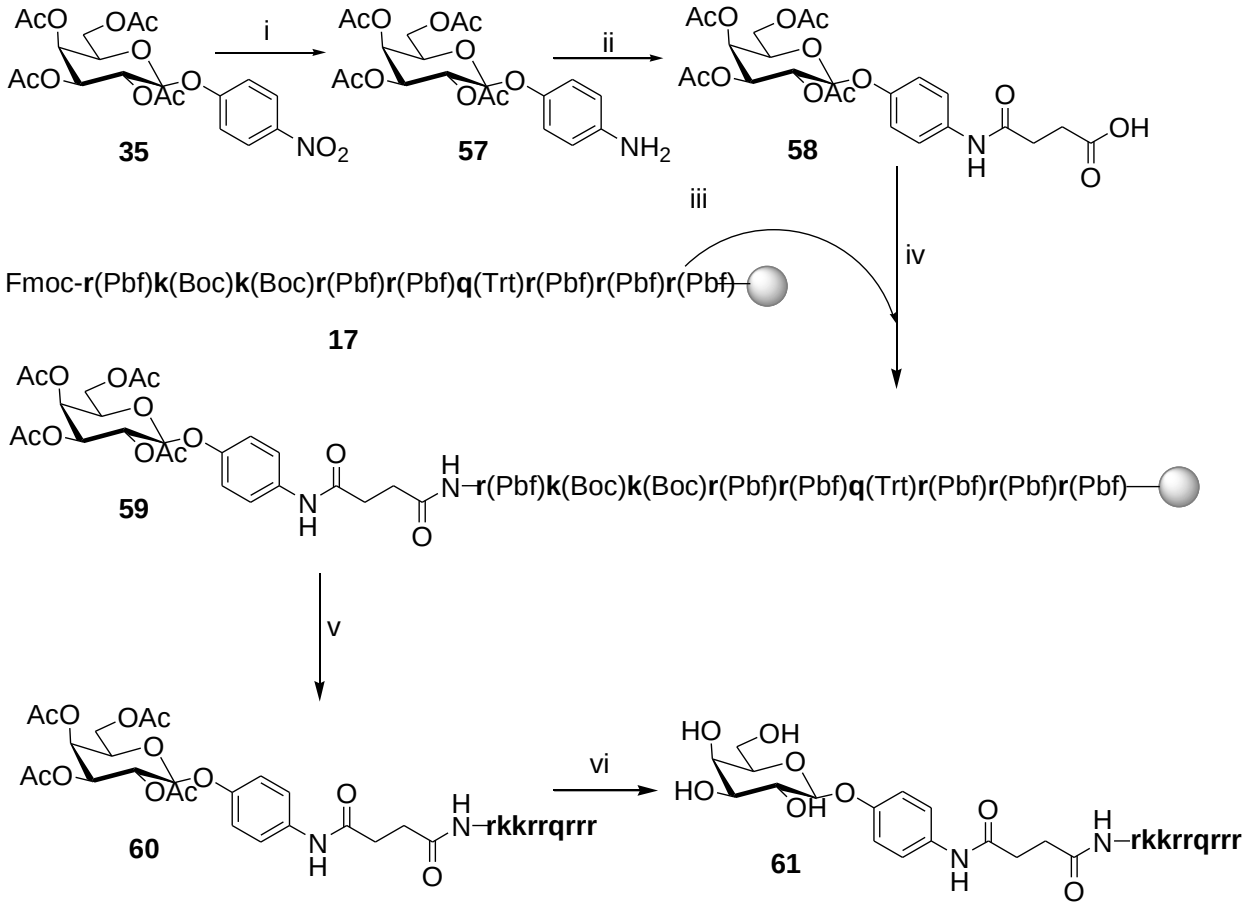

Scheme 11. Synthesis of **61**.

Reagents and conditions: i) H_2/Pd, EtOAc/EtOH (1:1 v/v), 5 h, rt; ii) succinic anhydride, pyridine, 12 h, rt; iii) 20% piperidine/DMF, 10 min (2x) iv) HATU, DIPEA, DMF, 3 h; v) TFA:m-crezol:TIPS-H_2O (90:5:2.5:2.5), 3 h; vi) NH_3/MeOH (7N).

The *O*-acetyl groups of **60** were removed with saturated methanolic ammonia (7N). The progress of deprotection was monitored by LC-MS. After the reaction was completed, the crude product was purified by RP-HPLC, lyophilized and characterized by ESI-MS (Fig 23). The detected molecular ions were consistent with the calculated mass of **61** (1692.93 g/mol).

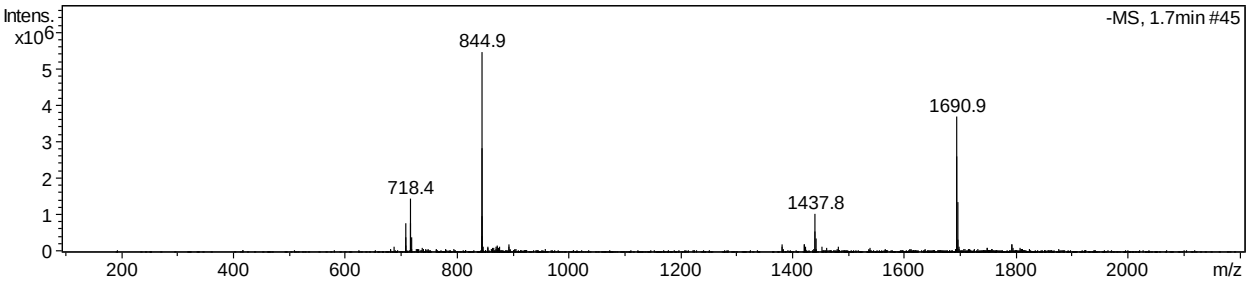

Figure 23. ESI-MS Spectrum of ligand **61** (negative mode).
Detected molecular ions m/z = 1690.9 ($(M-1H)^{1-}$), 844.9 ($(M-2H)^{2-}$), 1437.8 ($(M\text{-frag})-1H)^{1-}$) and 718.4($(M\text{-frag})-2H)^{2-}$), were consistent with the calculated mass of the product (1692.93 g/mol).

3.3.3 Evaluation of enzymatic activity on 54, 56 and 61

The investigated galactose conjugates **54** and **61** do not contain a chromophore residue, which release upon enzymatic reaction could be easily detected due to the observed changes in the absorbance. Therefore, an alternative colorimetric assay described by Diepenbrock et al.[216] was used to assess the enzymatic activity on **22** and **29** by quantitative determination of the formed galactose. The substrates were incubated first with *β*-galactosidase and reaction was stopped at various time points by removing the enzyme from samples by centrifugation using Nanosep Centrifugal Devices 10k with a MWCO 10000. Afterwards, the galactose content of these samples was determined using a two step procedure. In this method NADH was formed as result of the catalytic oxidation of galactose by D-galactose dehydrogenase, followed by its quantification in a second reaction with diaphorase, in which the colourless

p-iodonitrotetrazolium violet (INT) was transformed into a formazan showing an absorbance maximum at 492 nm. The amount of galactose was determined by using a galactose standard curve and was used to estimate the reaction rate of *β*-galactosidase at the indicated time points.

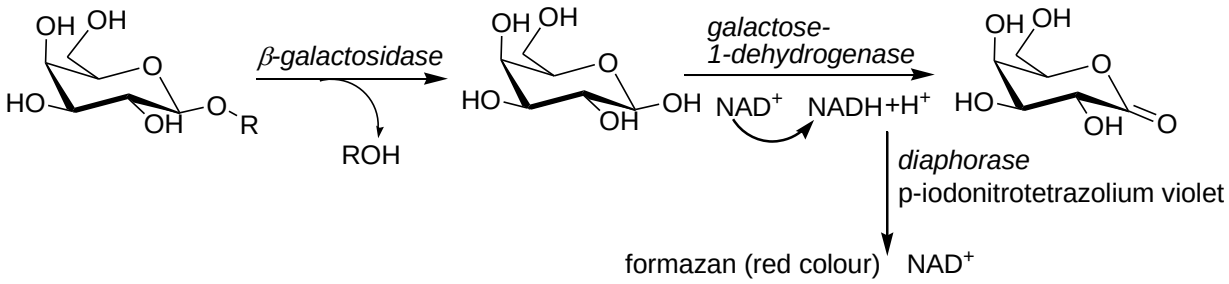

Figure 24. Colorimetric assay for determination of *β*-galactosidase activity.

The conversion of **54** and **61** using this assay was measured with an initial starting concentration of 0.5 mM calculated by weight. The real concentration of these conjugates was determined fitting the curve and were found to be 0.3 mM and 0.4 mM for **54** and **61**, respectively, (plateau phase, for details see Experimental part). The results demonstrated that the conversion rate of **54** with the alkyl linker was relatively slow (0.0018 µmol/min) as compared to **61** (0.0227 µmol/min) (Fig 25). Based on these results in can be concluded that linker incorporated between peptide and galactose has sidnificant influence on enzymatic conversion of such substrates. A longer incubation time of 6h with enzyme was required, for derivative **54** in order to observe its complete conversion to galactose and peptide. This might be attributed to the alkyl linker since most of low molecular weight substrates containing aryl groups are hydrolyzed faster as compared to alkyl-galactose or disaccharides[217,218]. On the other hand such an alkyl spacer as in **54** introduced a higher flexibility near to the galactose moiety. That could potentially influence the binding efficiency between enzyme and **22**.

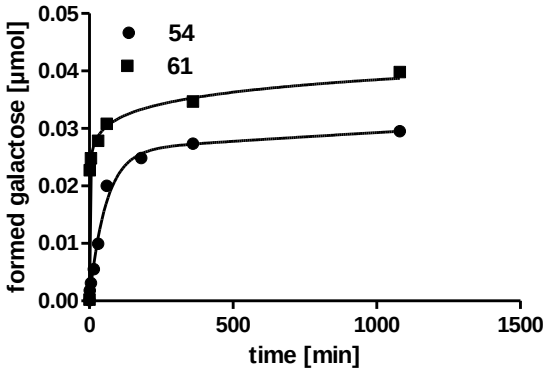

Figure 25. Conversion of **54** and **61** by *β*-galactosidase measured at different time points.
Conversion of **54** and **61** measured in the range of 0-18 h. Conjugate **54** reached plateau at ~ 0.03 µmol corresponding to a real concentration of ~0.3 mM (instead of 0.5 mM), conjugate **61** reached plateau at ~ 0.04 µmol corresponding to a real concentration of ~0.4 mM.

In order to examine whether the presence of FITC in the molecule has an influence on *β*-galactosidase activity, the derivative **56** was investigated.

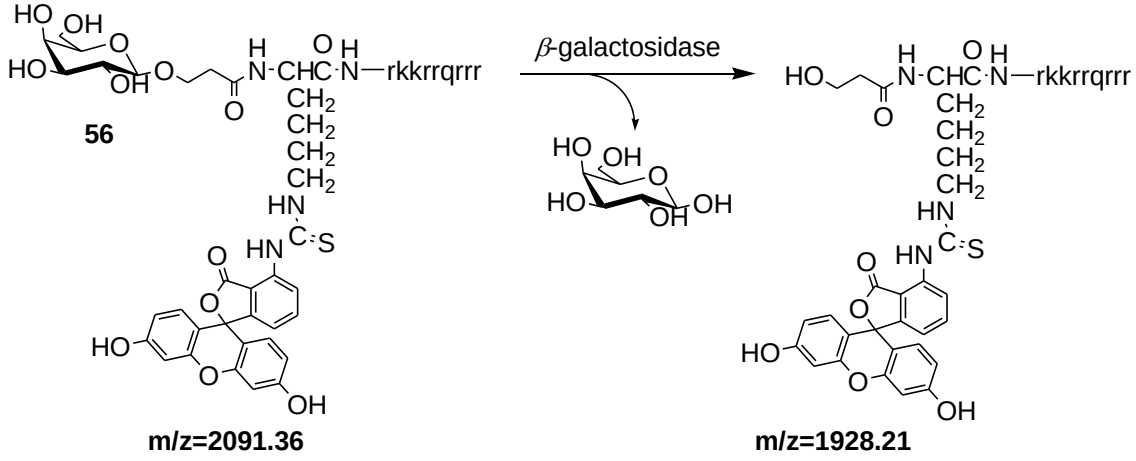

Figure 26. Schematic illustrations of enzymatic hydrolysis for **56.**

Since the absorbance maxima of FITC and formazan are almost at the same wavelength, the above described assay could not be applied. Thus, the *β*-galactosidase catalyzed reaction with **56**

after incubation for 0, 3 and 18 h (stopped like in case of **54** and **61**) was monitored by an ESI-MS (HCT Ultra, Bruker Daltonics, Bremen) with direct infusion alternating in positive and negative ion modus*. A complete conversion was observed already after 3 h at 37ºC (Fig 28). The detected molecular ions in mass spectra acquired from mixture before (Fig 27) and after enzymatic reaction (Fig 28) were consistent with the calculated mass of substrate **56** (2091.36 g/mol) and the cleaved Tat-FITC residue (1928 g/mol).

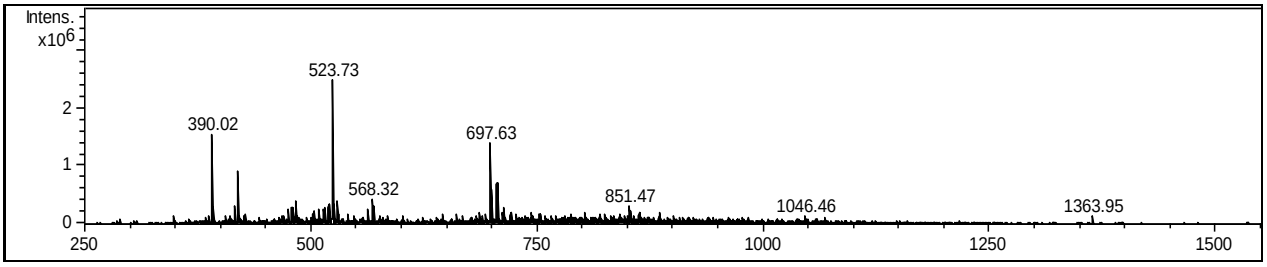

Figure 27. ESI-MS spectrum of **56** in solution without *β*-galactosidase.

Detected molecular ions m/z = 1046.7 $((M+2H)^{2+})$, 851.6 $((M\text{-}FITC)+2H)^{2+}$), 697.68 $((M+3H)^{3+})$, 568.32 $((M\text{-}FITC)+3H)^{3+}$) 523.73 $((M+4H)^{4+})$, 390 (FITC) consistent with the calculated mass of substrate (2091.36 g/mol).

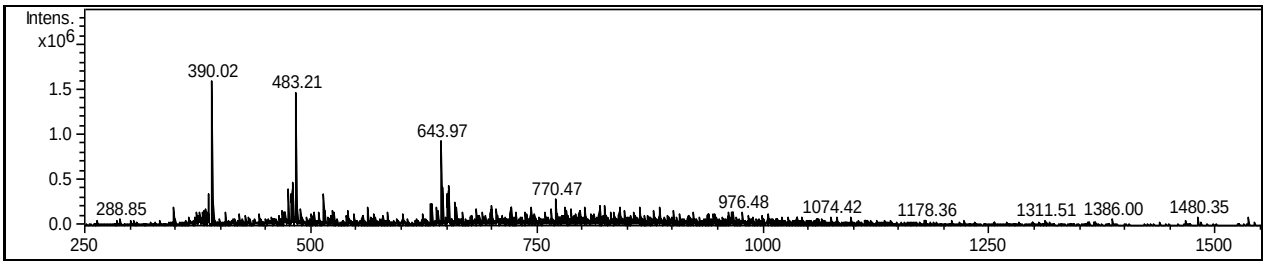

Figure 28. ESI-MS spectrum after cleavage of **56** by *β*-galactosidase (incubation 3h). Detected molecular ions m/z=770.47 $((M\text{-}FITC)+2H)^{2+}$), 643.97$((M+3H)^{3+}$), 482.21 $((M+4H)^{4+}$), 390.02 (FITC) were consistent with the calculated mass of expected product Tat-FITC of enzymatic reaction (1928.21 g/mol). *in collaboration with Dr. Guido Sauer, MPI for Developmental Biology, Tuebingen.

In general, mass spectrometry provides a good alternative to colorimetric assays since the enzymatic activity can be followed based on the intensity ratio of detected ion mass peaks of substrate and product in the reaction mixture[219]. It was found, that the attachment of FITC to the peptide did not affect the enzymatic activity on **56** as compared to **54**. These results showed that this method can also be used to monitor the enzymatic cleavage of **CA-1**.

3.4 Evaluation of *β*-galactosidase activity on CA-1

The studies presented in chapters 3.2.3 and 3.3.3 showed that modifications at the glycone part as well as the aglycone part of galactose moiety had a significant impact on the observed enzymatic activity of the *β*-galactosidase. These experiments assisted to establish the ESI-MS assay for the ultimate investigation of the activity of *β*-galactosidase on **CA-1**, which similarly to **54**, **56** or **61** does not contain chromogenic residues undergoing changes in absorbance upon the enzymatic reaction.

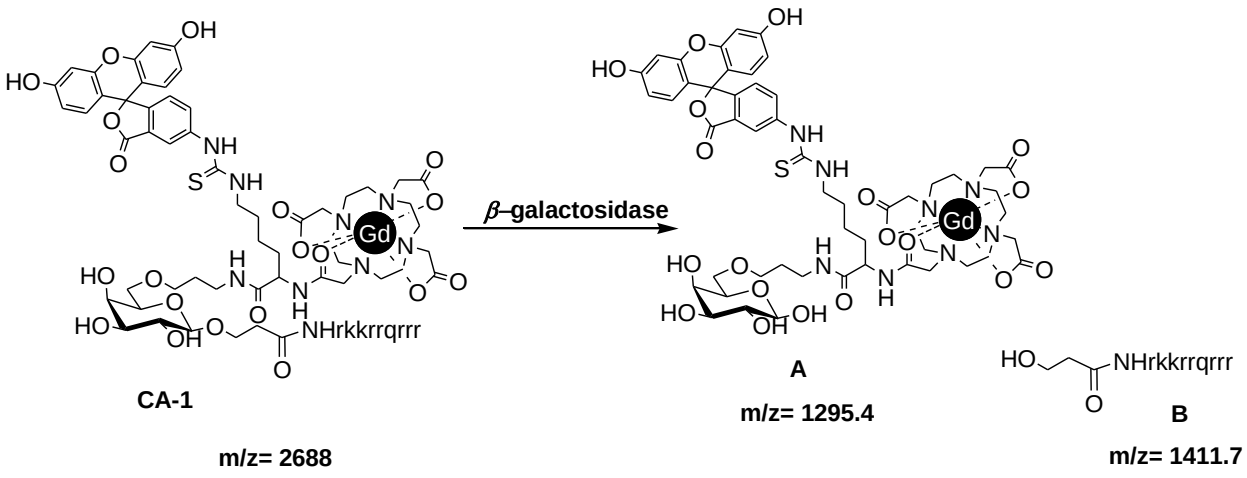

Figure 29. Expected products **A** (MW=1295.43) and **B** (1411.66 g/mol) as results of *β*-galactosidase catalysed hydrolysis of **CA-1**.

CA-1 was incubated with *β*-galactosidase at 37 ºC for defined time points (0, 0.5, 1, 3, 6 and 18 h) after which the reaction was stopped like in case of **54**. The obtained samples were further analyzed by ESI-MS. In the mass spectra of measured samples (Fig 30 and 31) a molecular ion

peak at 471.27 ($(M+3H)^{3+}$) was detected, which apparently corresponds to the molecular weight of **B** (1411.67 g/mol). This assignment was supported by the fact, that an identical mass peak increasing with incubation time was observed in mass spectra of **54** after *β*-galactosidase reaction. Subsequently, in the mass spectra of samples after incubation of **CA-1** with enzyme an increase in the intensity of ion mass peak 471.27 (B) was observed as compared to that of 673.0 (**CA-1**), indicating to an enzymatic conversion of **CA-1**. The exemplary mass spectra of samples after incubation times of 0 min (Fig 30) and 1 h (Fig 31) presented below shows this change in intensities of the investigated molecular peaks of substrate m/z=673 ($(M+4H)^{4+}$) and product 471.27 ($(M+3H)^{3+}$) with calculated ration between B and CA-1 equal 0.29 (B/CA-1) at 0 min and 1.01 (B/CA-1) at 1 h time points.

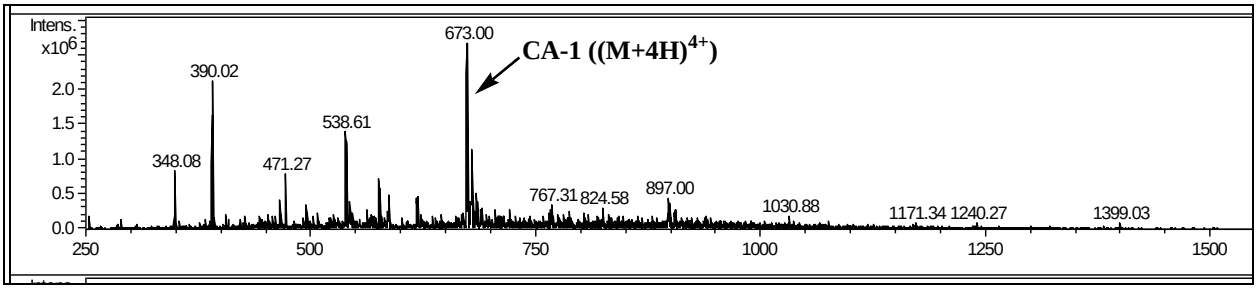

Figure 30. ESI-MS spectrum of sample of the immediately stopped *β*-galactosidase reaction (0 min). Detected molecular ions m/z = 897.0 ($(M+3H)^{3+}$), 673.0 ($(M+4H)^{4+}$), 390 (FITC) consistent with the calculated mass of **CA-1** (2688 g/mol).

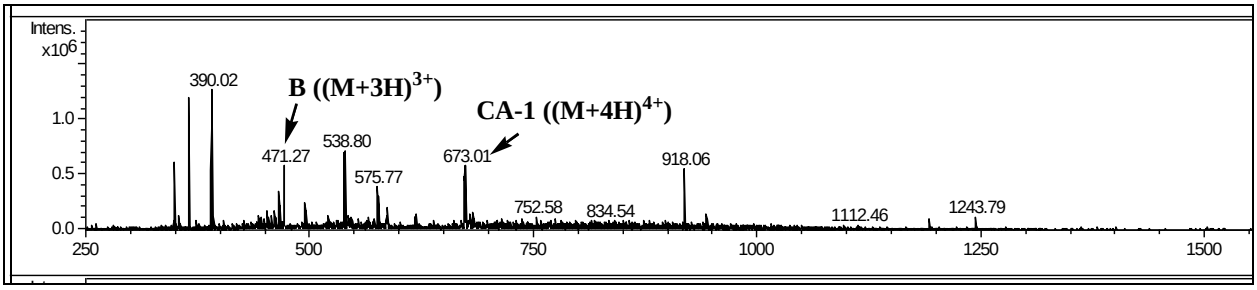

Figure 31. ESI-MS spectrum of sample after incubation with *β*-galactosidase for 1h.
Detected molecular ions m/z = 697.68 ($(M+4H)^{4+}$), 390 (FITC) consistent with the calculated mass of **CA-1** (2688 g/mol) and 471.27 ($(M+3H)^{3+}$) apparently corresponds to molecular weight of **B** (1411.66 g/mol).

The enzymatic conversion was also investigated by gel shift assay. This method is based on the different mobility of molecules in acrylamid gel depending on their molecular size and charge. The obtained samples of **CA-1** after incubation with enzyme for various time points were run on the gel (16.5%, Tris-Glycine SDS Page without urea) prepared as described by Fling & Gregerson[220] followed by silver staining, which is commonly used to visualize proteins and peptides separated through electrophoresis[221]. The product **B** (Fig 29) was expected in case of an enzymatic cleavage of **CA-1** by *β*-galactosidase. The gel separation of **CA-1** and the potential hydrolysis product **B** is difficult due to the relative small differences in size of these conjugates. For that reason, a derivative NH_2-k(FITC)-Tat_{49-57} (P) was used as reference, since its molecular weight (MW=1857.2 g/mol) is in the range between those of **CA-1** and **B** allowing to assign developed bands on the gel according to their size. In the silver stained gel (Fig 32) an additional band of a peptide in the molecular weight range of **B** was observed in the samples incubated with enzyme for definite time (0.5-18 h). In addition, the intensity of this band, which apparently was not visible at 0 min, increased time dependently between 0.5-3 h, what should be expected as consequence of longer incubation of substrate with *β*-galactosidase.

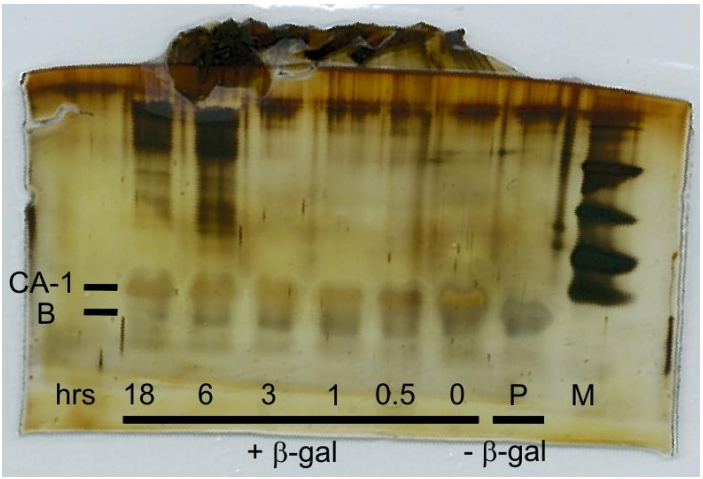

Figure 32. Gel shift assay of samples after incubation of **CA-1** with *β*-galactosidase for indicated time points. **CA-1** (MW= 2688 g/mol), **P**: NH_2-k(FITC)-Tat_{49-57} (MW=1857.2 g/mol) used as standard, **M**: molecular weight marker (3496, 6500, 14200, 17000, 26600 g/mol). After electrophoresis gel was fixed and silver stained.

The similar slow increase in observed hydrolyzed product was seen in case of model derivative **54** (data not shown). In case of the incubation of **CA-1** with enzyme for 6 h and 18 h dark brown bands appeared on the gel in the high molecular weight range above **CA-1**. However, their origin could not be explained and requires further investigation

The preliminary results obtained by ESI-MS and gel shift assay are comparable and apparently indicate that a slow conversion of **CA-1** by *β*-galactosidase was taking place. The evaluation of the enzymatic activity for **CA-1** proved to be difficult due to the complexity of its molecular structure and the several factors affecting its interaction with enzyme. Therefore, further studies are required to ultimately confirm these results and quantify the enzymatic activity.

3.5 Summary & conclusions

The *in vitro* evaluation of interaction between the cell-permeable **CA-1** and targeted *β*-galactosidase proved to be difficult. This was due to the complex molecular structure of **CA-1** comprising of MR and fluorescence reporters, the modified galactose moiety and cell-penetrating peptide. Each unit could potentially affect the enzyme activity towards hydrolysis of **CA-1**, dependent on the structure of glycon and aglycone. The series of model compounds with a modified galactose moiety (**CA-5** and **CA-6**) or various types of aglycone residues were synthesized and evaluated as *β*-galactosidase substrates. This approach was based on "breaking down" the structural complexity of **CA-1** into simpler and smaller elements in order to understand the influence of alternation in the molecule structure on its interactions with *β*-galactosidase. It was demonstrated that the modifications at the C-6 position of galactose reduced the conversion rate as compared to PNPG standard substrate. However, the introduced changes were still compatible with enzymatic hydrolyzobility. **CA-6** with a nonyl linker was a poor substrate for enzyme as compared to **CA-5**, showing that the length of the linker had a significant influence on the observed enzymatic activity. Thus, different spacers should be considered while designing an optimal substrate for enzymes.

The enzymatic studies on the galactose-peptide conjugates **54**, **56** and **61** demonstrated that the catalytic rate of the enzymatic reaction was strongly depending on the type of the linker connecting the anomeric center with the cell-permeable peptide. The derivatives with alkyl linker (**22** and **24**) required a longer time to be completely hydrolyzed. The slow hydrolysis of **54** most likely originated from the nature of this spacer as alkyl linker was cleaved generally slower in

comparison to aryl. It was observed that, the presence of a positively charged peptide affects the rate of enzymatic hydrolysis as compared to standard small size PNPG reference.

The preliminary results for **CA-1** indicated to its enzymatic conversion in the presence of *β*-galactosidase. Nevertheless, further experiments are required to clearly confirm these findings and to quantify enzymatic activity.

The results presented in this chapter showed, that a design of an efficient, cell permeable enzyme responsive MRI probe, which fulfills criteria for proper enzymatic activity, but also internalization and high relaxivity, is challenging. Modifications at the C-6 position of galactose mainly determined the interactions between *β*-galactosidase and **CA-1**. The type of the linker has a smaller influence on observed efficiency of enzymatic conversion as compared to alterations of the galactose moiety, but this impact is still substantial and should be taken into account when designing an optimal enzyme targeting probe. Further optimization of this first generation of *β*-galactosidase targeted CAs was required in order to achieve their more efficient enzymatic conversion. Therefore, the synthesis of a second generation of such CAs is under progress in which the galactose moiety was not modified. The self-imolative linker connecting galastose and MR chelate was introduced and in the future cell penetrating peptides showing cytosolic and non vesicular distribution will be appended to this structure.

Chapter 4

Dual-labeled contrast agents for MRI and optical imaging: design, synthesis and *in vitro* evaluation

4.1 Introduction

Multimodality imaging is a rapidly evolving field aimed at integrating the advantages of various imaging technologies (e.g. MRI, PET, SPECT, ultrasound, optical imaging), thus conquering their individual limitations to facilitate visualization of specific biological targets as well as biological pathways *in vivo*[222]. Hence, the development of suitable multimodal probes that incorporate two or more reporters visualized by different modalities emerges in many clinical and research areas[223]. Amongst the several multifunctional agents reported up to date[224,225], those combining the benefits of MRI and optical technologies remain most popular. The complementarity of these two techniques originates from deep tissue penetration along with a high spatial resolution for MRI and exceptional detection sensitivity for optical methods. These advantages compensate for the inherent low sensitivity of MRI and the light scattering associated with optical imaging.

A common approach to obtain dual-labeled reporter molecules involves the covalent attachment of a fluorescent molecule to T_1- or T_2-MRI contrast agents. The pioneering report on such dual MRI-optical probes was published in 1998 by Huber et al.[226], where CAs based on a polymeric scaffold (polylysine or polydextran) containing numerous DTPA chelates were functionalized with the fluorescent dye tetramethylrhodamine (TRITC). These polymeric agents **GRIP** (Gd-(DTPA)-tetramethylrhodamine-hydroxypropyl(D-lysine) and **GRID** (Gd-(DTPA)-tetramethylrhodamine-aminedextran) were successfully applied *in vivo* to study embryonic cell lineage in *Xenopus Laevis* embryos. In further application of these probes stem cells were labeled with **GRID** *prior* to transplantation, what enabled the tracking of their migration in the rat brain into ischemic lesions [142,143].

Besides Gd-based molecules, the use of T_2-based contrast agents has been extensively explored as a valuable platform to obtain multimodal probes. Weissleder and coworkers[227,228] first reported on dextran cross-linked iron nanoparticels (CLIO) derivatized with the cell permeable TAT peptide conjugated to FITC dye. Moreover, DTPA chelates were incorporated into the aminated dextran with purpose of radioisotope labeling. These triple-labeled particles showed an efficient cellular uptake in various cell lines and enabled in vivo mapping of progenitor cells. Further examples for the application of the multimodal and/or targeted CLIO nanoparticles as diagnostic tools include delineation of brain tumor boundaries using CLIO nanoparticles functionalized with a near-infrared fluorescent dye (Cy5.5)[229], imaging of mucin-1 tumor antigen (uMUC-1) as

characteristic sign of tumorigenesis[230], visualization of microvascular leakage as an indicator of insultis progression studied in mouse model of type 1 diabetes (T1D)[231] and imaging of apoptotic cells via the detection of the lipid target phosphatidylserine (PS)[232].

An alternative strategy to achieve multimodality imaging involves the administration of a mixture of monofunctional probes that are chemically equivalent. This approach was utilized by Aime and coworkers to visualize stem cells that are labeled with Gd-HPDO3A and Eu-HPDO3A complexes (HPDO3A=1,4,7-tris[carboxymethyl]-10-[2'hydroxypropyl]-1,4,7,10-tetraazacyclodo decane) by means of MRI and fluorescence microscopy[233]. The presented brief overview clearly highlighted the importance of this rapidly evolving field as future direction of the imaging methodologies.

The growing interest for the application of multimodality imaging in various research areas is indivisibly associated with the development of new multimodal probes. The commonly used protocols in the synthesis of Gd^{3+}-based bimodal contrast agents utilize a stepwise strategy. Thus, MR ligand and optical reporter are introduced „one by one" to the main core structure followed by complexation with the lanthanide metal ion. Whereas this approach works well for small size molecules, an identical procedure for the synthesis of dual-labeled macromolecules / multivalent CAs, which contain numerous MR chelates or fast degrading bioactive molecules, appears to be rather more complicated. The major drawbacks can be summed up as follows: solubility problems, possible underloading or overloading of MR ligands with Gd^{3+}, increased probability of non-specific binding of gadolinium inside macromolecular structures during complexation, stability as well as purity issues related to the number of synthetic transformations. To overcome some of these limitations, the design of pre-loaded bimodal Gd-precursors, which can be directly attached to a desired macromolecule in a single conjugation step, appeared as a valuable alternative to the classical stepwise strategy. Subsequently, a model precursor **CA-7** derived from the complex **CA-4** was synthesized. Both paramagnetic complexes consist of Gd-DOTA derivative and fluorescein isothiocyanate (FITC). These commonly used synthons in MR and optical imaging are linked together *via* a lysine spacer. Complex **CA-4** with a carboxylate group of lysine masked as methyl ester was initially designed as a bimodal, middle size contrast agents with potential cell-permeability. But it also proved later to be a feasible precursor of **CA-7**. Hence, the same synthetic strategy was utilized to obtain **CA-4** and **CA-7**. Moreover, given that the r_1 relaxivity of high molecular weight conjugates depends on the global

rotational correlation time further governed by the internal motions inside the molecule (see chapter 2), the α-amino group of lysine was preferentially selected over the ε-position for covalent attachment of the Gd-DOTA chelate while designing **CA-7**. The free α-carboxylate group of **CA-7** was chosen as feasible functionality for its further coupling to other molecules. To demonstrate the applicability of such a dual-labeled precursor in the synthesis of bulky molecules, the pre-metallated chelate **CA-7** was efficiently coupled to poly-L-glutamic acid (PGA) yielding the high molecular weight conjugate **CA-8**. This biodegradable and nontoxic anionic polymer has been commonly used as a macromolecular drug carrier[234]. In this chapter the synthesis, characterization as well as the biological evaluation and potential application of **CA-4**, **CA-7** and **CA-8** will be described.

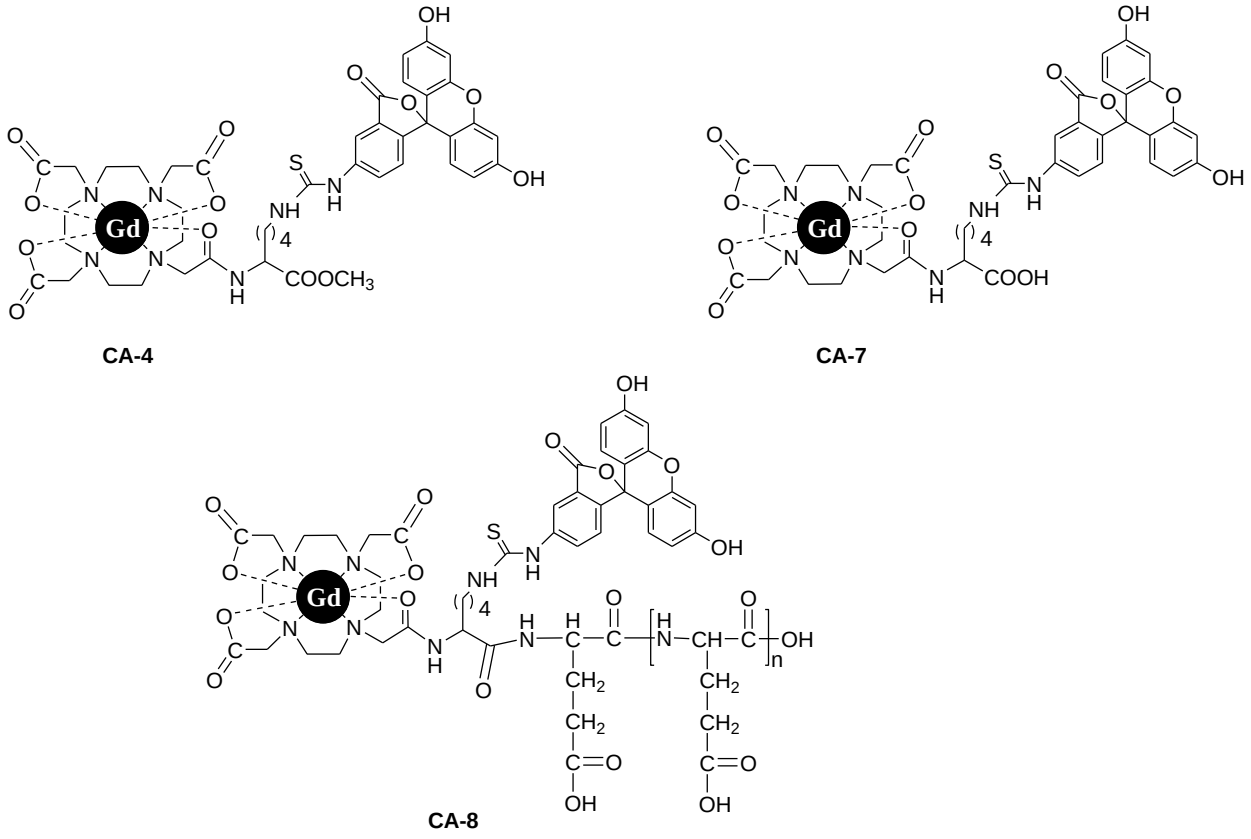

Figure 33. Designed dual-labeled contrast agents.

4.2 Synthesis of conjugates CA-4 and CA-7

The straightforward synthetic strategy to obtain the bimodal Gd^{3+} chelators **CA-4** and **CA-7** was established (Scheme12). At first, compound **62** was obtained with 59 % yield by coupling of DOTA tris(tert-butyl) ester **28** to the α-amino group of N-ε-carbobenzyloxy-lysine methyl ester hydrochloride in dry DMF using EDC/HOBt as activating agent and NMM base. Afterwards the N-ε-carbobenzyloxy group was removed from **62** by catalytic hydrogenation in a Parr-apparatus at 2 bar over 10% Pd/C yielding **63**. The incorporation of FITC into the ligand structure was approached by two ways. Initially, acid labile tert-butyl groups of **63** were deprotected using a mixture of TFA/DCM (6:4 v/v) and after co-evaporation with toluene, the crude intermediate **64** was reacted with FITC in water at pH 8.5 adjusted with aqueous Na_2CO_3. However, as monitored by LC-MS only a very poor conversion towards compound **66** was observed. Thus, an alternative approach was utilized, where **63** was first reacted with FITC in DMF in the presence of DIPEA base. After that, the crude intermediate **65** was further deprotected using a mixture of TFA/DCM (6:4 v/v) for 12 h, co-evaporated with toluene and purified by RP-HPLC as described in experimental section to give **66** with 62% yield after 2 steps. The exact concentration of the ligand was determined by UV-VIS measurements before performing the loading with $GdCl_3$ in order to avoid an excess of gadolinium in the sample. The complexation with the lanthanide was performed by stirring ligand **66** with $GdCl_3$ (ratio ligand: metal 1:0.9) in ultrapure water at 45 ºC for 12 h, followed by 2 days at room temperature. During the loading procedure, the pH of solution was maintained in the range of 6.5-7.5 since precipitation of **66** at lower pH occurred. The crude product **CA-4** was purified by RP-HPLC using acetonitrile/water. In order to obtain a pre-metallated complex **CA-7** for further conjugation to macromolecules, methyl ester protection was removed from carboxylate group by stirring a solution of **CA-4** in water at pH 10 for 2 h followed by RP-HPLC purification and lyophilization of the obtained product. Both complexes were characterized by ESI-MS mass spectrometry. The molecular ion peaks measured in the negative mode with the characteristic isotopic pattern distribution for Gd^{3+} complexes were consistent with the molecular weight of **CA-4** (1090 g/mol) and **CA-7** (1075 g/mol).

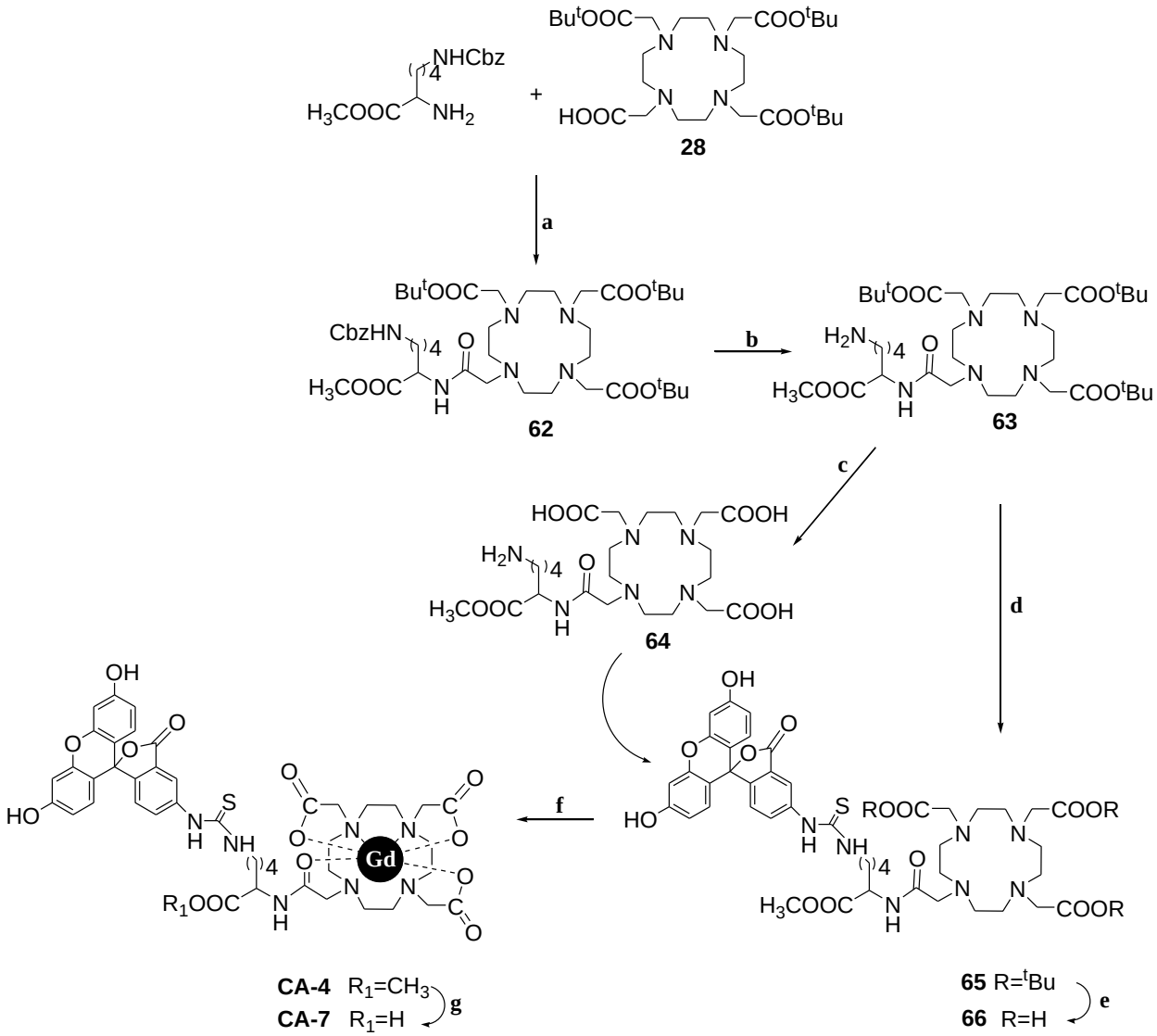

Scheme 12. Synthesis of **CA-4** and **CA-7** complexes

Reagents and conditions: a) EDC, NMM, DMF, 0°C-rt ; b) H_2/Pd , EtOH, rt; c) DCM/TFA 1:1v/v, 0°C-rt, 12 h d) FITC, DIPEA, DMF, 12 h, rt; e) DCM/TFA 1:1v/v, 0°C-rt, 12 h f) $GdCl_3x6H_2O$, 40ºC/12 h, rt 2 days; g) water, 1M NaOH aq., (pH~10), 2 h.

4.3 *In vitro* relaxometry and cell studies of CA-4

The longitudinal relaxation times T_1 of water protons for various concentrations of **CA-6** were measured in the range 5-40 µM at 128 MHz (3T) and room temperature. The real concentration of **CA-4** was determined to be 70% by weight based on FITC absorption measurements at 485 nm. This estimated concentration of the stock solution corresponded well to the gadolinium concentration obtained by BMS measurements. The determined relaxivity of **CA-4** was 9.15 $mM^{-1}s^{-1}$ and by this higher than that of the commercial available Gd-DOTA chelate (Dotarem®, 4.0 $mM^{-1}s^{-1}$). This behavior related to neighboring effect of FITC was already discussed in Chapter 2.

Given that lanthanide coordination complexes attached to hydrophobic chromophores could efficiently enter the cells as reported by Parker and collaborators[235,236], **CA-4** was further investigated for its ability to penetrate through the cell membrane. *In vitro* cell studies were performed, in which C6/LacZ cells were incubated with 10, 20 and 100 µM of **CA-4** in complete medium for 18 h. Indeed, **CA-4** proved to be cell-permeable as demonstrated by fluorescent spectroscopy (Fig 1a) with significant levels of intracellular accumulation at 100 µM, whereas at lower labeling concentrations of **CA-4** only poor cellular uptake was detected. Importantly, no apparent cytotoxicity of **CA-4** over the whole concentration range was observed as compared to control cells based on the Hoechst 33342 assay. Thus, this bimodal probe appeared to be well-tolerated for cells. Moreover, Trypan blue was included in the washing protocol of the cells as efficient quencher of extracellular fluorescence (bound to outer cell membrane or found in dead cells). This assay allowed for quantification of exclusively intracellulary located **CA-4** by means of fluorescent spectroscopy. The vesicular localization of CA-**4** (displayed as green spots) around the nucleus (blue) as shown in Figure 34 was distinctly visible in fluorescence microscopic images, however, only at higher labeling concentration (100 µM) of **CA-4** (images for lower concentration not shown).

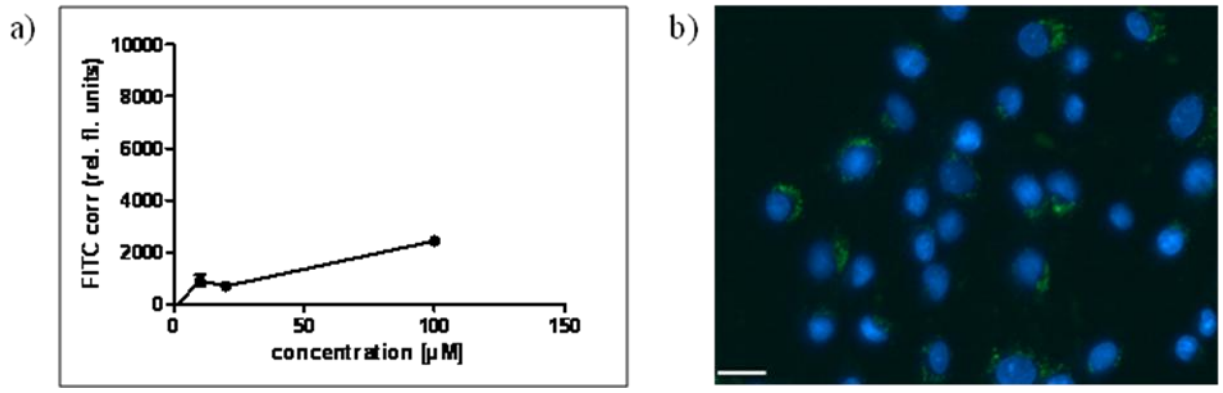

Figure 34. a) Cell internalization of **CA-4** into C6/LacZ cells measured by fluorescent spectroscopy. Cells were incubated with contrast agents at 10, 20 and 100 µM in medium containing serum for 18h. External fluorescence was quenched with Trypan Blue and subsequent washings with HBSS. b) Fluorescence microscopic images displaying the intracellular localization of **CA-4** in C6/ LacZ cells after incubation for 18 h with CA at 100 µM in complete medium. Cell nuclei were counterstained with Hoechst 33342 Nuclei: blue (Hoechst 33342), CA: green (FITC fluorescence). The bar represents 20 µm.

Subsequently, the effect of the cell-permeable conjugate **CA-4** on the cellular relaxation rates $R_{1,cell}$ was examined. C6/LacZ cells were incubated for 18 h with 10, 20 and 100 µM of this Gd^{3+}-complex and prepared for MR measurements as described in Chapter 2.2.4.3. Since only a faint uptake of **CA-4** was observable at lower labeling concentrations of CA and because of the sensitivity gap between MR and optical techniques, only incubation for 18 h was chosen to achieve an efficient accumulation of CA in the cells. The obtained MR results clearly demonstrated the capacity of **CA-4** to increase relaxation rates $R_{1,cell}$ in comparison to control cells (Fig 35). In harmony with the results obtained by fluorescent spectroscopy (Fig 34a), a small but statistically significant enhancement of $R_{1,cell}$ values (104% of control) was observed at 10 and 20 µM labeling concentration of **CA-4** with no difference between 10 and 20 µM. A more pronounced increase in $R_{1,cell}$ (115% of control) was detected after incubation with 100 µM of **CA-4**.

In summary, conjugation of the Gd-DOTA based chelate to a methyl protected lysine-FITC residue resulted in the formation of the bimodal contrast agent **CA-4** with the capacity to

penetrate the cell membrane and to increase the cellular relaxation rates $R_{1,cell}$ although to a much lower extent as compared to CPP-coupled **CA-1** and **CA-2**. No influence on cell viability was detected even at the highest labeling concentration indicating that **CA-4** was well-tolerated by the cells. Thus, MR and cell internalization studies clearly revealed a potential of **CA-4** to serve by itself as a bimodal cell-permeable CA for optical and MR imaging of cells.

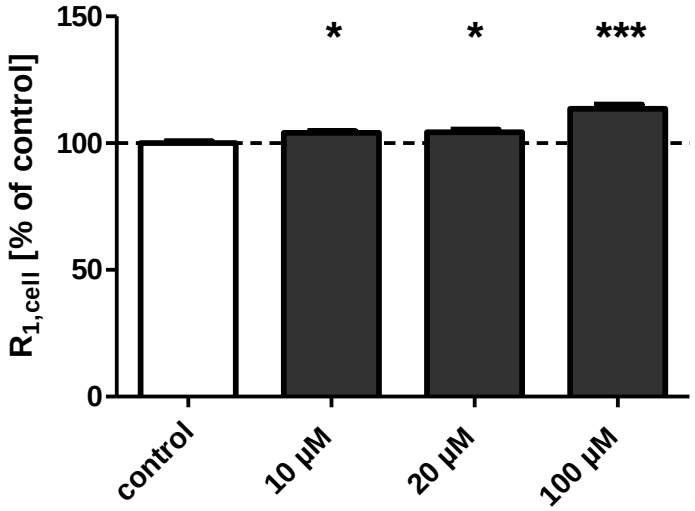

Figure 35. Cellular relaxation rate $R_{1,cell}$ in C6/LacZ cells after loading for 18 h with 10, 20 and 100 µM of **CA-4**. After incubation cells were trypsinized, centrifuged and re-suspended in 1.5 mL Eppendorf tubes at 2×10^7 cells /500 µL in complete DMEM for MR studies. Control: cells were incubated with culture medium without CA. *$p<0.05$, ***$p<0.001$, statistically significant compared to control;

4.4 Conjugation of pre-metallated CA-7 to poly(L-glutamic acid)

Poly(L-glutamic acid), PGA, as biodegradable and nontoxic anionic polymer has been reported to be a valuable macromolecular drug carrier[237,238]. Its applicability in the preparation of MRI blood-pool agents used for imaging of vascular abnormalities has been recently shown [239,240,241]. Although, many macromolecular MRI agents showed high relaxivities and increased blood retention sufficient for MRI examination, their application in clinical settings is still limited. The

reason is an incomplete or slow excretion from the body of currently existing MRI blood-pool agents, which raises safety issues regarding their toxicity[242]. In contrast, the polymeric PGA conjugated to Gd-chelates proved to be a valuable platform for developing a new class of macromolecular MRI CAs [240]. It was demonstrated that due to PGA biodegradation no apparent toxicity was observed during *in vivo* examination. Consequently, PGA was selected as a model for macromolecular carrier to evaluate the applicability of pre-metallated complex **CA-7.**

4.4.1 Synthesis of biomodal PGA-lysine-FITC/Gd-DOTA conjugate (CA-8)

The PGA-lysine-FITC/Gd-DOTA complex (**CA-8**) was obtained via a two-step reaction utilizing the NHS based strategy as illustrated in Scheme 13. At first, **CA-7** with a free carboxylate group was reacted for 20 min with NHS ester in the presence of EDC in aqueous 0.1 M MES buffer at pH= 5.5 to give the intermediate **67**. The exact concentration of **CA-7** was determined *prior* to the reaction in order to maintain the ratio of complex to EDC/NHS 1:1.5. Thus, a large excess of EDC/NHS reagents was avoided, which could otherwise lead to cross-coupling side reactions in the next step. The following conjugation of **CA-7** N-hydroxysuccinimide ester to the α-amino group of anionic PGA polymer (average MW~15000g/mol) was carried out in 0.1 M MES at pH~6.5 for 3 h at room temperature. The obtained crude sample (MW~ 16075 g/mol) was dialyzed for 48 h in the dark using a Float-A-Lyser (Spectrum Laboratories, Inc., USA) dialysis system with MWCO of 2000 to remove salts and unreacted complex. Afterwards, the remains were lyophilized to give conjugate **CA-8** with a yield of 72% with the content of **CA-8** of 95% in the sample estimated by FITC absorbance). Thus, it was observed that a pre-loading strongly reduced salt contamination as compared to protocol applied for **CA-1** and **CA-2** were 30% of compound was present in the sample.

The activation time of **CA-7** with EDC/NHS had a large influence on its conjugation efficiency to PGA. In case of an initially applied procedure with 1 h activation time followed by 3 h reaction of intermediate **67** with PGA less **CA-8** was found as determined by FITC absorbance. This observation was supported by the presence of **CA-7** in the outer solution of dialyzed samples (analyzed by ESI-MS) indicating to an incomplete coupling of the semi-stable NHS ester to the anionic polymer. Hence, the protocol with the shorter activation time of **CA-7** showed to be optimal to facilitate the formation of **CA-8**. The obtained PGA-lysine-FITC/Gd-

DOTA complex was further examined for its relaxometric properties as described in following chapter.

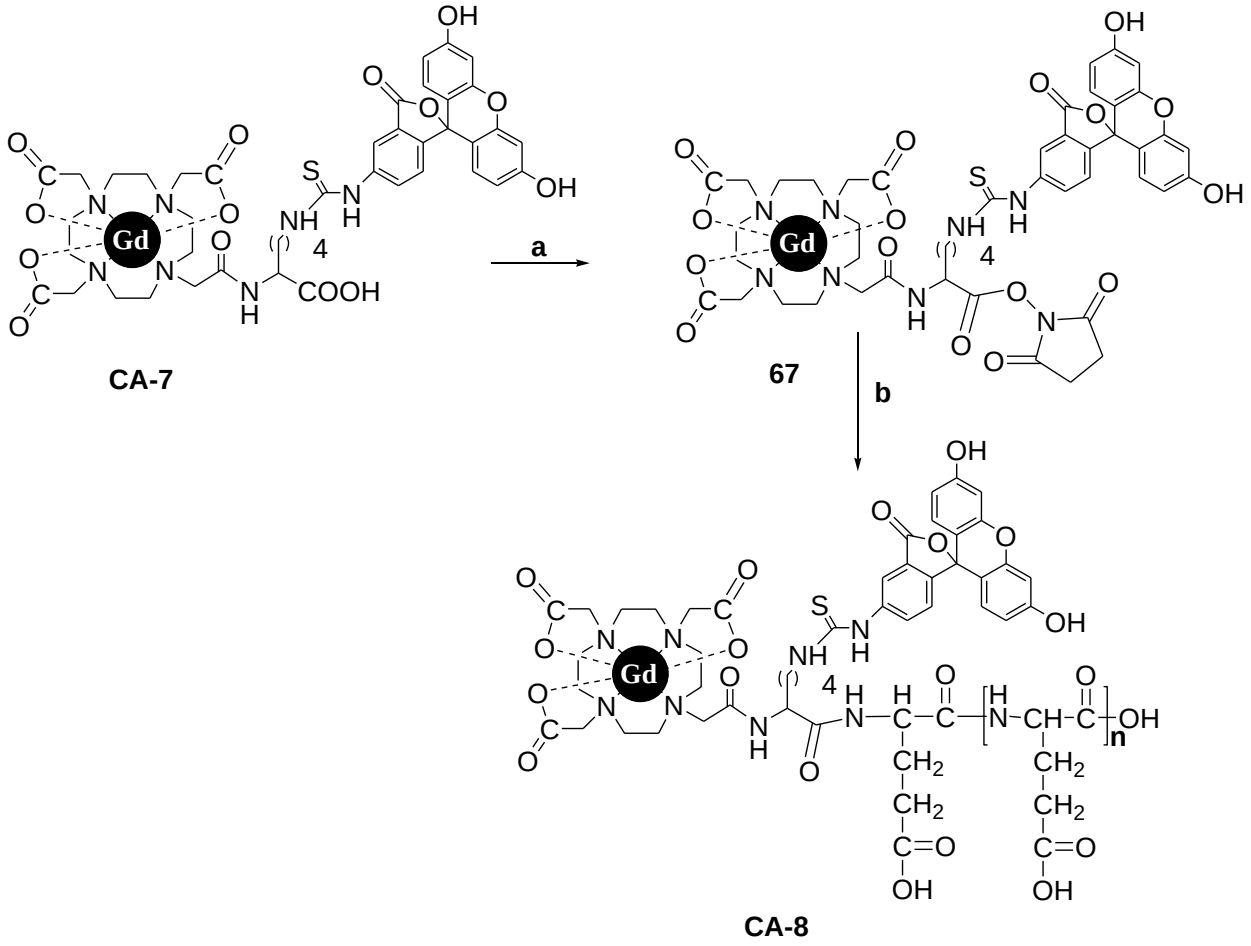

Scheme 13. Synthesis of the conjugate **CA-8**

Reagents and conditions: a) EDC, NHS, 0.1 M MES, pH=5.5 b) **41**, PGA, 0.1 M MES, pH=6.5

4.4.2 *In vitro* relaxometry studies of dual-labeled CA-8 conjugate

The paramagnetic properties of the high molecular weight conjugate **CA-8** were examined at 128 MHz (3T) and room temperature. The longitudinal relaxation times T_1 were measured for six different concentrations of **CA-8** in the range of 5-40 µM. **CA-8** showed reproducibly a relaxivity of 12 $mM^{-1}s^{-1}$. Hence, a significant increase in r_1 in comparison to **CA-4** was observed as summarized in Fig 3. Apparently a covalent attachment of **CA-7** complex to PGA resulted in an efficient decrease of the molecular tumbling rate, due to an increase in molecular weight, leading to the favorable gain in relaxivity. However, the obtained relaxivity of **CA-8,** even if

much higher than that of Gd-DOTA, was lower than expected with this large increase in molecular weight. This can be probably explained by too slow rotation of **CA-8**, that would be certainly profitable for r_1 at low magnetic field (<1.5T) but for higher magnetic fields as the applied 3T, an increase of molecular weight may work in disfavor of observed r_1 value as concluded by Caravan[24].

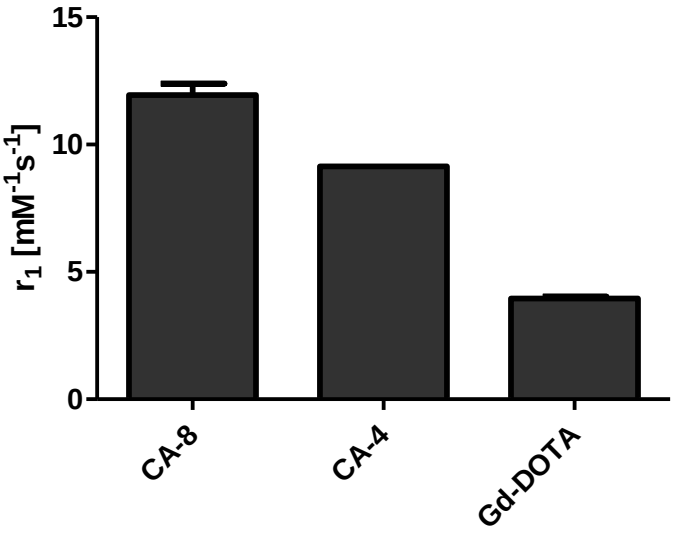

Figure 36. Comparison of r_1 values of **CA-4**, **CA-8** and **Gd-DOTA**.

In general, the established protocol using the pre-loaded bimodal complex **CA-7** for conjugation with PGA proved to be an excellent strategy to achieve efficient labeling of macromolecules for MR and optical imaging. Moreover, in comparison to published data by Lu et al.[239] for a PGA-cystamine-Gd^{3+}-DOTA conjugate the use of the pre-loading approach proved to be advantageous. As reported by the authors a large solubility problem occurred during the complexation of PGA-cystamine-DOTA with gadolinium due to formation of a precipitate after addition of $GdCl_3$. The reason for this was an unspecific binding of the metal ions to the carboxylic groups of PGA. EDTA had to be applied to strip off PGA-bound Gd^{3+}-metal. Furthermore, the described conjugate provided only a relaxivity of 2.5 $mM^{-1}s^{-1}$ per complex, hence, r_1 was much lower as compared to the reported value for Gd-DOTA as pointed out by the authors themselves. This was probably attributed to an incomplete loading of the attached chelates in the molecule. Such problems were not observed during the synthesis of our model

PGA conjugate **CA-8** since the gadolinium pre-loaded complex was used excluding problems associated with nonspecific binding and underloading of attached ligand.

4.5 Summary & Conclusions

A straightforward synthetic strategy was established to obtain middle-size complex **CA-4**. This dual-labeled imaging probe proved to be cell-permeable, however showing very poor uptake at low concentration typically used for CPP conjugated molecules. Thus, relatively high concentrations had to be applied to attain visible cellular accumulation. Such concentrations in the range of 50-100 µM were also typically used for literature reported middle size Gd-chelate with hydrophobic groups. On the other hand even if the observed internalization was modest a still statistically significant increase of cellular relaxation rates could be observed. This was probably due to relatively high relaxivity observed for **CA-4**, which enabled to acquire observable changes in $R_{1,cell}$. The relaxivity of **CA-4** was doubled as compared to Gd-DOTA, what can be ascribed to the potential neighboring effect of FITC and the higher rigidity in the close vicinity of the Gd-chelate. However, in order to understand this behavior in details additional relaxometric studies are required. Although high concentrations were applied, **CA-4** was still well tolerated by cells and therefore can be potentially used to for *in vitro* cell labeling protocols.

The facilitative approach towards the synthesis of bimodal high molecular weight conjugates was established based on application of precursor **CA-7**. The very efficient coupling of this dual-labeled and pre-loaded gadolinium complex to the macromolecular carrier PGA proved its utility for grafting into macromolecules (**CA-8**). The combination of attractive features ascribed to utilize precursor **CA-7** derives from its pre-loading with Gd^{3+} (elimination of nonspecific binding, under- or overloading), the incorporation of two imaging reporters for MR and fluorescent detection to targeted molecule in a single step, mild bioconjugation methods and easy synthesis. Morover as compared to standard procedure amount of salts in sample was significantly reduced. Therefore, the reported complex **CA-7** holds a great potential for efficient and easy labeling of a wide range of organic and/or biomolecules such as proteins, dendrimers, antibodies, polymers etc. as illustrated in Fig 37. In order to explore a feasible scope of its application a conjugation to peptides and proteins as well as further modifications are under progress.

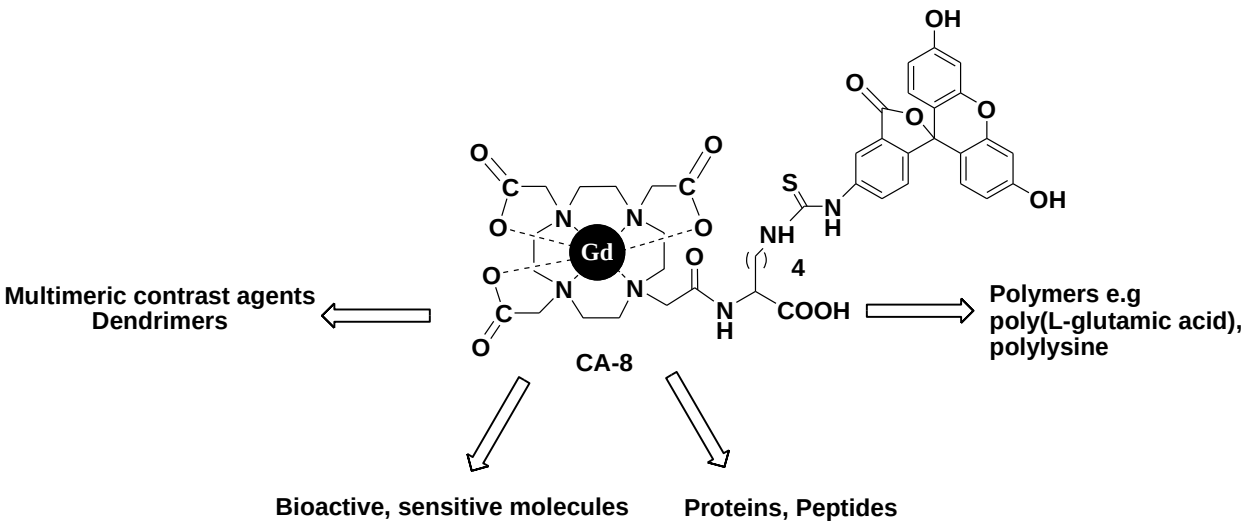

Figure 37. Potential applications of pre-metalated precursor **CA-7.**

5. Summary

The work presented in this doctoral thesis has been divided into three main sections.

In the first part a multistep synthesis was established leading to the successful formation of bimodal intracellular MR contrast agents **CA-1** and **CA-2** based on the galactose moiety serving as enzymatically cleavable spacer between MR reporter and CPP. These conjugates showed advantageously high relaxivity and this phenomenon were investigated by relaxometric comparison with model conjugates **CA-3** and **CA-4.** It was shown that increase in molecular weight and FITC neighboring mainly govern r_1 of **CA-1** and **CA-2**. The internalization studies by fluorescent spectroscopy and microscopy revealed intracellular localization of these conjugates. **CA-1** showed substantially higher levels of intracellular localization in C6/LacZ cells expressing *β*-galactosidase. Although both CAs could efficiently enhance intracellular relaxation rates, their mainly endosomal entrapment hindered the interactions with cytosolic *β*-galactosidase and only a tendency for higher accumulation in transgenic cell lines was observed by MR.

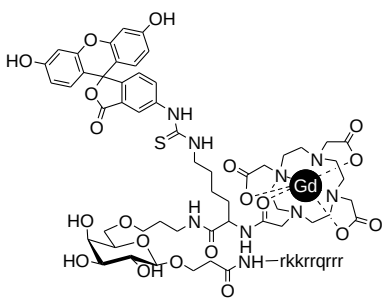

CA-1 (Tat_{49-57})

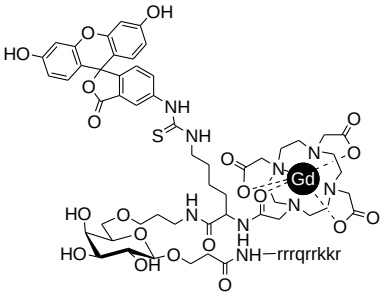

CA-2 (Tat_{57-49})

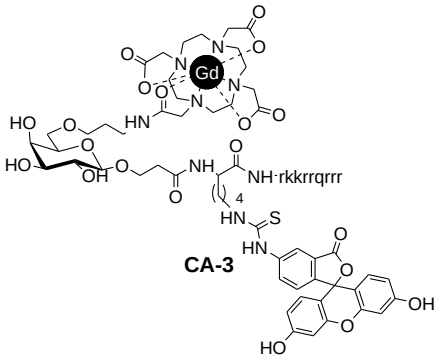

CA-3

In the second phase of the work an influence of molecular structure on enzymatic activity of β-galactosidase was investigated. In order to understand parameters that determine interactions of bulky intracellular MR contrast agents with targeted enzyme, a series of model molecules with introduced particular variations were synthesized and evaluated. Thus, an influence of the modification at glycon part (**CA-5**, **CA-6**) on β-galactosidase was elucidated by incorporation of MR reporters at C6 position of galactose moiety. Further in attempt to investigate an influence of

peptide as well as FITC incorporation via different spacer at C-1 position, a model conjugates **54**, **56** and **61** were synthesized. It was shown that substitution at C-6 position as well as the modifications at aglycone part decresed a rate of enzymatic reaction.

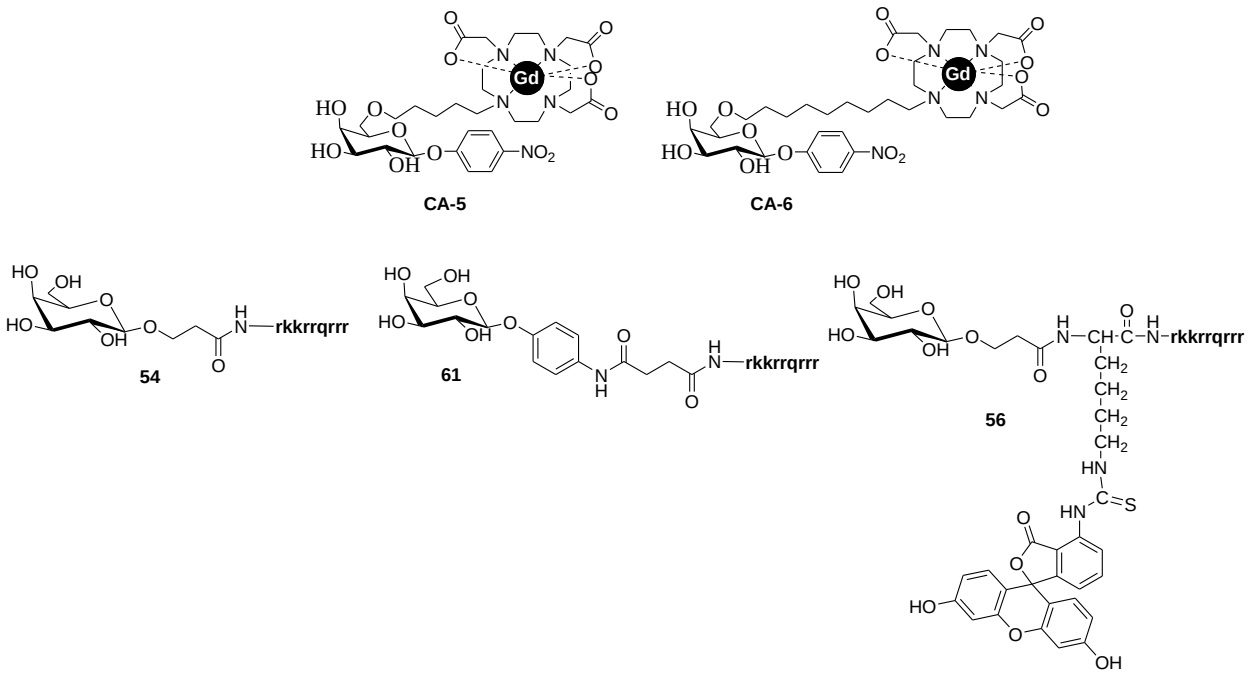

In the third phase of presented work on the base of experiences related to the complexity of synthesizing Gd-loaded dual-labeled bulky conjugates an efficient approach towards synthesis of such conjugates was established. The suitable precursor **CA-7** was obtained, that integrated benefits of preloading approach and bimodality. In order to prove its applicability **CA-7** was appended to macromolecular poly-L-glutamic acid (**CA-8**) using mild bioconjugation methods. In this chapter also middle size Gd^{3+} complex **CA-4** bearing hydrophobic FITC residue was considered as potential intracellular CA, which eventually showed the ability to penetrate across cell membrane.

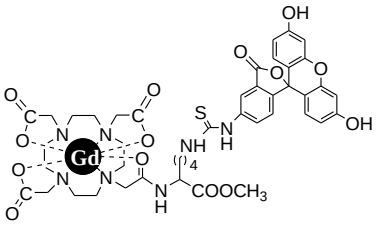

CA-4

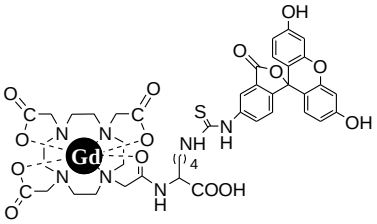

CA-7

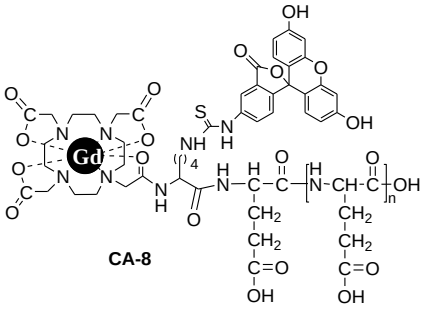

CA-8

6. Experimental part.

6.1 General remarks, materials and intrumentation

All reagents and solvents were purchased from Acros Organics, Fluka, Sigma Aldrich, Merck and used without further purification unless otherwise stated. Tetraazacyclododecane (cyclen) was obtained from Strem Chemicals (Newburyport, USA). The Fmoc protected amino acid derivatives, 2-(1H-benzotriazol-1-yl)-1,1,3,3-tetramethyluronium hexafluoro-phosphate (HBTU), and pre-loaded Wang resin were obtained from Novabiochem. 2-(1-H-7-azabenzotriazol-1-yl)-1,1,3,3-tetramethyluronium hexafluorophosphate (HATU) was purchased from McTony (Canada), dry, anhydrous solvents: N,N'-dimetylformamid (DMF), dichloromethane (DCM), acetonitrile (ACN) were purchased from Acros Organics as Sure-Seal bottles with molecular sieves. Water was purified using a Milipore Milli-Q Synthesis purifier.

Thin Layer Chromatography (TLC)

Aluminium sheet silica gel plates with 0.2-mm-thick silica gel 60 F_{254} (E. Merck, Germany) were used to run thin-layer chromatography using appropriate mobile phases as required. The compounds were visualized by UV_{254} light, were applicable, by charring with 5% H_2SO_4/EtOH (carbohydrates) or were developed in an iodine chamber (DOTA like compounds).

High Performance Liquid Chromatography (HPLC)

Analytical and semi-preparative reversed-phase high performance chromatography (RP-HPLC) were performed at room temperature on a Varian PrepStar Instrument (Australia) equipped with PrepStar SD-1 pump heads. UV absorbance was measured using a ProStar 335 photodiode array detector at 214 and 245 nm. Analytical RP-HPLC was performed in
a Polaris C_{18}-Ether column (4.6 × 250 mm, particle size 5 μm, particle pore diameter 100 Å, Varian, Advanced Chromatographic Solutions) and preparative RP-HPLC were performed in Polaris 5 C_{18}-Ether column (21.2 × 250 mm, 5 μm, 100 Å, Varian Advanced Chromatographic Solutions, flow rate 10 ml/min) or Polaris C8-Ether column (250x100 mm, 5 μm, 100 Å). The compounds were purified by HPLC using one of the following two methods. In Method 1: the linear gradient was used with the mobile phase starting from 90% of solvent A (0.1% TFA/water), 10% of solvent B (0.1 % TFA/acetonitile) isocratic for 5 min and increased to 60% B in 20 min, moving to 90% B in 3 min, and 90 % B isocratic up to 30 min. Alternatively, in

method 2, the linear gradient was used with the mobile phase starting from 80 % of solvent C (0.05% TFA/water), 10% of solvent B (0.05% TFA/acetonitile) isocratic for 5min and increased to 60% B in 20 min, moving to 90% B in 3 min, and 90% B isocratic up to 30 min. The flow rate generally used for analytical HPLC was 1ml/min and 10 ml/min or 4 ml/min for a preparative HPLC. All the injected solutions were filtered through a nylon-66 Milipore filter (0.45mm) prior to purification.

LC-ESI-MS

The analysis of samples was performed using an in house built system consisting of analytical RP-HPLC Beckmann System Gold LC 126 (Germany) and ESI-MS SL 1100 system (Agilent, Germany). The LC system was equipped with 508 Autosampler. UV absorbance was measured using UV 168 detector at 214 and 245 nm. RP-HPLC was performed using a Polaris C_{18}-Ether column (4.6 × 250 mm, particle size 5 µm, particle pore diameter 100 Å, Varian, Advanced Chromatographic Solutions).

NMR spectroscopy

^{1}H, ^{13}C, DEPT, HH-COSY and CH-COSY spectra were recorded on a Bruker 300 MHz or 400 MHz spectrometer (^{1}H; $CDCl_3$ internal reference at 7.27 ppm, DMSO at 2.5 ppm TMS at 0 ppm or D_2O at 4.5 ppm); 75 MHz (^{13}C, internal reference $CDCl_3$ at 77.0 ppm, DMSO at 39.51 or TMS at 0 ppm). All measurements were performed at room temperature.

Mass Spectrometry

Electrospray ionization-mass spectrometry (ESI-MS) spectra were measured on SL 1100 system (Agilent, Germany) with ion-trap detection in positive and negative modes. HR-FT-ICR mass spectra were performed on APEX 2 spectrometer (Bruker Daltonic) with ESI.

Optical Rotation

Optical rotations were measured at 20ºC with Perkin-Elmer Polarimeter 341using a 1dm quartz cell.

Preparative Column Chromatography

Column chromatography was performed using silica gel 60 (70-230 mesh, Merck). The used eleuent were given in each procedure.

6.2 Experimental procedures

2,3,4,6-tetra-O-acetyl-α-D-galactopyranoside bromide (1)

Penta-O-acetyl β-D-galactopyranoside (32 mmol, 12.6 g) was converted to **1** using previously decribed procedure[243]. The product was obtained as colorless oil (12.4 g, 95%), which crystallized upon storage in the fridge.

All spectral data was consistent with that reported in the literature [244]

2- (3-tert-butoxycarbonyl)ethyl-2,3,4,6-tetra-O-acetyl-β-D-galactopyranoside (2)

Method 1:

To **1** (10 mmol, 4.11 g) in dry DCM (100 ml) tert-butyl 3-hydroxypropionate (14 mmol, 2.05 g) and pulverized molecular sieves were added. A reaction mixture was stirred under nitrogen atmosphere for 10 min and temperature was decreases to -20ºC. Silver triflate (12 mmol, 3.08 g) was added and reaction was stirred for 1.5 h at -20ºC and further it was allowed to warm up to 0ºC with continuing the stirring for next 6 h. The progress of conversion was monitored by TLC (R_f=0.4, hexane/ethyl acetate 3:1). After completion, the reaction mixture was diluted with DCM (250 ml), filtered through Celite 545 and washed thoroughly with DCM. The collected filtrates were washed with saturated aqueous $NaHCO_3$, brine and water. The organic layer was dried over Na_2SO_4, filtered and concentrated under reduced pressure. The residue was purified by column chromatography on silica gel (hexane/ethyl acetate) to give 2.24 g (47%) of **3** as colorless syrup.

Method 2:

To a solution of **2** (9.3 mmol, 4.1 g) in dry DCM (320 ml) tert-butyl 3-hydroxypropionate (18.6 mmol, 2.71 g) and pulverized molecular sieves were added. After being stirred for 1 h at room temperature under nitrogen atmosphere, a reaction mixture was cooled to -50ºC and NBS (24.18 mmol, 4.3 g) was added followed by Me_3SiOTf (1.82 mmol, 0.4 g). The stirring was continued for next 1 h at -50ºC at which substrate **2** was consumed as detected by TLC (R_f=0.4, hexane/ethyl acetate 3:1). The reaction mixture was diluted with DCM (200 ml), filtered through Celite 545 and washed thoroughly with DCM. The collected filtrates were washed with saturated aqueous $NaHCO_3$, aqueous $Na_2S_2O_3$, brine and water. The organic layer was dried over Na_2SO_4,

filtered and concentrated *in vacuo*. The residue was purified by column chromatography on silica gel (hexane/ethyl acetate) to give 2.9 g (65%) of **3** as syrup.

$[\alpha_D]^{20}$= -6.2°(c=1.0, $CHCl_3$)

^{1}H-NMR (400 MHz, $CDCl_3$): δ= 1.45 (s, 9H, $C(CH_3)_3$) 1.97 (s, 3H, C*H*$_3$CO), 2.05 (bs, 6H, C*H*$_3$CO), 2.14 (s, 3H, C*H*$_3$CO), 2.4-2.6 (m, 2H,), 3.75-3.96 (m, 1H, OC*H*$_2$), 3.92 (pt, 1H, H-5, *J*=6.61 Hz), 3.98-4.11 (m, 1H, 1H, OC*H*$_2$), 4.11-4.23 (m, 2H, H-6), 4.53 (d, 1H, H-1, J_{1-2}=7.93 Hz), 5.01 (dd, 1H,H-3, J_{3-4}=3.4 Hz, J_{3-2}=10.3 Hz), 5.15 (odd, 1H, H-2, J_{2-1}=7.9 Hz, J_{2-3}=10.4 Hz), 5.98 (d, 1H, H-4, J_{4-3}=3.4 Hz).

^{13}C-NMR (100 MHz, $CDCl_3$): δ= 20.40, 20.48, 20.49, 20.58 (*C*H_3CO), 27.93 (C(*C*H_3)$_3$), 35.74 (*C*H_2), 61.15 (C-6), 65.36 (O*C*H_2CH$_2$), 66.93 (C-4), 68.58 (C-2), 70.51 (C-3), 70.80 (C-5), 80.57 (*C*$(CH_3)_3$), 101.18 (C-1), 169.23, 169.95, 170.07, 170.09, 170.19 (*C*OO).

HRMS(EI) (±) for $C_{21}H_{32}O_{12}$: $[M+Na]^+_{(calcd)}$= 499.17860, $[M+Na]^+_{(found)}$= 499.1788.

Phenyl 2,3,4,6-tetra-O-acetyl-β-D-galactopyranoside (3).

Penta-O-acetyl β-D-galactopyranoside (257 mmol, 100 g) was converted to **3** using previously decribed procedure[154]. The product was obtained as yellowish oil (79 g, 70%). The spectral data were consistent with that reported in the literature[245].

2- (3-tert-butoxycarbonyl)ethyl-β-D-galactopyranoside (4)

A compound **2** (5.8 mmol, 2.76 g) was dissolved in dry MeOH (30 ml) and sodium methoxide was added (pH~9-10). A reaction mixture was stirred for 2 h at room temperature with monitoring a progress of deprotection by TLC (R_f= 0.3, 1:9 MeOH/$CHCl_3$). After completion Dowex® 50Wx8-100 ion-exchange resin was added to neutralize pH of reaction mixture (pH~6-7), which was further filtered and concentrated to give **4** in quantitative yield (1.75 g, 98%) as syrup.

$[\alpha_D]^{20}$= -5.4°(c=1.0, $CHCl_3$)

^{1}H-NMR (400 MHz, DMSO-$_{d6}$): δ= 1.43 (s, 9H, $C(CH_3)_3$), 2.45-2.55 (m, 2H, C*H*$_2$), 3.20 (ps, 1H, H-4), 3.27 (pd, 1H, H-2), 3.43 (pt, 1H, H-5), 3.46-3.58 (m, 2H, H-6) 3.6-3.71 (m, 1H, 2H, H-3, OC*H*$_2$), 3.89-3.99 (m, 1H, OC*H*$_2$),4.08-4.13 (m, 1H, H-1), 4.5-5.05 (obs, 4H, O*H*).

^{13}C-NMR (75 MHz, $CDCl_3$): δ= 27.84 ($C(CH_3)_3$), 35.95 (CH_2), 60.41 (C-6), 64.42 (OCH_2), 68.07, 70.50, 73.53, 75.27, 79.99, 103.62 (C-1), 170.39 (*C*OO).

ESI-MS (+) for $C_{13}H_{24}O_8$ $[M+Na]^+_{(calcd)}$= 331.1, $[M+Na]^+_{(found)}$= 331.0.

2-(3-tert-butoxycarbonyl)ethyl-6-O-tert-butyldimethylsilyl-β-D-galactopyranoside (5)

Procedure 1:

A compound **4** (0.72 mmol, 0.22 g) was dissolved in dry DMF (4 ml) and imidazole (1.7 mmol, 0.12 g) was added. A reaction mixture was cooled to 0ºC and TBDMSCl (1 mmol, 0.15 g) was added portionwise. After 0.5 h at 0ºC a stirring was continued overnight at room temperature. The reaction mixture was poured into ice-cold water and aqueous layer was extracted with ethyl acetate (3x100ml), DCM (1x100ml). The combine dorganic layer were dried over Na_2SO_4, filtered and concentrated. The organic residue was purified by column chromatography on silica gel to give 0.07 g (30%) of **5** as sticky oil.

Procedure 2:

A solution of **4** (2 mmol, 0.61 g) in pyridine (10.4 ml) was cooled to -10ºC and TBDMSCl (3 mmol, 0.45 g) was added portionwise. Triethylamine (3.2 ml) was added dropwise over 10 min and reaction mixture was stirred for 2 h at 0ºC followed by further stirring overnight at room temperature (under nitrogen atmosphere). A progress of silylation was monitored by TLC (R_f=0.7, 1:9 MeOH/ethyl acetate). The reaction mixture was poured into ice-cold water (300ml) and aqueous layer was extracted with DCM (4x200ml). The combined organic layers were dried over Na_2SO_4 and concentrated under reduced pressure. The obtained residue was purified by column chromatography on silica gel (ethyl acetate/hexane) to give 0.42 g (50%) of **5** as sticky oil.

^{1}H-NMR (400 MHz, $CDCl_3$): δ= 0.06 (s, 6H, $SiCH_3$), 0.88 (s, 9H, $SiC(CH_3)_3$), 1.41 (s, 9H, $C(CH_3)_3$), 2.47-2.42 (m, 2H, CH_2), 3.28 (ps, 1H) 3.56-3.77 (m, 3H) 3.85-3.94 (m, 1H) 4.09-4.15 (pd, 1H) 4.40 (pd, 1H), 4.77 (pd, 1H), 4.82 (pd, 1H).

^{13}C-NMR (75 MHz, $CDCl_3$): δ= -5.03 ($SiCH_3$), 18.23, 26.03 ($C(CH_3)_3$), 28.0 ($C(CH_3)_3$), 36.22 (CH_2), 62.76 (C-6), 64.75 (OCH_2), 68.37, 70.57, 73.57, 75.35 (C-4, C-2, C-3, C-5) 80.08 ($C(CH_3)_3$), 103.88 (C-1), 170.39.

ESI-MS (+) for $C_{19}H_{38}O_8Si$ $[M+Na]^+_{(calcd)}$= 445.2, $[M+Na]^+_{(found)}$= 445.1.

Phenyl-1thio-β-Phenyl-1-thio-β-D-galactopyranoside (7)

O-acetyl deprotection of **2** (150 mmol, 66 g) was carried out in dry MeOH (500 ml) in the presence of sodium methoxide. The progress was monitored by TLC. After completion reaction mixture was neutralized with Dowex ®50Wx8-100 ion-exchange resin (pH~6), filtered and concentrated to give **7 (**40 g, 98%**)** in the form of oil**.** The spectral data were consistent with that reported in the literature[154].

m.p. 115-116°C (lit. 105-107°C) [154]

Phenyl 6-(O-tert-butyldimethylsilyl)-1-thio-β-D-galactopyranoside (8)

To a solution of **7** (78.96 mmol, 21.5 g) in dry pyrdine (310 ml) TBDMSCl (118.4 mmol, 17.84 g) was added portionwise, followed by Et_3N addition over 20 min at -10 ºC under nitrogen. The reaction mixture was stirred at -10 ºC for 1 h, slowly warmed up to room temperature and stirred for next 20 h until the starting material was consumed as monitored by TLC (R_f= 0.9, MeOH: EtOAc 9:1). The mixture was diluted with DCM (400 ml), poured into the ice-cold water and extracted with DCM (4x). The combined organic layers were washed with $NaHCO_3$ saturated, brine, dried over Na_2SO_4, filtered and concentrated. The organic residue was purified by column chromatography (hexane: ethyl acetate) to yield **4** as a yellow viscous oil (80%, 24.42 g).

$[\alpha_D]^{20}$= -45.6°(c=0.8, MeOH)

^{1}H-NMR (300 MHz, DMSO-$_{d6}$): δ= 0.05, 0.07 (2s, 2x3H, SiC*H*$_3$), 0.9 (s, 9H, C(C*H*$_3$)$_3$, 3.37-3.50 (m, 2H, H-2, H-3), 3.52-3.64 (m, 1H, H-5), 3.68-3.77 (m, 3H, H-6, H-4), 4.54 (pd, 1H, OH), 4.64 (d, 1H, $J_{1\text{-}2}$=9.1 Hz, H-1), 4.97 (pd, 1H, OH), 5.18 (pd, 1H, OH), 7.20-7.36 (m, 3H, Ar-*H*), 7.45-7.51 (m, 2H, Ar-*H*)

^{13}C-NMR (75 MHz, DMSO-$_{d6}$): δ=-5.28, -5.44 (Si*C*H$_3$), 17.98 (*C*(CH$_3$)$_3$), 25.81(C(*C*H$_3$)$_3$), 62.89 (C-6), 68.50, 69.16, 74.56 (C-4, C-2, C-3), 79.04 (C-5), 87.80 (C-1), 126.03 128.71, 129.07, 135.72 (ArH).

HRMS (EI) (±) for $C_{18}H_{30}O_5SSi$: $[M+Na]^+_{(calcd)}$= 409.14754, $[M+Na]^+_{(found)}$= 409.14752

Phenyl 2,3,4-tri-O-(*4*-metoxybenzyl)-6-(O-tert-butyldimethylsiloxypropyl)-1-thio-β-D-galactopyranoside (9)

To a solution of **8** (32.8 mmol, 12.64 g) and 4-methoxybenzyl bromide (115 mmol, 23 g, 16.6 ml) in anhydrous DMF (400 ml) at -10°C sodium hydride (115 mmol, 4.6 g, 60% dispersion in mineral oil) was added. The reaction mixture was stirred at -10°C for 30 min and next for 4 h at room temperature. The progress was monitored by TLC (hexane: ethyl acetate 1:1, R_f= 0.7). The reaction was cooled down to 0°C, diluted with cold water and extracted three times with diethyl ether, followed by ethyl acetate extraction. The combined organic layers were washed with water and brine, dried over Na_2SO_4, filter and concentrated under the vacuum. The residue was purified by column chromatography (ethyl acetate-hexane) to yield **9** as the yellowish, viscous oil (70%, 17.1 g).

$[\alpha_D]^{20}$= +1.6°(c=1.0, $CHCl_3$)

^{1}H-NMR (300 MHz, $CDCl_3$): δ= 0.02, 0.03 (2s, 6H, SiCH3), 0.87 (s, 9H, C(C*H*$_3$)$_3$)), 3.40 (pt, 1H, H-5, *J*=6.52), 3.54 (dd, 1H, H-3, $J_{3\text{-}2}$= 11.9 Hz, $J_{3\text{-}4}$= 2.64 Hz), 3.57-3.77 (m, 2H, H-6), 3.79, 3.81 (os, 9H, C*H*$_3$), 3.83-3.95 (m, 2H, H-4, H-2), 4.55 (d, 1H, *J*=11.4 Hz), 4.60 (d, 1H, H-1, $J_{1\text{-}2}$=9.63 Hz), 4.64-4.74 (m, 4H, OC*H*$_2$), 4.90 (d,1H, *J*=10.95 Hz),

^{13}C-NMR (75 MHz, $CDCl_3$): δ= -5.51, -5.27 (Si*C*H$_3$), 18.16 (*C*(CH$_3$)$_3$), 25.86 (C(*C*H$_3$)$_3$), 55.23 (CH3), 61.72 (C-6), 72.44 (OCH2), 73.14 (C-4), 74.00 (OCH2), 75.18 (OCH2), 77.03 (C-2), 78.96 (C-5), 83.92 (C-3), 87.79 (C-1), 113.51, 113.69, 113.77, 126.76, 128.69, 129.19, 129.30, 129.36, 129.92, 130.42, 130.49, 130.63, 131.13, 134.51, 158.99, 159.17, 159.22 (ArH).

HRMS (EI) (±) for $C_{42}H_{54}O_8SSi$: $[M+Na]^+_{(calcd)}$= 769.32009, $[M+Na]^+_{(found)}$= 769.32018

Phenyl 2,3,4-tri-O-(4-metoxybenzyl)-6-hydroxy-1-thio-β-D-galactopyranoside (10)

1M solution of TBAF in THF (15.6 ml) was added dropwise at 0ºC under nitrogen to a suspension of compound **9** (22.35 mmol, 16.67 g) and pulverized molecular sieves (4Å) in freshly distilled THF (117 ml). The reaction mixture was allowed to warm up to the room temperature (~1 h) and stirred for 6 h. After the completion as monitored by TLC, the reaction mixture was filtered through Celite 545, which was washed sorely with ethyl acetate. The collected filtrate was concentrated under the vacuum and residue was re-dissolved in ethyl

acetate, washed with saturated aqueous $NaHCO_3$ and water. The organic layer was dried over Na_2SO_4, filtered and concentrated in vacuo. The crude product was purified on silica gel by column chromatography using hexane/ethyl acetate as eluent (R_f =0.49, hexane: ethyl acetate 1:1) to afforded **10** in 69% as a white foam.

m.p. [120-121ºC]

$[\alpha_D]^{20}$= -2.4°(c= 0.8, $CHCl_3$)

^{1}H-NMR (300 MHz, $CDCl_3$): δ= 3.35-3.3.52 (m, 1H, H-5, 1H, H-6), 3.55 (dd, 1H, H-3, J_{3-2}= 9.3 Hz, J_{3-4}= 2.83Hz), 3.75-3.85 (m, 11H, H-6, CH_3, H-4), 3.90 (pt, 1H, H-2, *J*=9.44 Hz), 4.56 (d, 1H, OCH_2, *J*=11.52 Hz), 4.62 (d, 1H, H-1, J_{1-2}=9.63 Hz), 4.65-4.79 (m, 4H, OCH_2), 4.88 (d, 1H, *J*=11.33 Hz), 6.82-6.94 (m, 6H, ArH), 7.14-7.37 (m, 9H, ArH), 7.48-7.57 (m, 2H, ArH).

^{13}C-NMR (75 MHz, $CDCl_3$): δ= 55.23 (*C*H_3), 62.23 (C-6), 72.68 (O*C*H_2), 72.74 (C-4), 73.64 (O*C*H_2), 75.26 (O*C*H_2), 77.23 (C-2), 78.72 (C-5), 83.91(C-3), 87.75 (C-1), 113.71, 113.73, 113.84, 127.06, 128.79, 129.21, 129.90, 130.27, 130.37, 130.45, 131.37, 134.08, 159.26 (ArH).

HRMS (EI) (±) for C36H40O8S: $[M+Na]^+_{(calcd)}$= 655.23361, $[M+Na]^+_{(found)}$= 655.23398.

Phenyl 2,3,4-tri-O-(4-metoxybenzyl)-6-((benzyloxycarbonyl)amino)propyl)-1-thio-β-D-galactopyranoside (11)

Sodium hydride (47.6 mmol, 1.9 g, 60 % dispersion in mineral oil) was added portionwise at -10ºC to a solution of **10** (14.5 mmol, 9.16g) in DMF (95 ml) under nitrogen. The reaction mixture was stirred for 30 min. at -10ºC and N-benzyloxycarbonyl-3-bromopropylamine (58 mmol, 15.8 g) dissolved in DMF (13 ml) was added. The stirring was continued at -10ºC for half an hour and then at room temperature. The progress of the reaction was monitored by TLC. After 24 h the reaction mixture was cooled down to 0ºC, methanol (7 ml) was added slowly to destroy the excess of NaH, stirred for 10 min and diluted with ethyl acetate (250 ml). The reaction mixture was poured into ice-cold water, organic layer was separated and water layer was extracted with ethyl acetate (3x), DCM (1x). The combined organic extracts were dried over Na_2SO_4, filtered and concentrated in vacuo. The obtained residue was purified by silica gel column chromatography with hexane/ethyl acetate (5:1-3:1) as eluent (R_f= 0.6, hexane: ethyl acetate 1:1) to give 5.37 g (45%) of **11** after the purification as the white viscous oil.

$[\alpha_D]^{20}$= +6.8°(c= 0.9,$CHCl_3$)

^{1}H-NMR (300 MHz, $CDCl_3$): δ=1.63-1.75 (m, 1H, C*H*$_2$NH), 3.1-3.29 (m, 2H, C*H*$_2$NH), 3.3-3.65 (m, 5H, H-5, H-6, OC*H*$_2$CH$_2$, H-3,), 3.7-3.95 (m, 12H, H-6, C*H*$_3$, H-2, H-4), 4.54 (d, 1H, OCH$_2$, *J*=11.33 Hz), 4.60 (d, 1H, H-1, $J_{1\text{-}2}$=9.82 Hz)4.64-4.75 (m, 4H, OC*H*$_2$), 4.88 (d, 1H, OCH$_2$, *J*=11.33 Hz), 4.95-5.2 (2 os, 3H, PhCH2, NH)), 6.8-6.91 (m, 6H, Ar*H*), 7.1-7.4 (m, 14 H, ArH), 7.5-7.6 (m, 2H, ArH).

^{13}C-NMR (75 MHz, $CDCl_3$): δ= 22.60 (CH_2), 38.86 (CH_2NH), 55.22(*C*H$_3$), 66.47 (C-6), 69.47, 69.64 (O*C*H$_2$CH$_2$, O*C*H$_2$Ph) 72.43 (O*C*H$_2$),, 73.11 (C-4), 73.87, 75.20 (O*C*H$_2$), 77.20 (C-2), 77.30 (C-5), 83.92 (C-3), 87.77 (C-1), 113.55, 113.68, 113.78, 126.93, 128.0, 128.43, 128.69, 129.16, 129.48, 129.89, 130.38, 130.53, 130.81, 131.34, 134.36, 136.61, 156.29, 159.07, 159.17, 159.23 (ArH).

HRMS (EI) (±) for $C_{47}H_{53}NO_{10}S$: $[M+K]^+_{(calcd)}$= 862.30218, $[M+Na]^+_{(found)}$= 862.3021

Phenyl 6-((benzyloxycarbonyl)amino)propyl-1-thio-β-D-galactopyranoside (12)

Compound **11** (6.20 mmol, 5.2 g) was dissolved in DCM (90 ml) and water (3 ml) was added, followed by the DDQ (27.83 mmol, 6.32 g) addition. The reaction was stirred for 24 h at room temperature, diluted with DCM, filtered and washed with aqueous saturated NaHCO3, aqueous $Na_2S_2O_3$ and brine. The organic layer was dried over Na_2SO_4, filtered and concentrated. The residue was purified on silica gel by flush column chromatography (MeOH/DCM, R_f= 0.6 MeOH: EtOAc 1:9) to yield **12** as white solid (1.7 g, 60%).

$[\alpha_D]^{20}$= -30.2°(c=0.9, MeOH)

^{1}H-NMR (300 MHz, $CDCl_3$): δ=1.51-1.7 (pm, 1H, C*H*$_2$NH), 3.1-3.52 (m, 4H, C*H*$_2$NH, OC*H*$_2$CH$_2$), 3.54-3.7 (m, 4H, H-3, H-5, OH), 3.72-3.41 (m, 5H, H-6, H-2, H-4, OH), 4.55 (d, 1H, H-1, $J_{1\text{-}2}$=9.63 Hz), 5.04 (s, 2H, OCH$_2$Ph), 5.25 (bs, N*H*), 7.2-7.38 (m, 8H, Ar*H*), 7.45-7.55 (m, 2H, Ar*H*).

^{13}C-NMR (75 MHz, $CDCl_3$): δ= 29.72 (CH_2), 38.15 (CH_2NH), 66.64 (O*C*H$_2$Ph)), 68.76 (O*C*H$_2$CH$_2$), 68.94 (C-4), 69.54 (C-6), 69.97 (C-2), 74.78, 77.06 (C-5, C-3), 88.66 (C-1), 113.64, 113.71, 127.53, 128.04, 128.46, 128.86, 131.74, 133.48, 136.48, 156.65 (ArH)

HRMS (EI) (±) for $C_{23}H_{29}NO_7S$: $[M+K]^+_{(calcd)}$= 486.15569, $[M+Na]^+_{(found)}$= 486.15571

Phenyl 2,3,4-tri-O-acetyl-6-((benzyloxycarbonyl)amino)propyl-1-thio-β-D-galactopyranoside (13)

Pyridine (13 ml) was placed in the flask (under nitrogen), cooled to -10ºC and acetic anhydride (10.7 ml) was added. Compound **12** (1.57 g, 3.4 mmol) was dissolved in 3 ml of pyridine and added dropwise to a solution of pyridine/acetic anhydride (6ml/6 ml 3:2 v/v). The reaction mixture was allowed to warm up to the room temperature and stirred overnight. The progress of reaction was monitored by TLC. After 24 h a reaction mixture was diluted with ethyl acetate (100ml) and poured into ice-cold water. The organic layer was separated and the water layer was extracted with ethyl acetate (3x 150 ml). Combined organic layers were dried over Na_2SO_4, filtered and concentrated. The organic residue was purified by column chromatography (silica gel, hexane/ethyl acetate 3:1-2:1) to give **13** (1.7 g, 85%) as a colorless syrup (R_f= 0.7, hexane: EtOAc 1:1 v/v).

$[\alpha_D]^{20}$= +2.0°(c=0.9, $CHCl_3$)

^{1}H-NMR (300 MHz, $CDCl_3$): δ= 1.63-1.76 (m, 2H, CH_2), 1.97, 2.09, 2.11 (3s, 3x3H, C*H*$_3$CO), 3.14-3.30 (m, 2H, C*H*$_2$NH), 3.32-3.61 (m, 2H, H-6, 2H, OC*H*$_2$CH$_2$), 3.76-3.87 (m, 1H, H-5), 4.72 (d, 1H, H-1, $J_{1\text{-}2}$= 10 Hz), 4.99-5.18 (m, 4H, H-3, PhC*H*$_2$, N*H*), 5.24 (dd, 1H, H-2, $J_{2\text{-}1}$= 10 Hz, $J_{2\text{-}3}$= 10 Hz), 5.44 (pd, 1H, H-4, $J_{3\text{-}4}$= 3Hz), 7.24-7.39 (m, 8H, Ar*H*), 7.45-7.53 (m, 2H, Ar*H*).

^{13}C-NMR (75 MHz, $CDCl_3$): δ= 20.55, 20.62, 20.81 (CO*C*H3), 29.44 (*C*H$_2$CH$_2$NH), 38.30 (*C*H$_2$NH), 66.41 (PhCH$_2$), 67.49, 67.73 (C-2, C-4), 68.60 (OCH$_2$), 69.22 (C-6), 72.05 (C-3), 77.75 (C-5), 86.59 (C-1), 127.97, 128.86, 132.74, 136.74 (Ar), 156.45 (NH*C*OO), 169.45, 169.94, 170.34 (CH$_3$*C*O).

HRMS (EI) (±) for $C_{29}H_{35}NO_{10}S$: $[M+K]^+_{(calcd)}$= 628.16133, $[M+K]^+_{(found)}$= 628.16124

3-(2,3,4-tri-O-acetyl-6-((benzyloxycarbonyl)amino)propyl))-β-D-galactopyranos-1-yl)-propionate (14)

To a solution of **13** (2.6 mmol 1.53 g,) in dry DCM (90 ml) under nitrogen tert-butyl 3-hydroxypropionate (5.2 mmol, 0.76 g,) in DCM (1 ml) and pulverized molecular sieves (4Å)

were added. The reaction mixture was stirred for 1 h at room temperature and then cooled down to -50ºC. NBS (6.72 mmol, 1.2 g) was added followed by Me_3SiOTf (0.5 mmol, 0.11g) addition and stirring was continued for next 45 min at which time the substrate **13** was fully consumed as detected by TLC. The reaction mixture was diluted with DCM (150 ml), filtered through Celite 545 and washed thoroughly with DCM. The collected filtrate was washed with saturated aqueous $NaHCO_3$, aqueous $Na_2S_2O_3$, brine and water. The organic layer was dried over Na_2SO_4, filtered and concentrated in vacuo. The residue was purified by column chromatography (silica gel, hexane/ethyl acetate 3:1, R_f= 0.45) to give **14** (0.81 g, 50%) as a colorless syrup.

$[\alpha_D]^{20}$= -6.9°(c=0.9, $CHCl_3$)

^{1}H-NMR (300 MHz, $CDCl_3$): δ= 1.44 (s, 9H, C(C*H*$_3$)$_3$), 1.61-1.84 (m, 2H, C*H*$_2$CH$_2$), 1.97, 2.04, 2.13 (3s, 3x3H, C*H*$_3$CO), 2.28-2.62 (m, 2H, C*H*$_2$COO), 3.08-3.63 (m, 6H, C*H*$_2$O, C*H*$_2$NH), 3.67-3.87 (m, 2H, H-5, H-6), 3.93-4.10 (m, 1H, H-6), 4.48 (d, 1H, $J_{1,2}$=7.7 Hz, H-1), 5.0 (dd, 1H, H-3, J_{3-2}=10.4 Hz, J_{3-4}=3.4 Hz), 5.09 (os, 2H, Ph*C*H$_2$O)5.11-5.27 (m, 2H, H-2, N*H*), 5.41 (d, 1H, H-4, $J_{3,4}$=3.1 Hz), 7.24-7.43 (m, 5H, Ar*H*)

^{13}C-NMR (75 MHz, $CDCl_3$): δ= 20.56, 20.65, 20.74 (CO*C*H3), 28.04 (C(*C*H$_3$)$_3$), 29.43 (CH$_2$), 35. 83 (*C*H$_2$) 38.41 (*C*HNH), 65.45 (*C*H$_2$O$_{C-6}$), 66.40 (*C*H$_2$O$_{C-1}$), 67.63 (C-4), 68.47 (C-6), 68.96 (C-2), 69.35 (Ph*C*H$_2$O), 71.01 (C-3), 71.89 (C-5), 80.69 (*C*(CH$_3$)$_3$), 101.30 (C-1), 127.98, 128.01, 128.44 (Ph), 136.77 (Ph), 156.46 (NH*C*O), 169.45, 170.05, 170.27 (CH$_3$*C*O), 170.44 (CH$_2$*C*OO)

HRMS (EI) (±) for $C_{30}H_{43}NO_{13}$: $[M+NH_4]^+_{(calcd)}$= 643.30736, $[M+NH_4]^+_{(found)}$= 643.30736

3-((2,3,4-tri-O-acetyl-6-((N-9-fluoroenylmethoxycarbonyl)amino)propyl))-β-D-galactopyranos-1-yl)-propanoic acid (16)

To a solution of **14** (1.27 mmol, 0.56 g) in DCM (24 ml) a neat TFA (24 ml) was added at 0ºC and the mixture was stirred at room temperature for 15 h, then evaporated and co-evaporated with toluene to give a mixture of crude **15** and partially deprotected intermediate with remaining Cbz group. The organic residue was dissolved in ethanol (50 ml), 10% Pd/C (0.2 g) and few drops of formic acid (pH~4) were added. The reaction mixture was flushed with N_2, then with H_2 and stirred for 8 h under a hydrogen atmosphere (2 bars). After flushing with nitrogen, the solution was filtered by Celite 545, sorely washed with ethanol and concentrated to give crude

15. This material was dissolved in the mixture of dioxane and water (90 ml, 1:1v/v) and solid Na_2CO_3 (3.0 mmol, 0.32 g) was added. The reaction mixture was ultrasonicated for 15 min, cooled down to 0ºC, Fmoc-OSu (1.9 mmol, 0.64 g) was added and stirring was continued for next 6 h. The reaction mixture was acidified with aqueous HCl to pH ~ 5, diluted with water and water layer was extracted three times with DCM. The collected organic layers were dried over Na_2SO_4, filtered and concentrated in vacuo. The organic residue was purified on silica by column chromatography (starting with DCM and slowly increased to 5% MeOH/DCM) to yield 0.5 g (64%) of **16** as greenish oil after three steps.

$[\alpha_D]^{20}$= +2.8°(c=1.0, $CHCl_3$)

^{1}H-NMR (300 MHz, $CDCl_3$): δ= 1.65- 1.8 (m, 2H, C*H*$_2$CH$_2$NH), 1.97, 2.04, 2.14 (3s, 3x3H, COC*H*$_3$, 2.53-2.69 (m, 2H, C*H*$_2$COOH), 3.1-3.6 (m, 6H, C*H*$_2$NH, CH$_2$OC*H*$_2$, H$_a$-6, H$_b$-6), 3.75-3.94 (m, 2H, H-5, OC*H*$_2$CH$_2$COOH), 4.0-4.15 (m, 1H, OC*H*$_2$CH$_2$COOH), 4.17-4.29 (pt, 1H, C*H*Fmoc), 4.32-4.57 (m, 3H, OC*H*$_2$Fmoc, H-1), 4.95-5.09 (dd, 1H, $J_{3\text{-}4}$= 3.2 Hz, $J_{3\text{-}2}$= 10.4 Hz, H-3), 5.12-5.22 (dd, 1H, H-2, $J_{2\text{-}1}$= 8.0 Hz, $J_{2\text{-}3}$= 10.4 Hz), 5.3 (s, 1H, NH), 5.42 (pd, 1H, H-4), 7.27-7.35 (t, 2H, Fmoc), 7.36-7.45 (t, 2H, Fmoc), 7.60 (d, 1H, Fmoc), 7.76 (d, 1H, Fmoc).

^{13}C-NMR (75 MHz, $CDCl_3$): δ= 20.53, 20.64 (CO*C*H$_3$), 29.36 (*C*H$_2$CH$_2$NH), 34.68 (*C*H$_2$COOH), 38.19 (*C*H$_2$NH), 47.25 (*C*HFmoc), 65.37 (OC*H*$_2$CH$_2$COOH), 66.36 (NHCOO*C*H$_2$), 67.64 (C-4), 68.37 (C-6), 68.92 (C-2), 69.09 (CH$_2$O*C*H$_2$), 70.90 (C-3), 71.90 (C-5), 101.57 (C-1), 119.91, 124.99, 126.98, 127.62, 143.91 (Fmoc), 156.62 (NH*C*O), 169.61, 170.08, 170.52 (*C*OCH$_3$), 175.19 (COOH)

HRMS (EI) (±) for $C_{33}H_{39}NO_{13}$: $[M+K]^+_{(calcd)}$= 696.20530, $[M+K]^+_{(found)}$= 696.20540

Synthesis of CA-1 and CA-2

Solid phase synthesis of peptides 17 and 18

Peptides were synthesized manualy using Heidolph Synthesis 1 synthesizer by the Fmoc SPPS method on the pre-loaded polysterene-based Wang resin containing Fmoc/Pbf protected arginine (loading 0.4 mmol/g). The resin (0.08 mmol, 200 mg) was initially washed with DCM (2x) and swollen for 30 min in DCM, followed by a further washing with DMF (6x). The Fmoc group

was removed by treatment with 20% piperidine/DMF (2x10 min). The resin was drained and washed with DMF (4x) after each deprotection and coupling step. The amino acids were coupled to the resin by adding a pre-activated mixture of an appropriate Fmoc-protected amino acid (4 eq)[Fmoc/Boc-lysine, Fmoc/Pbf-arginine, Fmoc/Trt-glutamine, HBTU (3.6 eq)/HOBt (3.6 eq) in DMF (2 ml) and DIPEA (8 eq) and allowing the mixture to stir for 1 h under nitrogen. All coupling steps were followed by a Kaiser test on the resin to indicate presence (deprotection) or absence (coupling) free amino group. The Fmoc-protected peptides D-$Tat_{47\text{-}59}$ ($FmocR_{(Pbf)}K_{(Boc)}K_{(Boc)}R_{(Pbf)}R_{(Pbf)}Q_{(Trt)}R_{(Pbf)}R_{(Pbf)}R_{(Pbf)}$) and D-$Tat_{59\text{-}47}$ ($FmocR_{(Pbf)}R_{(Pbf)}$ $R_{(Pbf)}$ $Q_{(Trt)}$ $R_{(Pbf)}$ $R_{(Pbf)}$ $K_{(Boc)}$ $K_{(Boc)}$ $R_{(Pbf)}$) bound to the Wang resin were obtained. The aliquots of resin bound Fmoc protected D-Tat-peptides were cleaved with TFA/water/TIPS/m-cresol (90:5:2.5:2.5) and analyzed by ESI-MS. The observed masses were consistent with the calculated molecular weight (1560.9) of the D-Tat peptides.

ESI-MS (+): m/z= 781.6 ($(M+2H)^{2+}$) , 521.6 ($(M+3H)^{3+}$)

Conjugation of "sugar core" 16, 28 and FITC with D-Tat peptides

The resin bound peptide was deprotected with 20% piperidine/DMF and washed thoroughly with DMF (6x). Coupling of sugar building block **16** was performed by adding of pre-activated solution of Fmoc protected compound **16** (3eq), HATU (3 eq) in DMF (3 ml) and DIPEA (6 eq) to the resin. After 3 h of coupling under nitrogen atmosphere, the resin was washed with DMF (4x). After Fmoc group deprotection of intermediate **19**, Fmoc-Lys(Dde)-OH residue was coupled to the free amino group of sugar. The Fmoc-Lys(Dde)-OH (4eq) and HATU (4 eq) were dissolved in DMF (3 ml), DIPEA (8 eq) was added and resulting solution was added to the reaction mixture and was allowed to react for 3 h under nitrogen to afford **20.** The Fmoc group was removed by treatment with piperidine and resin was washed with DMF (4x). Coupling of DOTA tris(*tert*-butyl) ester to the α-NH_2 group of Lys was carried out by adding a pre-activated solution of HATU (4eq), DOTA tris(tert-butyl) ester (4 eq) in DMF (3 ml) and DIPEA to the resin and reacted for 24 h under nitrogen. The Dde group of intermediate **21** was removed by treatment with 2% hydrazine hydrate in DMF (2x4min) and FITC was reacted with ε-NH_2 group of Lys (FITC (4 eq): DIPEA (8 eq), DMF (3ml)) within 12 h. All coupling steps were followed by a Kaiser test on the resin.

Cleavage of conjugates 24a, 24b from the resin

The resin was washed with DMF (4x), DCM (4x) and MeOH (6x) and dried under vaccum. The resin attached conjugates **22** were cleaved off the resin with TFA/water/TIPS/m-cresol (90:5:2.5:2.5 v/v/v/v) cocktail for 4 h and washed with TFA. The crude product was precipitated with cold (-20ºC) tert-butyl methyl ether (MTBE). The obtained precipitant was washed with additional amount of MTBE (2x), centrifuged and re-suspended in neat TFA. After precipitation with cold MTBE and centrifugation, the crude product was dissolved in H_2O/t-BuOH (2:1v/v) and lyophilized to afford crude **24a** and **24b** as the orange powder. These conjugates were purified by semi-preparative reversed phase HPLC column using a method A (flow rate 10 ml/min). The obtained products were characterized by ESI-MS. The detected molecular ions were consistent with the calculated mass of **24a** and **24b** (2659.34).

24a

ESI-MS (+): m/z= 1331.2 $((M+2H)^{2+})$, 1136.1 $((M\text{-}FITC)+2H)^{2+})$, 887.8 $((M+3H)^{3+})$, 758.2 $((M\text{-}FITC)+3H)^{2+})$ 666.1 $((M+4H)^{4+})$, 390 (FITC)

24b

ESI-MS (+): m/z =1331.2 $((M+2H)^{2+})$, 887.8 $((M+3H)^{3+})$, 757.9 $((M\text{-}FITC)+3H)^{2+})$ 666.1 $((M+4H)^{4+})$, 390 (FITC)

***O*-acetyl deprotection of 24a** or **24b (23a** and **23b)**

The acetyl protected compound (**24a** or **24b)** was dissolved in dry MeOH, cooled to 0ºC and hydrazine hydrate (in the ratio 1:6 v/v with MeOH) was added slowly. The resulting reaction mixture was stirred at 0ºC for 30 min and then stirring was carried out at room temperature. The progress of the reaction was monitored by LC-MS system. After 12 h the reaction mixture was cooled to 0ºC and acetone was added slowly until resulting pH~5. The organic solvents were removed in vacuo. The obtained crude product **23a** and **23b** were re-dissolved in water, lyophilized and purified by semi-preparative RP-HPLC column using a method 1 (flow rate 10 ml/min). The obtained fractions were collected and solvents removed under vacuum, followed by dissolving the sample in ultra pure water and lyophilisation. The obtained ligands **23a** and **23b** were characterized by ESI-MS. The detected molecular ions were consistent with the calculated mass of **23a** and **23b** products (2533.31).

23a

ESI-MS (+): m/z =1268.5 ((M+2H)$^{2+}$), 1073.4((M-FITC)+2H)$^{2+}$), 845.9 ((M+3H)$^{3+}$), 716.2 ((M-FITC)+3H)$^{2+}$) 634.7 ((M+4H)$^{4+}$), 390 (FITC)

23b

ESI-MS (+): m/z = 1268.5 ((M+2H)$^{2+}$), 1074.4 ((M-FITC)+2H)$^{2+}$) 845.9 ((M+3H)$^{3+}$), 716.1 ((M-FITC)+3H)$^{2+}$) 634.6 ((M+4H)$^{4+}$), 390 (FITC)

Preparation of Gd^{3+} complexes of ligands 23a and 23b (CA-1 and CA-2)

The real concentration of ligand **23a**, **23b** was determined based on the absorbance of FITC. Ligand **23a** or **23b** (1eq) was dissolved in ultrapure water. The titrated solution of $GdCl_3x6H_2O$ (0.9 eq) in water was added dropwise (pH was kept above 5.5 for the duration of the gadolinium addition). The pH was adjusted to 6-6.5 with 0.1M NaOH. The solution was stirred at 40 ºC for 12 h and then stirring was continued at room temperature for 3 days. The pH was checked periodically and adjusted to 6.5. The reaction mixture was freeze dried and further purified by semi-preparative reversed phase HPLC column using a method 2 and 0.05% TFA in water/acetonitrile gradient as mobile phase (flow rate 4 ml/min). The obtained product after lyophilization was characterized by ESI-MS with observed appropriate isotopes pattern. The detected molecular ions were consistent with the calculated mass of **CA-1** and **CA-2** (2688.21g/mol).

CA-1

ESI-MS (-): m/z= 2687.0 ((M-H)$^{1-}$), 1343.5 ((M-2H)$^{2-}$).

ESI-MS (+): m/z= 1345.6 ((M+2H)$^{2+}$), 897.0 ((M+3H)$^{3+}$), 767.6 ((M-FITC)+3H)$^{2+}$), 673.0 ((M+4H)$^{4+}$), 538.7 ((M+5H)$^{5+}$), 390 (FITC)

CA-2

ESI-MS (+): m/z =1345.8 ((M+2H) $^{2+}$), 897.8 ((M+3H)$^{3+}$), 768.6 ((M-FITC)+3H)$^{2+}$) 390 (FITC)

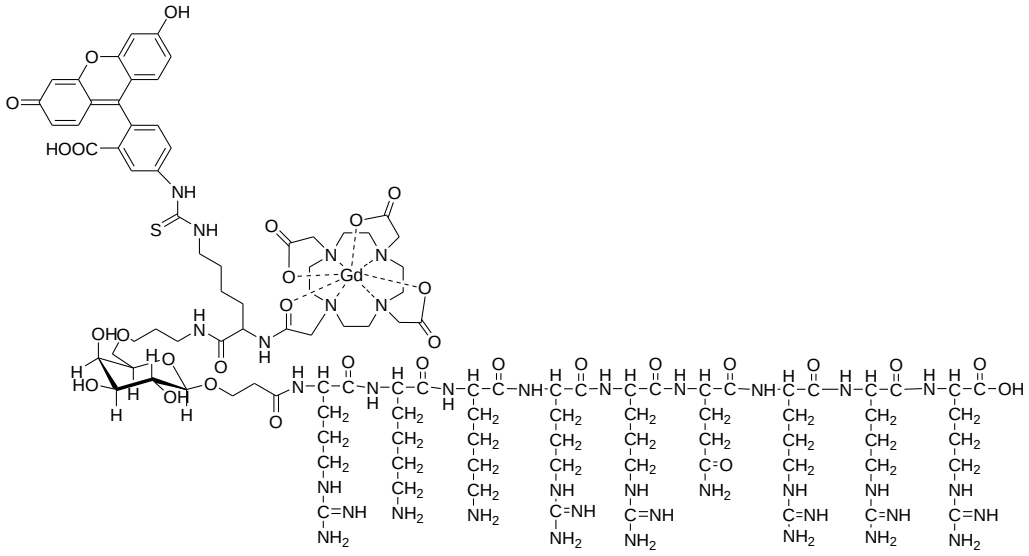

Chemical structure of **CA-1**

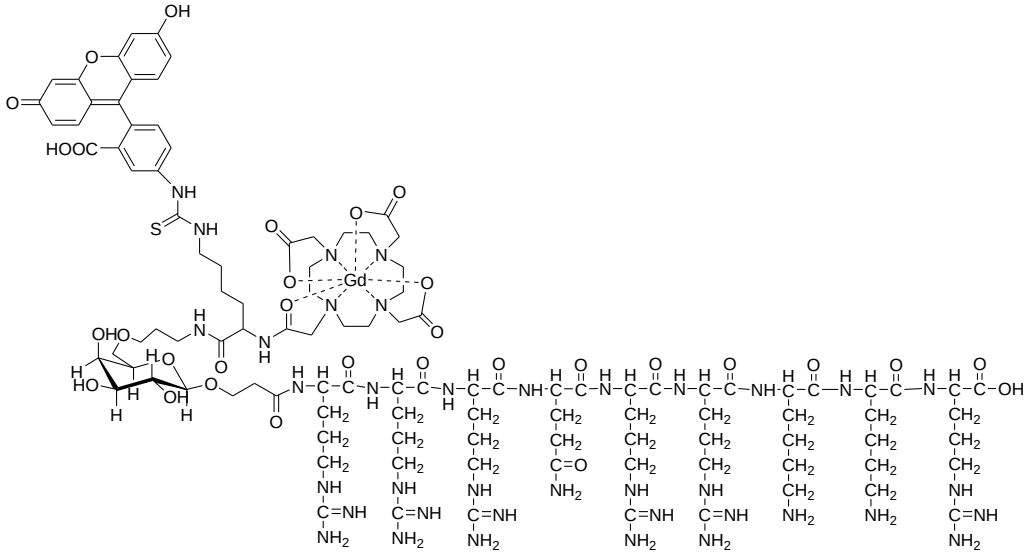

Chemical structure of **CA-2**

Synthesis of conjugate 34

Peptide **17** was synthesized as described for **24a** on pre-loaded Wang resin (0.08 mmol, 200 mg). Fmoc group was removed by treatment with 20 % piperidine/DMF (2x) and resin was washed with DMF. Next Fmoc-Lys (Dde)-OH pre-activated with HBTU (3.6 eq)/HOBt (3.6 eq) in DMF

(2 ml) and DIPEA (8 eq) was added and reaction was allowed to stir for 1 h under nitrogen atmosphere to give **18**. The Fmoc group was further deprotected and Fmoc group of resin bound peptide **18** was deprotected with 20% piperidine/DMF and washed thoroughly with DMF (6x). Coupling of sugar building block **16** was performed by adding of pre-activated solution of Fmoc protected compound **16** (3eq), HATU (3eq) in DMF (3 ml) and DIPEA (6eq) to the resin. After 3 h of coupling under nitrogen atmosphere, the resin was washed with DMF (4x). After Fmoc group deprotection of intermediate **30**, DOTA tris(*tert*-butyl) ester was coupled to the α-NH_2 group of Lys by adding a pre-activated solution of HATU (4eq), DOTA tris(*tert*-butyl) ester(4eq) in DMF (3 ml) and DIPEA to the resin and reacted for 24 h under nitrogen. The Dde group of intermediate **31** was removed by treatment with 2% hydrazine hydrate in DMF (2x4min) and FITC was reacted with ε-NH_2 group of Lys (FITC (4eq): DIPEA (8 eq), DMF (3ml)) within 12 h to give **32**. All coupling steps were followed by a Kaiser test on the resin. The resin bound **32** was cleaved off the resin by applying procedure described for **24a** and **24b**. The obtained crude **33** was analyzed by ESI-MS and afterwards acetyl groups were deprotected accordingly to procedure described for **23a** and **23b**. The obtained **34** was purified by semi-preparative RP-HPLC using a method 1 (flow rate 10 ml/min). The obtained fractions were collected and solvents removed under vacuum, followed by dissolving the sample in ultra pure water and lyophilisation. The ligand **34** was further characterized by ESI-MS. The detected molecular ions were consistent with the calculated mass of **34** (2533.31g/mol).

ESI-MS (+): m/z = 1268.2 $((M+2H)^{2+})$, 1137.1$((M\text{-}FITC)+2H)^{2+})$, 845.9 $((M+3H)^{3+})$, 716.0 $((M\text{-}FITC)+3H)^{2+})$ 634.6 $((M+4H)^{4+})$, 537.3 $((M\text{-}FITC)+4H)^{4+})$, 390 (FITC)

Preparation of Gd^{3+} complexes of ligands 34 (CA-3)

The complexation of **34** with titrated solution of $GdCl_3$ was performed as described for **CA-1** and **CA-2**. After complexation was completed a reaction mixture was freeze dried and further purified by semi-preparative RP-HPLC column using a method 2 (flow rate 4 ml/min). The obtained product after lyophilization was characterized by ESI-MS with observed appropriate isotopes pattern. The detected molecular ions were consistent with the calculated mass of **CA-3** (2688.21).

ESI-MS (+): m/z = 1346.2 ($(M+2H)^{2+}$), 897.6 ($(M+3H)^{3+}$), 767.4 ($(M-FITC)+3H)^{2+}$), 672.7 ($(M+4H)^{4+}$), 390 (FITC)

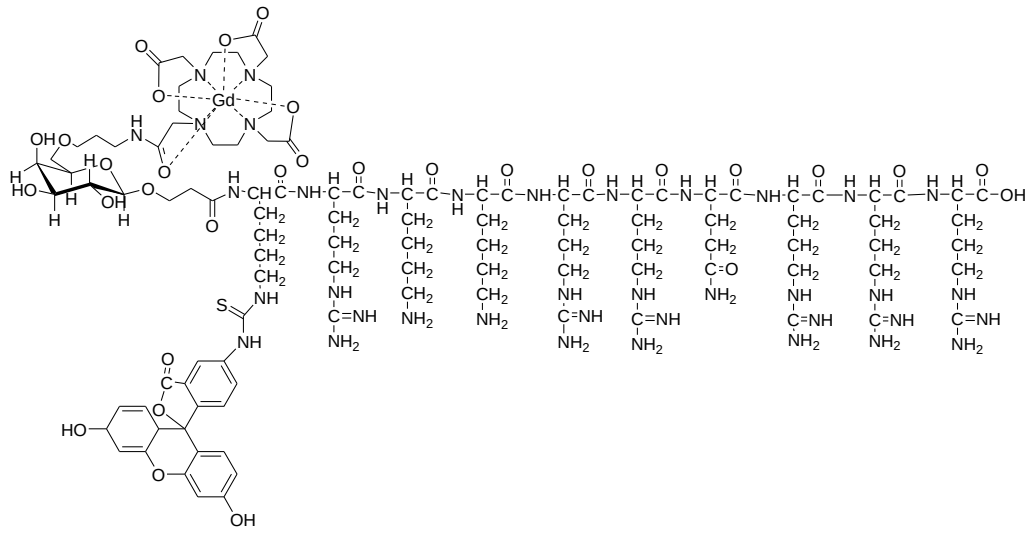

Chemical structure of **CA-3**

1,4,7-tris-(tert-butoxycarbonylmethyl)-1,4,7,10-tetraazacyclododecane-10 acetic acid (28).

To a solution of **26**[165] (20 mmol, 10.4 g) in dry acetonitrile (160 ml) under nitrogen potassium carbonate (31 mmol, 4.38 g) was added and reaction mixture was stirred for 30 min at room temperature. Next benzyl bromide (31 mmol, 7.1 g) was added dropwise with further stirring for 15 h at room temperature. The reaction mixture was filtered and concentrated under reduced pressure. The obtained residue was purified by column chromatography on silica gel using 10% MeOH/DCM eluent to give 11.5 g (87%) of **27** as beige foam. To a solution of **27** (17 mmol, 11.3 g) in MeOH (100ml) 10% Pd/C (1 g) was added and reaction mixture was vigorously shaked under hydrogen atmosphere (2 bar) for 5 h at room temperature. The reaction mixture was filtered by Celite 545, concentrated and obtained residue was purified by column chromatography using 10% MeOH/DCM eluent to give 6.8 g (70%) of **28** as slightly yellowish foam. The spectral data were in the agreement with that literature reported[165].

p-nitrophenyl 2,3,4,6-tetra-O-acetyl-β-D-galactopyranoside (35)

Potassium carbonate (50 mmol, 6.91 g) and benzyltrimethylammonium chloride (2 mmol, 0.37 g) were added to dry chloroform (15 ml). After being stirred for 10 min at room temperature, p-nitrophenyl (10 mmol, 1.39 g) was added and stirring was continued for next 30 min. Next, a solution of **1** (20 mmol, 8.22g) in chloroform (5 ml) was added and reaction mixture was stirred overnight at room temperature (under nitrogen atmosphere). The reaction mixture was diluted with chloroform (250 ml), neutralized with 1M HCl aq. and poured into ice-cold water. The layers were separated and organic layer was washed with water (1x), saturated $NaHCO_3$ (3x) and brine (2x). The combined organic layers were dried over Na_2SO_4, filtered, concentrated and an obtained residue was crystallized from ethanol to give 3.0 g (65%) of **35** as yellowish fine powder.

The obtained ^{1}H-NMR and ^{13}C-NMR were in the agreement with literature reported data[246]

p-nitrophenyl β-D-galactopyranoside (36)

To a solution of **35** (50 mmol, in dry MeOH (300 ml) sodium methoxide was added (pH~9-10) and reaction mixture was stirred for 2 h at room temperature with monitoring a progress of deprotection by TLC (R_f= 0.2, 1:9 MeOH:EtOH). After completion Dowex®50x8-100 ion exchange resin was added portionwise with stirring until pH was adjusted to ~6. The reaction mixture was filtered, resin washed sorely with MeOH and concentrated to give **36** with quantitative yield.

The obtained ^{1}H-NMR and ^{13}C-NMR were in the agreement with literature reported data [246] .

p -nitrophenyl 2,3,4-Tri-O-benzoyl-6-O-trityl-β-D-galactopyranoside (38)

A **36** (26.56 mmol, 8 g) was tritylated and subsequently benzolyted accordingly to previously method described[209]. The crude product was crystallized from ethanol to give 20.4 g (90 %) of **38** as slightly yellowish fine powder. The obtained spectral data were in the agreement with that literature described[209].

p-nitrophenyl 2,3,4-Tri-O-benzoyl-β-D-galactopyranoside (39)

A **38** (12 mmol, 10.2 g) was dissolved in 90% acetic acid in water (200ml). After being stirred for 1.5 h at 60 ºC more of solution 90% acetic acid in water (200 ml) was added and stirring was

continued for the next 1 h. A progress of deprotection was monitored by TLC (R_f= 0.3, 1:4 ethyl acetate/toluene). The reaction mixture was cooled and solvents were removed by co-evaporation with toluene under reduced pressure. The obtained residue was purified by column chromatography on silica gel (ethyl acetate/toluene) to give 8.71 g of **39** (85%) as white foam. The obtained ^{1}H-NMR and ^{13}C-NMR were in the agreement with literature reported data[209].
m.p. 197-198°C.

p-nitrophenyl ((2,3,4-Tri-O-benzyol)-6-O-(5-bromopentyl))-β-D-galactopyranoside (40)

A solution of **39** (3 mmol, 1.83 g) in dry DMF under nitrogen (50 ml) cooled to -30ºC fresh sodium hydride (9 mmol, 0.36 g) was added. After reaction was stirred for 5min 1,5-dibromopentane (62.55 mmol, 8.4 ml) was added to the solution and stirring was continued at -30ºC for the next 5 min. At this point, a reaction flask was taken out of the cooling mixture and reaction was stirred for 15 min at room temperature with monitoring a progress of conversion by TLC (R_f = 0.7 ethyl acetate/hexane 1:3). After that, a reaction was diluted with diethyl ether (200 ml) and saturated NH_4Cl (100 ml) was carefully added. The ether layer was washed with water (200 ml), after their separation, the aqueous lazer was further extracted with ethyl acetate (3x200ml). The combined organic layers were dried over Na_2SO_4, filtered and concentrated under reduced pressure. The residual syrup was purified by silica gel column chromatography (ethyl acetate/hexane) to give 0.8 g (35%) of **40** as syrup.

$[\alpha_D]^{20}$= +38.7°(c=1.0, $CHCl_3$)

^{1}H-NMR (300 MHz, $CDCl_3$): δ= 1.2-1-1.75 (m, 6H, alkyl), 3.05-3.17 (m, 2H, C*H*$_2$Br), 3.62-3.73 (m, 1H, OC*H*$_2$), 3.85-3.96 (m, 1H, OC*H*$_2$) ,4.05 (dd, 1H, H-2, $J_{2\text{-}1}$= 7.8 Hz, $J_{2\text{-}3}$= 10 Hz), 4.4-4.51(m, 1H, H-5, 1H, H-6$_a$) 4.58-4.71 (m, 1H, H-6$_b$), 5.26 (d, 1H, H-1, $J_{1\text{-}2}$= 7.6 Hz), 5.24 (dd, 1H, H-3, $J_{3\text{-}2}$= 10 Hz, $J_{3\text{-}4}$= 3.4 Hz), 5.94 (d, 1H, H-4, $J_{4\text{-}3}$= 3.4 Hz) 7.1-7.2 (m, 2H, Ar*H*), 7.31-7.4 (m, 2H, Ar*H*), 7.42-7.57 (m, 5H, Ar*H*), 7.59-7.69 (m, 2H, Ar*H*), 7.85-7.93 (m, 2H, Ar*H*), 7.96-8.04 (m, 2H, Ar*H*),8.06-8.15 (m, 4H, Ar*H*)

^{13}C-NMR (75 MHz, $CDCl_3$): δ= 24.64 (*C*H$_2$), 29.17 (*C*H$_2$), 32.29 (*C*H$_2$), 33.27 (C*H*$_2$Br), 62.26 (C-6), 68.03 (C-4), 71.90 (C-5), 72.71 (C-3), 73.33(O*C*H$_2$), 77.05 (C-2),100.81(C-1), 116.56, 125.72, 128.43, 128.54, 128.65 128.99, 129.12, 129.24, 129.61, 129.64, 129.91, 133.42, 133.58, 133.69, 142.97, 161.42, 165.36, 165.39, 165.87 (ArH)

HRMS (EI) (±) for $C_{38}H_{36}BrNO_{11}$: $[M+Na]^+_{(calcd)}$= 784.1364, $[M+Na]^+_{(found)}$= 784.1360

p-nitrophenyl ((2,3,4-Tri-O-benzyol)-6-O-(9-bromononyl))-β-D-galactopyranoside (41)

A solution of **39** (3 mmol, 1.83 g) in dry DMF under nitrogen (50 ml) cooled to -30ºC and fresh sodium hydride (9 mmol, 0.36 g) was added. After reaction was stirred for 7 min 1,5-dibromopentane (62.55 mmol, 8.4 ml) was added to the solution and stirring was continued at -30ºC for the next 5 min. At this point, a reaction flask was taken out of the cooling mixture and reaction was stirred for 15 min at room temperature with monitoring a progress of conversion by TLC (R_f = 0.7 ethyl acetate/hexane 1:3). After that, a reaction was diluted with diethyl ether (200 ml) and saturated NH_4Cl (100 ml) was carefully added. The ether layer was washed with water (200 ml), after their separation, the aqueous layer was further extracted with ethyl acetate (3x200ml). The combined organic layers were dried over Na_2SO_4, filtered and concentrated under reduced pressure. The residual syrup was purified by silica gel column chromatography (ethyl acetate/hexane) to give 0.34 g (14%) of **41** as yellowish syrup.

$[\alpha_D]^{20}$= +43.6°(c=1.0, $CHCl_3$)

^{1}H-NMR (400 MHz, $CDCl_3$): δ= 0.98-1.35 (m, 12H, alkyl), 1.37-1.52 (m, 2H, alkyl), 1.7-1.8 (m, 2H, alkyl), 3.35-3.17 (t, 2H, C*H*$_2$Br, *J*=6.82 Hz), 3.62-3.72 (m, 1H, OC*H*$_2$), 3.85-3.95 (m, 1H, OC*H*$_2$) ,4.05 (dd, 1H, $J_{2\text{-}1}$= 7.8, Hz, $J_{2\text{-}3}$= 9.9 Hz), 4.42-4.57(m, 1H, H-5, 1H, H-6$_a$) 4.63 (odd, 1H, H-6$_b$), 5.28 (d, 1H, H-1, $J_{1\text{-}2}$= 7.6 Hz), 5.51 (dd, 1H, H-3, $J_{3\text{-}2}$= 9.8 Hz, $J_{3\text{-}4}$= 3.28 Hz), 5.95 (d, 1H, H-4, $J_{4\text{-}3}$= 3.28 Hz) 7.15 (d, 2H, Ar*H*, *J*=9.09 Hz), 7.36 (t, 2H, Ar*H*, *J*=7.83 Hz), 7.44-7.58 (m, 5H, Ar*H*), 7.6-7.68 (m, 2H, Ar*H*), 7.9 (d, 2H, Ar*H*, *J*=7.33 Hz), 8.01-8.04 (m, 2H, Ar*H*),8.06-8.12 (m, 4H, Ar*H*)

^{13}C-NMR (100 MHz, $CDCl_3$): δ= 25.82, 27.93, 28.44, 29.04, 29.08 , 29.93, 32.60 (*C*H$_2$), 33.95 (C*H*$_2$Br), 62.21 (C-6), 67.97 (C-4), 71.79 (C-5), 72.68 (C-3), 73.71 (O*C*H$_2$), 76.86 (C-2),100.74 (C-1), 116.49, 125.64, 128.31, 128.48, 128.59, 128.94, 129.12, 129.19, 129.59, 129.85, 133.28, 133.53, 133.63, 142.82, 161.46, 162.45, 165.32, 165.81 (ArH).

HRMS (EI) (±) for $C_{42}H_{44}BrNO_{11}$: $[M+Na]^+_{(calcd)}$= 840.1999, $[M+Na]^+_{(found)}$= 840.1997

1,4,7-tris(carboethoxymethyl)-1,4,7,10-tetraazacyclododecane (43)

Cyclen (10 mmol, 1.72 g) was added in dry chloroform (50 ml) containing sodium bicarbonate (10 mmol, 0.84 g). A mixture was stirred for 30 min and afterwards cooled to -20ºC. Ethyl bromoacetate (30 mmol, 5.01 g) was diluted with chloroform (5 ml) and added gradually dropwise to solution of cyclen. Afterwards a reaction mixture was allowed to warm up to room temperature and stirring was continued for 2 days at room temperature. Then, the reaction mixture was filtered and solvent was removed under reduced pressure. The obtained residue was purified on silica gel by column chromatography using MeOH/DCM as eluent (R_f= 0.45 1:9 MeOH/DCM) yielding 2.6 g of **43** (60%) of as oil.

The obtained ^{1}H-NMR and ^{13}C-NMR were in the agreement with literature reported data[247].

ESI-MS (+) for $C_{20}H_{38}N_4O_6$ $[M+H]^+_{(calcd)}$= 431.27, $[M+H]^+_{(found)}$= 431.3

2,3,4-tribenzyol-6-O-(5-(1-(4,7,10-trismethylcarboxymethyl-(1,4,7,10-tetraazacyclododecyl)))pentyl)-1-(p-nitrophenyl)-β-galactopyranoside (44)

To a solution of cyclen (6.8 mmol, 1.17 g) in dry chloroform (160 ml) **40** (0.85 mmol, 0.73 g) dissolved in $CHCl_3$ (10 ml) was added slowly dropwise at 0ºC. The reaction mixture was allowed to warm up to room temperature and stirring was continued for 8 h. After that, a temperature was increased and reaction was stirred overnight at 50ºC (12 h). The progress was monitored by ESI-MS. Next, the reaction mixture was filtered through G-4 sintered funnel and collected filtrate was evaporated under reduced pressure. The obtained residue was dissolved in DCM, water was added (200 ml) and aqueous layer was extracted with DCM (4x150 ml). The organic layers were combined and dried over Na_2SO_4, filtered and concentrated under vacuum to give 0. 47 g of **42** as yellow syrup that was used in the next step without purification. The derivative **42** was dissolved in dry acetonitrile (60 ml), sodium carbonate (2.28 mmol, 0.26 g) was added and the mixture was stirred for 20 min at room temperature under nitrogen atmosphere. Next, methyl bromoacetate (2.48 mmol, 0.26 g) was added dropwise and the reaction mixture was stirred for 1 h at room temperature. After that temperature was increased and stirring was continued at 55ºC overnight. The progress of reaction was monitored by TLC (R_f= 0.5 10% MeOH/CH_2Cl_2) and ESI-MS. After completion, the reaction mixture was filtered and concentrated under reduced

pressure. The organic residue was purified by column chromatography on silica gel (eluent MeOH/CH_2Cl_2) to give 0.36 g (40%) of **44** as brownish syrup.

^{1}H-NMR (300 MHz, $CDCl_3$): δ= 1.1-1.6 (m, 6H, alkyl), 2.0-3.09 (m, 18H, C*H*$_2$), 3.1-3.43 (m, 6H, C*H*$_2$), 3.55-3.8 (m, 9H, C*H*$_3$, 1H OC*H*$_2$), 3.87-3.98 (m, 1H, OC*H*$_2$), 4.04 (pt, 1H, H-2), 4.42-4.56 (m, 1H, H-5, 1H, H-6$_a$) 4.58-4.67 (m, 1H, H-6$_b$), 5.32 (d, 1H, H-1, J_{1-2}= 8.7 Hz), 5.24 (dd, 1H, H-3, J_{3-2}= 9.8 Hz, J_{3-4}= 3.02 Hz), 5.93 (d, 1H, H-4, J_{4-3}= 3.02 Hz) 7.19 (d, 2H, *J*= 9.06 Hz, Ar*H*), 7.33-7.41 (m, 2H, Ar*H*), 7.42-7.58 (m, 5H, Ar*H*), 7.59-7.68 (m, 2H, Ar*H*), 7.89 (d, 2H, *J*= 7.93 Hz, Ar*H*), 8.02 (m, 2H *J*= 7.93 Hz, Ar*H*),8.05-8.13 (m, 4H, Ar*H*)

^{13}C-NMR (75 MHz, $CDCl_3$): δ= 24.03, 25.30, 29.52, 29.87 (*C*H$_2$), 52.34, 52.53 (C*H*$_3$COO), 53.35, 53.78, 55.24, 55.77 (*C*H$_2$), 62.14 (C-6), 67.89 (C-4), 71.70 (C-5), 72.58 (C-3), 73.65 (O*C*H$_2$), 77.09 (C-2), 100.51(C-1), 116.49, 125.61, 128.35, 128.41, 128.57, 129.49, 129.54, 129.75, 133.36, 133.45, 133.65, 142.77, 161.36, 165.18, 165.27, 165.79 (ArH), 173.94, 174.62 (*C*OOCH$_3$)

ESI-MS (+) for $C_{55}H_{67}N_5O_{17}$: $[M+H]^+_{(calcd)}$= 1070.45, $[M+H]^+_{(found)}$= 1070.5

2,3,4-tribenzoyl-6-O-(5-(1-(4,7,10-trisethylcarboxymethyl-(1,4,7,10-tetraazacyclododecyl)))pentyl)-1-(p-nitrophenyl)-β-galactopyranoside (45)

To solution of DO3A-(tris-ethyl) ester (0.6 mmol, 0.26 g) in dry DMF (40 ml) potassium carbonate (1.2 mmol, 0.17 g) was added. After the mixture was stirred for 20 min at room temperature, a solution of **40** (0.8 mmol mmol, 0. 62 g) in DMF was added and reaction mixture was stirred for 1h at room temperature, followed by stirring at 55ºC for 24 h. The progress of conversion was monitored by TLC (R_f= 0.4, 10% MeOH/CH_2Cl_2) and ESI-MS. After completion, the reaction mixture was filtered and concentrated under reduced pressure. The organic residue was purified by column chromatography on silica gel (eluent MeOH/DCM) to give 0.57 g (85%) of **45** as yellow gum.

^{1}H-NMR (300 MHz, $CDCl_3$): δ= 1.15-1.7 (m, 18H, alkyl, C*H*$_3$), 2.0-3.75 (m, 25H, C*H*$_2$, C*H*$_2$O), 3.85-3.98 (m, 1H, OC*H*$_2$), 4.0-4.32 (m, H-2, C*H*$_2$CH$_3$), 4.43-4.55 (m, 2H, H-6, H-5), 4.57-4.75 (m, 1H, H-6), 5.31 (d, 1H, H-1, J_{1-2}= 7.55 Hz), 5.51 (dd, 1H, H-3, J_{3-2}= 9.8 Hz, J_{3-4}= 3.4 Hz),

5.92 (pd, 1H, H-4, J_{4-3}= 3.2 Hz), 7.17 (d, 2H, *J*= 9.08 Hz, Ar*H*), 7.30-7.7 (m, 9H, Ar*H*), 7.89 (d, 2H, *J*= 7.74 Hz, Ar*H*), 7.99-8.23 (m, 6H, Ar*H*).

^{13}C-NMR (75 MHz, $CDCl_3$): δ= 13.99 (*C*H_3), 24.13, 25.38, 29.57, 29.92 (alkyl) 53.91, 55.36, 55.93, 55.98 (*C*H_2), 61.47, 61.66 (*C*H_2), 62.18 (C-6), 67.91 (C-4), 71.80 (C-5), 72.62 (C-3), 73.72 (O*C*H_2), 77.15 (C-2), 100.65 (C-1), 116.54, 125.65, 128.40, 128.46, 128.62, 128.91, 129.13, 129.20, 129.55, 129.59, 129.81, 133.39, 133.51, 133.70, 142.86, 161.41, 165.30, 165.82 (ArH) 173.51, 174.23 (*C*OO).

HRMS (EI) (±) for $C_{58}H_{73}N_5O_{17}$: $[M+H]^+_{(calcd)}$= 1112.5074, $[M+H]^+_{(found)}$= 1112.5082

2,3,4-tribenzoyl-6-O-(9-(1-(4,7,10-trisethylcarboxymethyl-(1,4,7,10-tetraazacyclododecyl)))nonanyl)-1-(p-nitrophenyl)-β-galactopyranoside (46)

A **41** (0.41 mmol, 0.33 g) was reacted with **43** (0.36 mmol, 0.15 g) using procedure described for **45**. The obtained residue was purified by column chromatography on silica gel (eluent MeOH/DCM) to give 0.29 g (70%) of **46** as yellow gum.

^{1}H-NMR (300 MHz, $CDCl_3$): δ= 1.14-1.87 (m, 23H, alkyl, C*H*$_3$), 2.25-3.95 (m, 26H, C*H*$_2$, OC*H*$_2$), 3.97-4.35 (m, 7H, H-2, C*H*$_2$CH$_3$), 4.40-4.55 (m, 2H, H-6, H-5), 4.57-4.72 (m, 1H, H-6), 5.30 (d, 1H, H-1, J_{1-2}= 7.55 Hz), 5.51 (dd, 1H, H-3, J_{3-2}= 10.1 Hz, J_{3-4}= 3.4 Hz), 5.94 (pd, 1H, H-4, J_{4-3}= 3.4 Hz), 7.10-7.21 (m, 2H, Ar*H*), 7.28-7.69 (m, 9H, Ar*H*), 7.89 (d, 2H, *J*= 7.93 Hz, Ar*H*), 8.15-8.78 (m, 6H, Ar*H*).

^{13}C-NMR (75 MHz, $CDCl_3$): δ= 14.0 (*C*H_3), 25.56, 25.71, 29.15, 29.49, 29.85, 31.24, 32.58 (alkyl), 50.10, 52.98, 55.83, 56.0 (*C*H_2), 62.61 (C-6), 67.92 (C-4), 71.63 (C-5), 72.63 (C-3), 73.6 (O*C*H_2), 76.78 (C-2), 100.62 (C-1), 116.42, 125.53, 128.22, 128.37, 128.50, 129.49, 129.74, 129.47, 133.19, 133.41, 133.54, 142.71, 161.41, 165.25, 165.72, 173.40, 174.09.

ESI-MS (+):$C_{55}H_{67}N_5O_{17}$: $[M+H]^+_{(calcd)}$= 1168.56, $[M+H]^+_{(found)}$= 1168.6

6-O-(5-(1-(4,7,10-triscarboxymethyl-(1,4,7,10-tetraazacyclododecyl)))pentyl)-1-(4-nitrophenyl)-β-galactopyranoside (47)

To a solution of **45** (0.45 mmol, 0.5 g) in dry MeOH (20 ml) was added 30 % sodium methoxide/methanol solution dropwise until pH~11 was reached and reaction mixture was stirred for next 5 h at room temperature. A progress of deprotection was monitored by TLC (R_f = 0.3 1:9 MeOH/DCM) and ESI-MS. After completion Dowex®50x8-100 ion exchange resin was added portionwise with stirring until pH of solution was adjusted roughly to 6. The reaction mixture was filtered, resin washed sorely with MeOH and concentrated under vacuum. The obtained residue was dissolved in ultra pure water (10 ml), a solution was cooled to ~8ºC and 1N NaOH was added (~2.1 ml) until pH of mixture was adjusted to roughly 10-11. A progress of deprotection was monitored by ESI-MS. After being stirred for 2 h at room temperature deprotection was completed and reaction mixture was neutralized with 0.1N HCl (pH~6.5) and lyophilized. The obtained solid residue was purified by RP-HPLC using MeOH/water to give 0.18 g (55%) of **47** after lyophilization as white fluffy powder.

^{1}H-NMR (400 MHz, D_2O): δ= 1.25-1.33 (m, 2H, alkyl), 1.54-1.68 (m, 4H, alkyl), 2.86-3.53 (m, 21H), 3.61-3.94 (m, 10 H), 3.98 (pd, 1H, H-4, J_{4-3}=3.03 Hz), 5.23 (d, 1H, H-1, J_{1-2}=7.83 Hz), 7.22 (d, 2H, *J*=9.35 Hz, Ar*H*), 8.22 (d, 2H, *J*=9.35 Hz, Ar*H*).

^{13}C-NMR (100 MHz, D_2O): 22.74, 23.16, 29.13 (*C*H_2, alkyl), 49.28, 51.54, 54.02, 56.0, 56.43 (*C*H_2), 61.02 (C-6), 68.82 (C-4), 72.40 (C-2), 73.30 (O*C*H_2), 75.88 (C-3), 79.20 (C-5), 100.23 (C-1), 116.81, 126.57, 142.84, 162.08 (ArH), 173.28 (*C*OOH).

ESI-MS (+) for $C_{31}H_{49}N_5O_{14}$: $[M+H]^+_{(calcd)}$= 716. 3, $[M+H]^+_{(found)}$= 716.4

6-O-(5-(1-(4,7,10-triscarboxymethyl-(1,4,7,10-tetraazacyclododecyl)))nonyl)-1-(p – nitrophenyl)-β-galactopyranoside (48)

A **46** (0.24 mmol, 0.28g) was deprotected using method described for **47**. The obtained solid residue was purified by RP-HPLC using MeOH/water to give 0.08 g (40 %) of **48** after lyophilization as white fluffy powder.

^{1}H-NMR (400 MHz, D_2O): δ= 0.95-1.3 (m, 10H, alkyl), 1.40-1.65 (m, 4H, alkyl), 2.85-3.53 (m, (m, 22 H), 3.61 (pt, 1H), 3.68-3.87 (m, 8H), 3.97 (pd, 1H, H-4, J_{4-3}=3.03 Hz), 5.16 (d, 1H, H-1, J_{1-2}=7.58 Hz), 7.15 (d, 2H, *J*=9.09 Hz, Ar*H*), 8.13 (d, 2H, *J*=9.09 Hz, Ar*H*).

^{13}C-NMR (100 MHz, D_2O): 22.77, 25.80, 26.37, 28.63, 28.77, 29.10, 29.63 (*C*H_2, alkyl), 49.13, 50.09, 51.58, 54.29, 55.32, 56.14,(*C*H_2), 60.99 (C-6), 68.66 (C-4), 72.44 (C-2), 73.57(O*C*H_2), 75.82 (C-3), 79.03 (C-5), 100.33 (C-1), 116.72, 126.44, 142.59, 162.23 (ArH), 173.33 (*C*OOH).

ESI-MS (+) for $C_{35}H_{57}N_5O_{14}$: $[M+H]^+_{(calcd)}$= 772. 4, $[M+H]^+_{(found)}$= 772.4

Preparation of Gd^{3+} complexes of ligands 47 and **48 (CA-5 and CA-6)**

To a solution of ligand **47** or **48** (1 eq) in ultra pure water (pH~6.5) a titrated aqueous solution of $GdCl_3$ (0.9 eq) was added dropwise and pH was kept in the range 6.5-7 by addition of 0. 1 M $NaOH_{aq}$ if required. The reaction mixture was stirred for 3 days at room temperature with pH periodically checked and adjusted with 0. 1 M $NaOH_{aq}$. After this time pH was not changed and compexation was considered to be completed. The absence of free Gd^{3+} was checked with xylenol orange indicator. Afterwards water was removed by evaporation under reduced pressure and product was purified by preparative RP-HPLC using acetonitrile/water and lyophilized to give Gd^{3+} complexes as white powder with detected Gd^{3+} isotope pattern.

CA-5 ESI-MS (-): $C_{31}H_{46}GdN_5O_{14}$ $[M-H]^{1-}_{(calcd)}$= 869.2 $[M-H]^{1-}_{(found)}$= 869.1

CA-6 ESI-MS (-): $C_{35}H_{54}GdN_5O_{14}$ $[M-H]^{1-}_{(calcd)}$= 925.2, $[M-H]^{1-}_{(found)}$= 925.1

3-((2,3,4,6-tetra-O-acetyl-β-D-galactopyranosyl)oxy)-propanoic acid (49)

To a solution of **3** (2.4 mmol, 1.14 g) in dry DCM (20 ml) neat TFA (20 ml) was added at 0ºC. After being stirred for 1 h at 0ºC, a reaction mixture was allowed to warm up to room temperature and stirring was continued for next 24 h. A progress of deprotection was moniored by TLC (R_f=0.3, 10% MeOH/DCM). Next, the solvent were removed by co-evaporation with toluene and obtained residue was purified by column chromatography on silica gel (eluent MeOH/DCM) to give 0.61g (60%) of **49** as colorless syrup.

$[\alpha_D]^{20}$= +3.7°(c=1.0, $CHCl_3$)

^{1}H-NMR (300 MHz, $CDCl_3$): δ= 1.99 , 2.04, 2.06, 2.14 (4s, 12H, C*H*$_3$CO), 2.57-2.75 (m, 2H, C*H*$_2$), 3.8-3.97 (m, 1H, H-5, 1H, OC*H*$_2$), 4.04-4.27 (m, 1H, OC*H*$_2$, 2H, H-6), 4.52 (d, 1H, H-1, J_{1-2}=7.93 Hz), 5.02 (dd, 1H,H-3, J_{3-4}=3.4 Hz, J_{3-2}=10.3 Hz), 5.18 (odd, 1H, H-2, J_{2-1}=8 Hz, J_{2-3}=10.6 Hz), 5.98 (d, 1H, H-4, J_{4-3}=3.4 Hz), 7.57 (bs, 1H, O*H*).

^{13}C-NMR (75 MHz, $CDCl_3$): δ= 20.54, 20.59, 20.60, 20.64 (*C*H_3CO), 34.58 (*C*H_2), 61.23 (C-6), 65.15 (O*C*H_2CH_2), 66.99 (C-4), 68.65 (C-2), 70.67 (C-3), 70.79 (C-5), 101.48 (C-1), 169.64, 169.95, 170.20, 170.30, 170.52 (CH_3*C*O), 176.04 (*C*OO).

HRMS(EI) (±) for $C_{17}H_{24}O_{12}$: $[M+Na]^+_{(calcd)}$= 443.1160, $[M+Na]^+_{(found)}$= 443.1157

Synthesis of *O*-acetyl protected 52

Fmoc protected D-Tat $_{49-57}$ peptide was synthesized manually as described in the chapter on pre-loaded Wang (scale 0.08 mmol), followed by Fmoc group deprotection with 20% piperidine/DMF and washing of resin with DMF (6x). Subsequently, a mixture of carbohydrate (3 eq)/ HATU (3 eq) in DMF (3 ml) stirred for 5min and DIPEA (6 eq) were added to the resin. After being stirred for 3h under nitrogen atmosphere, coupling was completed as confirmed by Kaiser test and resin was washed with DMF (DMF (4x), DCM (4x) and MeOH (6x) and dried under vaccum. The cleavage cocktail TFA/water/TIPS/m-cresol (90: 2.5:2.5:5 v/v/v/v) cocktail (5 ml) was added and stirring was continued for 4 h. Afterwards filtrate was collected and resin was additionally washed with TFA (0.5 ml) followed by precipitation with cold (-20ºC) tert-butyl methyl ether (MTBE). The obtained precipitant was washed with additional amount of MTBE (2x), centrifuged and re-suspended in neat TFA. After precipitation with cold MTBE and centrifugation, the obtained residue was dissolved in ultra pure water and lyophilized and further purified by RP-HPLC using a method A (flow rate 10 ml/min). The collected fractions were combined and solvents were evaporated under reduced pressure. The obtained product was dissolved in ultra pure water with adjusting pH to ~7 and lyophilized to give 60 mg (43%) of **52** as white light powder. The obtained product was characterized by characterized by ESI-MS and detected molecular ions were consistent with the calculated mass of **52** (1741.95 g/mol).

ESI-MS (+): m/z = 871.5 ($(M+2H)^{2+}$), 581.5 ($(M+3H)^{3+}$), 436.5 ($(M+4H)^{4+}$).

_O_-acetyl deprotection of 52 (54)

O-acetyl protected **52** (25 mg) was dissolved in 7N NH_3/MeOH (15 ml) at 0ºC and after 30 min at 0ºC a stirring was continued at room temperature. After 8.5 h deprotection was completed as detected by ESI-MS and solvent was evaporated under reduced pressure. The obtained residue was purified by RP-HPLC using a method A (flow rate 10 ml/min) and the collected fractions were combined and solvents were evaporated under reduced pressure. The obtained product was dissolved in ultra pure water with adjusting pH to ~7 using 0.01 M NaOH and lyophilized to give 18 mg (80%) of **54** as white hygroscopic powder. The obtained product was characterized by ESI-MS and detected molecular ions (m/z) were consistent with the calculated mass of the product (1573.81 g/mol).

ESI-MS (+): m/z = 1575.2 $((M+1H)^{1+})$, 787.6 $((M+2H)^{2+})$, 525.4 $((M+3H)^{3+})$.

Synthesis of conjugate 55

Fmoc protected Lys-Tat $_{49\text{-}57}$ was synthesized (scale 0.08 mmol) and Fmoc group was removed with 20% piperidine/DMF followed by washing with DMF (6x). Subsequently **49** (3eq) activated with HATU (3 eq)/DIPEA (6 eq) in DMF (3ml) was added to the resin. After shaking for 3h, resin was washed with DMF (4x) and coupling was completed as confirmed by Kaiser test. Next, resin was treated with 2% hydrazine hydrate/DMF (2x) and washed with DMF (8x). A mixture of FITC (3 eq) dissolved in DMF (2 ml) and DIPEA (8 eq) was added to the resin with shaking continued for 12h at room temperature in the dark. After coupling completion, a resin was washed with DMF (4x), DCM (4x) and MeOH (6x) and dried under vaccum. The resin attached conjugate was cleaved off the resin accordingly to the same procedure as describe for **52** and purified by RP-HPLC using method A to give 64 mg (35%) of **55** after lyophilization as light orange powder. The detected molecular ions were consistent with the calculated mass of **55** (2258.51 g/mol).

ESI-MS (+): m/z = 1130.5 $((M+2H)^{2+})$, 935.6 $((M\text{-}FITC+2H)^{2+})$, 754.0, $((M+3H)^{3+})$, 624.3$((M\text{-}FITC+3H)^{3+})$, 565.8 $((M+4H)^{4+})$, 452.7 $((M+5H)^{5+})$, 390 (FITC).

_O_-acetyl deprotection of 55 (56)

_O_-acetylated **55** (30 mg) was dissolved in 7N NH_3/MeOH at 0ºC (20 ml) and stirred for 12 h at room temperature. A progress of deprotection was monitored by ESI-MS. The solvent was evaporated under reduced pressure and the obtained residue was dissolved in ultra pure water followed by lyophilization. A crude product was purified by RP-HPLC using method A to give 8.5 mg (31%) of **56** after lyophilization as light orange powder. The product was characterized by ESI-MS and detect molecular ions measured in positive and negative modus were consistent with the calculated mass of **56** (2090.07 g/mol).

ESI-MS (+): m/z = 1046.7 $((M+2H)^{2+})$, 851.6 $((M\text{-}FITC)+2H)^{2+})$, 698.0 $((M+3H)^{3+})$, 568.6 $((M\text{-}FITC)+3H)^{3+})$ 523.9 $((M+4H)^{4+})$, 390 (FITC).

ESI-MS (-): m/z = 2089.5 $((M-H)^{1-})$, 1044.7 $((M-2H)^{2-})$.

2,3,4,6-tetra-O-acetyl-1-(4-aminophenyl)-β-D-galactopyranoside (57)

To a solution of **35** (5 mmol, 2.35 g) dissolved in a mixture of ethyl acetate/ethanol (30 ml 1:1 v/v) 10 % Pd/C (0.2 g) was added and a reaction mixture was stirred in Parr-apparatus for 5 h under hydrogen atmosphere (3 bar). After completion, a solution was filtered through Celite 545 and concentrated to give 2.08 g (95%) of expected **57** as dark brown oil.
The obtained ^{1}H-NMR and ^{13}C-NMR data were in the agreement with literature reported[246]

4-oxo-4-((4-((2,3,4,6-tetra-O-acetyl-β-D-galactopyranos-1-yl)oxy)phenyl)amino)-butanoic acid (58)

To a pre-cooled solution of **57** (2 mmol, 0.89 g) in pyridine (26 ml) succinic anhydride (2.5 mmol, 0.25 g) was added portionwise and stirred for 1 h at 0ºC. After this time, stirring was continued at room temperature for next 2 h. The progress of reaction was monitored by TLC (R_f= 0.25, 10% MeOH/CH_2Cl_2). After completion reaction mixture was diluted with ethyl acetate (200ml) and poured into ice-cold water. The layers were separated and aqueous layer was extracted with ethyl acetate (1x200ml) and DCM (2x200ml). The combined organic layers were dried over Na_2SO_4, filtered and concentrated under reduced pressure. The residue was purified by column chromatography on silica gel to give 0.7g (65%) of **58** as brownish syrup.

$[\alpha_D]^{20}$= +2.6°(c= 0.75, $CHCl_3$)

^{1}H-NMR (300 MHz, $CDCl_3$): δ= 2.01, 2.03, 2.06, 2.17 (4s, 12H, C*H*$_3$CO), 2.4-3.1 (m, 4H, C*H*$_2$), 3.91-4.29 (m,2H, H-6, 1H, H-5), 4.98 (d, 1H, H-1, J_{1-2}=7.74 Hz), 5.12 (dd, 1H, H-3, J_{3-4}=2.93 Hz, J_{3-2}=10.4 Hz), 5.4-5.7 (m, 2H, C-2, C-4 6.85-7.0 (m, 2H, ArH), 7.39-7.55 (m, 2H, ArH)

^{13}C-NMR (75 MHz, $CDCl_3$): δ= 20.47, 20.52, 20.54, 20.63 (*C*H_3CO), 45.23 (*C*H_2), 61.26 (C-6), 66.89, 68.65(C-2, C-4), 70.73(C-3), 70.89(C-5), 100.06 (C-1), 117.42, 121.28, 133.89, 153.22 (ArH), 169.39, 170.01 (CH_3*C*O), 170.17 (NH*C*O), 170.34 (*C*OOH).

ESI-MS (-) for $C_{23}H_{27}NO_{13}$: $[M-H]^{1-}_{(calcd)}$= 538.1, $[M-H]^{1-}_{(found)}$= 538.0.

Synthesis of conjugate 61

A conjugate **61** was synthesized using the same procedure like described for **52** on the pre-loaded Wang resin (scale 0.04 mmol, 100 mg of resin). The obtained crude O-acetylated **60** was dissolved in 7N NH_3/MeOH (30 ml) at 0ºC (20 ml) and stirred for 12 h at room temperature. A progress of deprotection was monitored by ESI-MS. The solvent was evaporated under reduced pressure and the obtained residue was dissolved in ultra pure water followed by lyophilization. The residue was purified by RP-HPLC using method B and collected fractions were concentrated under reduced pressure. The obtained product was dissolved in ultra pure water with adjusting pH using 0.01 M NaOH and after lyophilization 20 mg (29%) of **61** was obtained as white hygroscopic powder. The obtained product was characterized by ESI-MS and detect molecular ions were consistent with the calculated mass of **61** (1692.93 g/mol).

ESI-MS (+): m/z = 1690.9 ($(M+1H)^{1+}$), 844.9 ($(M+2H)^{2+}$), 1437.8 ($(M\text{-frag}+H)^{1+}$), 718.4 ($(M\text{-frag}+2H)^{2-}$).

1-(2-(6-(benzyloxycarbonylamino)-1-metoxy-1-oxohexane-2-ylamino)-2-oxoethyl)-4,7,10-(tris-tertbutoxycarbonyl)-1,4,7,10-tetracyclododecane (62)

28 (2.7 mmol, 1.54g) was dissolved in DMF (25 ml) cooled to 0ºC and N-ε-Cbz-D-lysine methyl ester (3.24 mmol, 1.07 g), NMM (5.4 mmol, 546 mg), HOBt (3.24 mmol, 437 mg) were added. The reaction mixture was stirred for 15 min and EDC (3.24 mmol, 0.5 g) was added followed by stirring continued at 0º C for 30 min and then at room temperature overnight (17 h). The progress of reaction was monitored by TLC (R_f= 0.4, 10% MeOH/DCM). After completion, the reaction

mixture was diluted with DCM (200 ml) and poured into ice-cold water. The layers were separated on aqueous layer was extracted with DCM (3x 100 ml). The collected organic layers were dried over Na_2SO_4, filtered and evaporated under reduced pressure. The residue was purified by column chromatography on silica gel (eluent MeOH/DCM) to give 1.36 g (59%) of **62** as white foam.

^{1}H-NMR (300 MHz, $CDCl_3$): δ= 1.3-1.95 (m, 6H, CH_2, 27H $(CH_3)_3C$)), 1.9-3.4 (m, 24H, CH_2CH_2 macrocycle, CH_2COO) 3.45-3.7 (m, 2H, CH_2), 3.66 (s, 3H, CH_3OOC), 4.22-4.35(m, 1H, C*H*), 5.09 (s, 2H, CH_2OPh), 6.33 (bs, 1H, N*H*) 7.22-7.5 (m, 5H, Ph), 9.08 (bs, 1H, N*H*)

^{13}C-NMR (75 MHz, $CDCl_3$): δ= 22.9 (CH_2), 27.68, 27.75, 27.85 ($C(CH_3)_3$), 29.48 (CH_2CH_2NHCO), 29.65 (CH_2CH), 39.60 (CH_2NH), 51.79 (*C*HNHCO), 53.23 ($COOCH_3$), 55.19, 55.54 (CH_2CH_2,macrocycle), 55.90 (CH_2COO), 65.77 ($NHCOOCH_2$), 81.61, 81.65, 81,71 ($C(CH_3)_3$), 127.39 (Ph), 127.58 (Ph), 128.13 (Ph), 137.12 (Ph), 156.68 ($NHCOCH_2$), 171.71 (NH*C*O), 172.19 ($COOC(CH_3)_3$), 172.47 ($COOC(CH_3)_3$) , 172.84 ($COOCH_3$)

HRMS (EI) (±) for $C_{43}H_{72}N6O_{11}$: $[M+Na]^+_{(calcd)}$= 871.5151 $[M+Na]^+_{(found)}$= 871.5155

1-(2-(6-amino-1-metoxy-1-oxohexane-2-ylamino)-2-oxoethyl)-4,7,10-(tris-tertbutoxycarbonyl)-1,4,7,10-tetracyclododecane (63)

A solution of **62** (1.6 mmol, 1.36 g), 10% Pd/C (0.3 g) in EtOH (50 ml) was vigorously stirred at room temperature under H_2 pressure (2 bar) in Parr-apparatus for 6 h. After completion, a reaction mixture was filtered by Celite 545, sorely washed with ethanol and filtrate was concentrated to give syrup residue. After flash column chromatography on silica gel (MeOH/DCM) 0.68g (60%) of **63** was obtained as yellowish foam.

^{1}H-NMR (300 MHz, $CDCl_3$): δ= 1.27-1.89 (m, 31 H, CH_2, $(CH_3)_3C$)), 1.91-3.57 (m, 24H, CH_2), 3.68 (os, 3H, CH_3OOC), 3.82 (ps, 4H, CH_2), 4.22-4.35 (m, 1H, C*H*), 8.92 (bs, 1H, N*H*).

^{13}C-NMR (75 MHz, $CDCl_3$): δ= 22.69 (CH_2), 27.68, 27.74, 27.85 ($C(CH_3)_3$), 29.79 (CH_2CH_2NHCO), 30.26 (CH_2CH), 40.01 (CH_2NH), 51.87 (*C*HNHCO), 52.97 ($COOCH_3$), 55.23, 55.53 (CH_2CH_2,macrocycle), 55.92 (CH_2COO), 81.58, 81.61, 81.66 ($C(CH_3)_3$), 171.78 (NH*C*O), 172.22 ($COOC(CH_3)_3$), 172.49 ($COOC(CH_3)_3$), 172.86 ($COOCH_3$).

ESI-MS (+) for $C_{35}H_{66}N_6O_9$: $[M+Na]^+_{(calcd)}$= 737.49, $[M+Na]^+_{(found)}$= 737.5

1-(2-(6-(fluoresceinthiourea)-1-metoxy-1-oxohexane-2-ylamino)-2-oxoethyl))-1,4,7,10-tetraazacyclododecyl-4,7,10-triacetic acid (66)

A compound **63** (0.81 mmol, 0.58 g) was dissolved in DMF (35 ml) under nitrogen and FITC was added (1.21 mmol, 0.48 g), followed by addition of DIPEA (1.62 mmol, 0.81 ml). The reaction mixture was stirred at dark for 12 h and progress of the reaction was monitored by TLC (R_f= 0.3, 10% MeOH/DCM). After completion, the solvent was evaporated under a reduced pressure and the crude **65** was dissolved in DCM (17 ml). The reaction mixture was further cooled down to 0ºC and neat TFA (25 ml) was added. After 30 min at 0ºC, the stirring was continued at room temperature for 12 h with monitoring the progress of reaction by ESI-MS. The reaction mixture was evaporated with toluene and the residue was purified by preparative RP-HPLC using acetonitrile/ water and lyophilized to give **66** (0.47 g, 62%) as dark orange downy powder.

^{1}H-NMR (300 MHz, $CDCl_3$): δ= 1.3-1.83 (m, 6H, CH_2), 2.5-3.95 (m, 29H, $CH_2C\mathit{H}_2$ $C\mathit{H}_2COO$, $C\mathit{H}_2$, CH_3(overlapped s 3.74)) , 4.30-4.51 (m, 1H, C*H*), 6.58 (overlapped ps, 4H, ArH), 7.09 (overlapped ps, 3H, ArH) 7.49 (bs, 1H, ArH), 7.82 (bs, 1H, ArH).

ESI-MS (-) for $C_{44}H_{53}N_7O_{14}S$: $[M-H]^{1-}_{(calcd)}$= 934.3, $[M-H]^{1-}_{(found)}$= 934.3.

Preparation of Gd^{3+} complex of 66 (CA-4)

A compound **66** (0.064 mmol, 70 mg) was dissolved in ultrapure water (10 ml) and titrated $GdCl_3$ solution (0.9 eq) in water (2 ml) was slowly added with maintaining pH in the range 6.2-7 (at lower pH observed precipitation). The reaction mixture was stirred at dark for 12 h at 50ºC and followed by 24 h at room temperature with periodical pH adjustment using 0.1 M NaOH. Next, the reaction mixture was cooled down and stirred with Chelex-100 for 3 h to trap eventually free Gd^{3+}. The water was removed under reduced pressure and remaining residue was purified by RP-HPLC using acetonitrile/water. After lyophilization **CA-4** was obtained in the form of dark orange powder.

ESI-MS (-) for $C_{44}H_{50}GdN_7O_{14}S$: $[M-H]^{1-}_{(calcd)}$= 1089.2 $[M-H]^{1-}_{(found)}$= 1089.1

HRMS (EI) (±) for $C_{44}H_{50}GdN_7O_{14}S$: $[M-2H]^{2-}_{(calcd)}$= 544.1123 $[M-2H]^{2-}_{(found)}$= 544.1117.

Synthesis of CA-7

To a solution of **CA-4** in ultra pure water 1M NaOH was added dropwise until pH~10 and reaction mixture was stirred for 2 h at room temperature at the dark. The progress of reaction was monitored by ESI-MS. After completion pH was brought back to 7 and solvent was removed under reduced pressure. The obtained residue was purified by RP-HPLC (method) using acetonitrile/water as eluents, lyophilized and gave **CA-7** in 70% yield as dark orange powder.

ESI-MS (-) for $C_{43}H_{48}GdN_7O_{14}S$: $[M-H]^{1-}_{(calcd)}$= 1075.2, $[M-H]^{1-}_{(found)}$= 1075.0

Synthesis of CA-8

A concentration of pre-loaded was first determined by absorbance measurements of FITC. Next, the solution of **CA-7** (3.7mg, 3.43 µmol) in ultra pure water (3 ml) was diluted 1:1 with 0.1M MES buffer (pH~5.5). Poly-L-glutamic acid (34 mg, 2.29 µM with assumption MW~15000g/mol) was dissolved in 1ml of 0.1M MES buffer and pH was adjusted to roughly 6.5. After that, N-hydroxysuccinimide (NHS) (5.15 µmol, 0.6 mg) and EDC (5.15 µmol, 0.65mg) each dissolved in 1 ml of 0.1M MES (pH~5.5) were mixed together and added to the solution of **CA-7** with stirring continued for 20 min at room temperature. This mixture containing NHS-ester **67** was added to the solution of PGA and reacted for 3 h at the room temperature in dark. Subsequently the solution of crude product (MW~16075g/mol) was continuously dialyzed for 48 h in the dark using Float-A-Lyser and then lyophilized to give 27 mg (72%) of **CA-8** as dark orange powder.

6.3 Cell experiments

Cell culture

C6 rat glioma cells were a kind gift of Prof. Bernd Hamprecht (University of Tuebingen, Germany). LacZ cells (C6/lacZ7, ATCC® No.: CRL-2303™) expressing β-galactosidase were obtained from ATCC, USA. Cells were cultured as a monolayer at 37°C with 5% CO_2 in DMEM supplemented with 10% fetal bovine serum (FBS), 4 mM L-glutamine, 100 µg/mL streptomycin and 100 U/mL penicillin (all purchased from Biochrom AG, Germany) for C6. The culture medium of LacZ cells was additionally supplemented with 0.1 mM non-essential amino acids.

All cells were passaged by trypsinization with trypsin/EDTA 0.05/0.02% (w/v) in phosphate-buffered saline (PBS; Biochrom AG, Germany) every second to third day.

Concentration estimation of FITC-labeled compounds

Compounds were dissolved in MilliQ water to obtain a 10 mM solution by weight (if possible). The pH was adjusted to about 6.5 by the use 0.1 M NaOH or 0.1M HCl. Especially for peptide conjugates this has to be done carefully since pH values >7 should be avoided due to (poorly reversible) precipitation.

(In more detail: Compounds were solved in about 40-50 µl less than calculated, pH was adjusted by dropwise (5 µl) addition of base or acid, volume was filled up to the required one with water.)

For the determination of the real concentration, these stock solutions were diluted 1:100 in Dulbecco's Modified Eagle's Medium (DMEM; Biochrom AG, Germany). The absorbance of the solutions was measured in a multiplate reader (BMG Labtech, Germany) at 485 nm with ratiometric correction of turbidity at 690 nm. The concentrations of the stock solutions were calculated assuming $\varepsilon_{\text{fluorescein 485 nm}}$=81,000 l/(mol·cm) and all further dilutions were done according to this calculated concentration.

Internalization

Internalization experiments on cells were performed in 96well microplates. At 70-80 % confluency (after 24 h), cells were incubated with different concentrations of CAs in complete culture medium for indicated time points (2 – 18 h) at routine culture conditions. After incubation, the labeling CA were removed and cells were incubated with Bisbenzimid 33342 (Hoechst 33342), a nuclear stain, in complete medium for 30 min (100µl/well) in order to estimate the cell number. The supernatant was removed and extracellular fluorescence was quenched by incubation with cold Trypan Blue (0.05 % (w/v) in PBS, 100µl/well) for 3 min followed by two washes with 200 µl cold HBSS (Biochrom AG, Germany) and the addition of 200µl pre-warmed HBSS. Cell-related FITC fluorescence (Ex 485 nm/Em 530 nm) and cell number (Ex 346 nm/ Em 460 nm) was evaluated in the multiplate reader.

Cell number corrected internalized fluorescence was calculated by the following equation:

$$fluorescence_{(FITC)}/fluorescence_{(Hoechst)} \times 1000$$

and was expressed as corr. fluorescence units (corr. f.u.).

Cells incubated in the absence of CA were used as control and wells without cells but treated with Hoechst, Trypan Blue and washed as described above were used as blank.
Hoechst fluorescence could also be used for the evaluation of cytotoxicity of compounds.
Experiments were run at least two times for each CA with six replicates.
The cells in plates processed for fluorescence spectroscopic measurement, as mentioned above, were used for complementary fluorescence microscopy. Microscopy was performed without fixation using a Zeiss Axiovert 200 M microscope (Germany) with an LD Plan NeoFluor 40X objective. The imaging conditions were kept constant for the observation of all the different samples. Cellular localization and distribution of the peptide was observed by irradiating with blue light (Ex 470/40 nm) and observing at Em 525/50 nm. Apart from FITC fluorescence, the nuclear labeling by Hoechst was observed by Ex 365/15nm and Em 460/50 nm and Trypan Blue fluorescence viewed by Ex 535/50 and Em 645/75 nm. Also phase contrast images with differential interference contrast (DIC) microscopy of the same area were made to observe if the cells maintain their normal morphology in the presence of CAs. Volocity Acquisition and Visualization software (Improvision, England) was used for high speed image capture and high resolution rendering of data sets as images.

6.4 Relaxation rates in cells

For MR imaging of cells, exponentially growing cells were labeled with different concentrations of CAs in 175 cm^2 tissue culture flasks for 18 h. After two times washing with HBSS and once with PBS, cells were trypsinized, centrifuged and re-suspended in 1.5 mL Eppendorf tubes at a density of 2×10^7 cells in 500 µl complete medium. Cells were allowed to settle before MR measurements. Tubes with medium only and cells without CA were used as controls.
MR imaging of the cell pellets at room temperature (~21 ˚C) was performed in a 3 T (123 MHz) human MR scanner (MAGNETOM Tim Trio, Siemens Healthcare, Germany), using a 12-channel RF Head coil and slice selective measurements from a slice with a thickness of 1 mm positioned through the cell pellet.
T_1 was measured using an inversion-recovery sequence, with an adiabatic inversion pulse followed by a turbo-spin-echo readout. Between 10 and 15 images were taken, with the time

between inversion and readout varying from 23 ms to 3000 ms. With a repetition time of 10 s, 15 echoes were acquired per scan and averaged six times. For T_2, a homewritten spin-echo sequence was used with echo times varying from 19 ms to 1000 ms in about 10 steps and a repetition time of 8 s. Diffusion sensitivity was reduced by minimizing the crusher gradients surrounding the refocusing pulse. All experiments scanned 256^2 voxels in a field-of-view of 110 mm in both directions resulting in a voxel volume of $0.43 \times 0.43 \times 1$ mm^3.

Data analysis was performed by fitting to relaxation curves with self-written routines under MATLAB 7.1 R14 (The Mathworks Inc., United States). The series of T_1 and T_2 relaxation data were fitted to the following equations:

a) T_1 *series with varying* $t = T_I$: $S = S_0 (1 - \exp(-t / T_1) + S(T_I = 0) \exp(-t / T_1)$

b) T_2 *series with varying* $t = TE$: $S = S_0 \exp(-t / T_2)$

Nonlinear least-squares fitting of three parameters S_0, $S_{(TI = 0)}$, and T_1/T_2 was done for manually selected regions-of-interest with the Trust-Region Reflective Newton algorithm implemented in MATLAB. The quality of the fit was controlled by visual inspection and by calculating the mean errors and residuals.

The obtained T_1 and T_2 values of the pellet were converted to $R_{1,cell}$ (= $1/T_1$) and $R_{2,cell}$ (=$1/T_2$). These were expressed in % of control ($R_{1,cell}$ and $R_{2,cell}$ of cells incubated similar in absence of CA).

6.5 Relaxivity in solution

800 µl of 3 – 5 concentrations in the range of 5 – 40 µM were prepared in MilliQ water. Pure water was used as blank. Two times 200 µl of each sample were transferred to a 96well plate and the absorbance was measured at 485nm to check the exact concentration again. Afterwards, samples for each concentration were combined again and 380µl aliquots were transferred to Eppendorf cups for MR measurement (two replicates per concentration). Parameters and evaluation were the same as for cell measurements.

Relaxation rate values were plotted on the exact concentration (in mM) and linear regression was done. The slope of the obtained curve is the corresponding relaxivity.

Alternatively, relaxivity can also be calculated from each concentration by following equation:

$(R_{1,conc.} - R_{1,blank})/c$

$R_{1,conc}$, relaxation rate for sample with CA at concentration c (in mM)

$R_{1,blank,}$ relaxation rate for blank

c, concentration of CA in mM

6.6 Enyzmatic assays

Enzymatic assay *β*-galactosidase (nitrophenol-galactopyranose)

The activity of *β*-galactosidase was determined by monitoring the formation of the p-nitrophenyl anion for reaction at 37°C, pH 7.3 (0.1 Phosphate buffer: 7.7 eq. 0.1 M Na_2HPO_4 + 2.3 eq. 0.1 M KH_2PO). The standard enzyme diluent was made by mixing 10 mM Tris/HCl, $MgCl_2$, pH=7.3 in ratio 1:1, 2M mercaptoethanol in water (freshly prepared, 140 µl/ml), 6U/ml β-Galactosidase (dilution in enzyme diluent according to enzyme activity in stock). The 10 mM substrate stock solution was prepared and further diluted as required. The substrate premix was prepared by mixing 15eq. Phosphate buffer, 1 eq 20 mM $MgCl_2$, 1eq. 2 M mercaptoethanol and 1eq. substrate (end concentration in premix: 555 µM). The enzyme solution (20 µl/well) was added to 90 µl/well of substrate premix (substrate end concentration in well: 454 µM or 50nmol) in a 96well plate and was immediately read in a plate reader by measuring absorbance in kinetic mode for 15 min (1 point per min). PNPG were measured as standard. The obtained reaction rate (slope ΔE/min) of the kinetic curves for the synthesized substrates was compared to the one of PNPG (100%).

Enzymatic assay *β*-galactosidase (via evaluation of formed galactose)

The substrate solution was prepared by mixing 0.2 M Phosphate buffer (pH=7.3) and 20 mM $MgCl_2$ (pH=7.3) to obtain an end concentration of 0.5 mM. The *β*-galactosidase (75.48U/ml) was diluted 1:1000 with enzyme diluent. Afterwards, 20 µl of *β*-galactosidase were added to 100µl aliquots of substrate solution. After indicated time points the reaction was stopped by centrifugation through PALL Nanosep 10K omega filters (MWCO 10000; VWR, Germany). The galactose content was determined in a two step reaction. Galactose-dehydrogenase (GADH, 1.1mg/ml with 94U/mg corresponds to 103U/ml), diaphorase (solved in 6 ml water to give 1.3U/ml) and Iodonitrotetrazolium violet (INT, stock solution 2.2 mM) were used. First a NAD premix was prepared by mixing 150 µl NAD^+ (stock solution: 29.8 mg/ml), 47 µl water, 166 µl

0.2 M Tris, and 1.5µl GADH (corresponds to 0.155U). The dye premix containing INT and the enzyme Diaphorase was prepared by mixing 1:1 both stocks solution. A galactose standard curve was obtained by adding 20 µl of enzyme diluent to 100 µl of standard galactose solutions (0.031, 0.0625, 0.125, 0.25, 0.5 mM). The reaction was started by adding to 120 µl of samples after reaction with β-galactosidase or standards 40 µl Tris, 40 µl water, 50 µl NAD premix. After incubation for 1 h at 37 °C, 20µl INT/Diaphorase premix was added. Absorbance of the formed formazan dye has to be measured at 495 nm after 10 min in the dark and is directly correlated to the galactose content in the samples. The calculated amount of galactose in the samples (from the standard curve) is plotted vs. the incubation time with β-galactosidase and the curve was fitted to obtain the initial reaction rate (initial slope) and the real concentration in the stock solution of substrates (corresponding concentration at plateau of the fitted curve).

6.7 Preparation of CA-1 sample for ESI-MS and gel shift analysis

The standard enzyme diluent was made by mixing 10 mM Tris/HCl, $MgCl_2$, pH=7.3 in ratio 1:1, 3U/ml *β*-Galactosidase (dilution in enzyme diluent according to enzyme activity in stock). The substrate solution contained 0.0835M Phosphate buffer (pH 7.3), 1.1 mM $MgCl_2$, and 0.138 mM of **CA-1**. The enzyme solution (20 µl/well) was added to 100 µl/well of substrate solution (end concentration per well 13.8 nmol). The samples were incubated for 0, 0.5, 3, 6 and 18 h at 37°C with shaking. After indicated time points the reaction was stopped by centrifugation through PALL Nanosep 10K omega filters (MWCO 10000; VWR, Germany). The obtained samples were analysed by ESI-MS and gel shift assay.

ESI-MS analysis of CA-1 samples after enzymatic reaction

Each sample 10 µl was diluted 1:10 with 0.1% HCOOH/water and analyzed by ESI-MS (HCT Ultra, Bruker Daltonics, Bremen) with direct infusion altering in negative and positive modus.

Gel shift assay analysis of CA-1 samples after enzymatic reaction

Electrophoresis was performed according to procedure described by Fling and Gregerson[220].The samples after incubation with *β*-galactosidase were electrophoresed in a gel containing 16,5% Tris-Glycine SDS PAGE gel without urea using Pharmacia Fine Chemicals system. Gel fixation

was done with methanol, followed by washing with ethanol and silver staining according to a previously described protocol[221].

7. References

1) Cassidy P.J., Radda G.K., *J. Release Soc*., **2005**, 1-12.

2) Weissleder R. Mahmood U., *Radiology*, **2001**, 219, 316-333.

3) Weissleder R., *Radiology*, **1999**, 212, 609-614.

4) Massoud T. F. , Gambhir S. S., *Genes & Dev.*, **2003**, 17, 545-580.

5) Constantine G., Shan K., Flamm S. D., U Sivananthan M., *Lancet*, **2004**, 363, 2162–71.

6) Traboulsee A.L., Li D.K., *Adv. Neurol*., **2006**, 98,125-46.

7) Jerningan T.L., Salmon D.P., Butters N., Hesselink J.R., *Biol. Psych*., **1991**, 29, 68-81.

8) Pirko I., Fricke S. T., Johnson A. J., Rodriguez M., Macura S. I., *J. Am. Soc. Exper. NeuroTher.*, **2005**, 2, 250–264.

9) Bradley W.G., *Noninv. Med. Imagining*, **1984**, 1, 93-204.

10) Hermann P., Kotek J., Kubíček V., Lukeš I., *Dalton Trans.*, **2008**, 3027-3047.

11) Krause W., *Top. Curr. Chem*., Springer-Verlang Berlin Heidelberg, **2002**, 221, 125-128.

12) Pollet R., Marx D., *J. Chem. Phys.*, **2007**, 126, 181102.

13) Yazyev O.V., Helm L., *Eur. J. Inorg. Chem.* **2008**, 201–211.

14) Cacheris W.P., Quay S.C., Rocklage S.M., *Magn. Reson. Imaging*, **1990**, 8, 467-481.

15) Caravan P., Ellison J.J., McMurry T.J., Lauffer R.B., *Chem. Rev*., **1999**, 99, 2293-352.

16) Strijkers G.J., Mulder W.J., van Tilborg G.A.F., Nicolay K., *Anti-Can. Agents in Med. Chem.*, **2007**, 7, 291-305.

17) Solomon I., *Phys. Rev*., **1955**, 99, 559-565.

18) Bloemberg N., Morgan L.O., *J. Chem. Phys*., **1961**, 34, 842-850.

19) Merbach A., Toth E., *The Chemistry of Contrast Agents in Medical Magnetic Resonance Imaging, John Wiley,& Sons, Ltd., New York.*, **2001**.

20) Borel A., Yerlay F., Helm L., Merbach A.E., *CHIMIA*, **2004**, 58, 200-203.

21) Pereira G.A., Geraldes C.F.G.C., *Ann. Magn. Reson.*, 2007, 6, 1-33.

22) Doble D.M.J., Melchior M., O'Sullivan B., Siering C., Xu J., Pierre V.C., Raymond K.N., *Inorg. Chem.*, **2003**, 42, 4930-4937.

23) Major J.L., Meade T.J., *Accounts. Chem. Res*., **2009**, 42, 893-903.

24) Caravan P., *Chem. Soc. Rev.*, **2006**, 35, 512-523.

25) Werner E. J., Datta A., Jocher C. J., Raymond K. N., *Angew. Chem. Int. Ed. Engl*., **2008**, 47, 8568-8580.

26) Supkowski R.M., Horrocks W.D., *Inorg. Chem.*, **1999**, 38, 5616-5619.

27) Aime S., Calabi L., Cavallotti C., Gianolio E., Giovenzana G. B., Losi P., Maiocchi A., Palmisano G., Sisti M., *Inorg. Chem.*, **2004**, 43, 7588-7590.

28) Xu J., Franklin S.J., Whisenhut D.W., Raymond K.N., *J. Am. Chem. Soc*., **1995**, 117, 7245-7246.

29) Pierre V.C., Raymond K.N., *Bioconjugate Chem*., **2005**, 16, 3-8.

30) Werner E.J., Avedano S., Botta M., Hay B.P., Moore E.G., Aime S., Raymond K.N., *J. Am. Chem. Soc*., **2007**, 129, 1870-1871.

31) Pierre V.C., Botta M., Aime S., Raymond K.N., *J. Am. Chem. Soc*., **2006**, 128, 5344-5345.

32) Barge A., Cravotto G., Robaldo B., Gianolio E., Aime S., *J. Incl. Phenom. Macrocycl. Chem*., **2007**, 57, 489–495.

33) Nakamura E., Makino K., Okano T., Yamamoto T., Yokoyama M., *J. Controlled Release,* **2006**, 114, 325–333.

34) Aime S., Geninatti Crich S., Frulanno L., *Angew. Chem. Int. Ed. Engl.*, **2002**, 114, 1059-061.

35) Sipkins D.A., Cheresh D.A., Kazemi M.R., Nevin L.M., Bednarski M.D., Li K.C.P., *Nat. Med*., **1998**, 4, 623-626.

36) Leclercq F., Cohen-Ohana M., Mignet N., Sbarbati A., Herscovici J., Scherman D., Byk G., **2003**, *Bioconjugate Chem.*, 14, 112-119.

37) Bertini I., Bianchini F., Calorini L., Colagrande S., Fragai M., Franchi A., Gallo O., Gavazzi C., Lunchinat C., **2004**, *Magn. Reson. Med*., 52, 669-672.

38) Lattuada L., Lux G., *Tetrahedron Lett.* **2003**, 44, 3893-3895.

39) Lokling K.E., Skurtveit R., Bjornerud A., Fossheim S.L., *Magn. Reson. Med.*, **2004**, 51, 688-696

40) Lokling K.E., Fossheim S.L., Klaveness J., Skurtveit R., *J. Controlled Release,* **2004**, 98, 87-95.

41) Aime S., Botta M., Fasano M., Terreno E., *The Chemistry of Contrast Agents in Medical Magnetic Resonance Imaging, John Wiley,& Sons, Ltd., New York.,* **2001**,193.

42) Qu M.-H., Tu C.-H., Tsai S.-C., Lee W.-T., Liu G.-C., Wang Y.-M., *Inorg. Chem*., **2006**, 45, 244-254.

43) Gianolio E., Giovenzana G.B., Longo D., Longo I., Menegotto I., Aime S., *Chem. Eur. J.*, **2007**, 13, 5785-5797.

44) Casali C., Janier M., Canet E., Obadia J.F., Benderbous S., Corot C., Revel D., *Acad. Radiol.* **1998**, 5, S214-218.

45) Rohrer M., Baur H., Mintorovitch J., Requardt M., Weimann H.J., *Invest. Radiol.*, **2005**, 40, 715-724.

46) Anderson E.A., Isaacman S., Peabody D.S., Wang E.Y., Canary J.W., Kirshenbaum K., *Nano Lett.*, **2006**, 6, 1160-1164.

47) Prasuhn D.E. Jr, Yeh R.M., Obenaus A., Manchester M., Finn M.G., *Chem. Commun*., **2007**, 1269-1271.

48) Allen M., Bulte J.W.M., Liepold L., Basu G., Zywicke H.A., Frank J.A., Young M., Douglas T., *Magn. Reson. Med*., **2005**, 54, 807-812.

49) Datta A., Hooker J.M., Botta M., Francis M.B., Aime S., Raymond K.N., *J. Am. Chem. Soc*., **2008**, 130, 2546-2552.

50) Zhang Z., Greenfield M.T., Spiller M., McMurry T.J., Lauffer R.B., Caravan P., *Angew. Chem. Int. Ed. Engl.*, **2005**, 44, 6766-6769.

51) Port M., Corot C., Raynal I., Idee J.-M., Dencausse E., Lancelot D., Meyer B., Bonnemain B., Lautrou J., *Invest. Radiol.*, **2001**, 36, 445-454.

52) Yoo B., Pagel M., *Front. Biosci.*, **2008**, 13, 1733-1752.

53) Aime S., Berge A., Botta M., Howard J.A.K., Kataky R., Lowe M.P., Parker D., de Sousa A.S., *Chem. Commun*., **1999**, 1047-1048.

54) Zhang S., Wu K., Sherry A.D., *Angew. Chem. Int. Ed. Engl*., **1999**, 38, 3192-3194.

55) Zhang S., Malloy C.R., Sherry A.D., *J. Am. Chem. Soc*., **2005**, 127, 17572-17573.

56) Punnia-Moorthy A., *J. Oral. Pathol*., **1987**, 16, 36-44.

57) Fukumura D., Jain R.K., *APMIS*, **2008**,116, 695-715.

58) Martin G.R., Jain R.K., *Cancer Res*., **1994**, 54, 5670-5674.

59) Lowe M.P., Parker D., Reany O., Aime S., Botta M., Castellano G., Gianolio E., Pagliarin R., *J. Am. Chem. Soc*., **2001**, 123, 7601-7609.

60) Woods M., Kiefer G.E., Bott S., Castillo-Muzquiz A., Eshelbrenner C., Michaudet L., McMillan K., Mudigunda S.D. K., Ogrin D., Tircso G., Zhang S., Zhao P., Sherry A.D., *J. Am. Chem.Soc.*, **2004**, 126, 9248-9256.

61) Aime S., Botta M., Geninatti Crich S., Giovenzana G., Palmisano G., Sisti M., *Bioconjugate Chem.*, **1999**, 10, 192-199.

62) Li W.H,, Fraser S.E., Meade T.J., *J. Am. Chem. Soc*., **1999**, 121, 1413-1414.

63) Berridge M.J., Lipp P., Bootman M.D., *Nat. Rev. Mol. Cell Biol.*, **2000**, 1, 11-21.

64) Angelovski G., Fouskova P., Mamedov I., Canals S., Toth E. and Logothetis N. K., *ChemBioChem*., **2008**, 9, 1729-1734.

65) Vallee B.L., Falchuk K.H., *Physiol. Rev.*, **1993**, 73, 79-118.

66) Frederickson Ch. J., Koh J.-Y., Bush A. I., *Nat. Rev. Neurosci.*, **2005**, 6, 449-462

67) Lee J.–M., Zipfel G. J., Park K. H., He Y. Y., Hsu C. Y. , Choi D. W., *Neurosci.*, **2002**, 115, 871-878.

68) Hanaoka K., Kikuchi K., Urano Y., Narazaki M., Yokawa T., Sakamoto S., Yamaguchi K., Nagano T., *Chem. Biol.*, **2002**, 9, 1027-1032.

69) Major J.L., Parigi G., Luchinat C., Meade T.J., *PNAS*, **2007**, 104, 13881-13886.

70) Major J.L., Boiteau R. M., Meade T.J., *Inorg. Chem.*, **2008**, 47, 10788-10795.

71) Comblin, V., Gilsoul, D., Hermann, M., Humbelt, V., Jacques V., Mesbahi, M., Sauvage, C., Desreux, J. F., *Coord. Chem. Rev.* **1999**, 451, *185-186*.

72) Metzler D.E., *Biochemistry The Chemical Reactions of Living Cells*, Academic *Press, Inc. London, Ltd.*, **1977**, 300-349.

73) Knippschild U., Wolff S., Giamas G., Brockschmidt C., Wittau M.,Uwe Würlf P., Eismann T., Stöter M., *Onkologie*, **2005**, 28, 508–514.

74) Bloomer J. R., *J. Invest. Derm.*, **1981**, 77, 102–106.

75) Farmer P.M., *Ann. Clin. Labor. Sci.*, **1980**, 10, 263-268.

76) Bogdanov A. Jr, Weissleder R., *Trends in Biotech.*, **2002**, 20, S11-S18.

77) Bhaumik S., Gambhir S. S., *Proc. Natl. Acad. Sci. U.S.A*, **2002,** 99, 377–382

78) Wu J. C., Inubushi M., Sundaresan G., Schelbert H. R., Gambhir S. S., *Circulation*, **2002**,106, 180-183.

79) Gilad A.A., Winnard P.T., van Zijl P.C.M., Bulte J.W.M., *NMR Biomed*., **2007**, 20, 275-290.

80) Maidment N. T., Tan A. M., Bloom D. C., Anton B., Feldman L.T., Stevens J. G., *Exper. Neurology*, **1996**, 139, 107-114.

81) Liu L., Kodibagkar V. D., Yu J.-X., Mason R. P., *FASEB J.*, **2007**, 21, 2014-2019.

82) Louie A.Y,, Huber M.M., Ahrens E.T., Rothbacher U., Moats, Jacobs R.E., Fraser S.E., Meade T.J., *Nat. Biotechnol*., **2000**, 18, 321-325.

83) Urbanczyk-Pearson L.M., Meade T.J., *Nat.Protoc*. *2008*, 47, 3, 341-350.

84) Urbanczyk-Pearson L.M., Femia F.J., Smith J., Parigi G., Duimstra J.A., Eckermann A.L., Luchinat C., Meade T.J., *Inorg. Chem*., **2008**, 47, 56-68.

85) Moats R.A., Fraser S.E., Meade T.J., *Angew. Chem., Int. Ed. Engl*., **1997**, 36, 726-728.

86) Duimstra J.A., Femia F.J., Meade T.J., *J. Am. Chem. Soc*., **2005**, 127, 12847-12855.

87) Lauffer R.B., McMurry T.J., Dunham S.O., Scott D.M., Parmelee D.J., Dumas S., *WIPO Patent Applic.05/115105*, **2005**.

88) Hanaoka K., Kikuchi K., Terai T., Komatsu T., Nagano T., *Chem. Eur. J.*, **2008**, 14, 987-995.

89) Nivorozhinkin A.L., Kolodziej A.F., Caravan P., Greenfield M.T., Lauffer R.B., McMurry T.J., *Angew. Chem. Int. Ed. Engl.,* **2001**, 40, 2903-2906.

90) Aime S., Cabella C., Colombatto S., Geninatti Crich S., Gianolio E., Maggioni F., *J. Magn. Reson. Imaging*, **2002**, 16, 394-406.

91) Bogdanov A. Jr, Matuszewski L., Bremer C., Petrovsky A., Weissleder R., *Mol. Imaging*, **2002**, 1, 16-23.

92) Chen J.W., Wellington Pham, Weissleder R., Bogdanov A. Jr., *Magn. Reson. Med.*, **2004**, 52, 1021–1028.

93) Brennan M.L., Penn M.S., Van Lente F., Nambi V., Shishehbor M.H., D.O., Ronnier J. A., Goormastic M., Pepoy M.L., McErlean E.S. , Topol, E.J., Nissen S.E., Hazen S.L.F., *N. Engl. J. Med.*, **2003**, 349, 1595-1604.

94) Querol M., Chen J.W., Weissleder R., Bogdanov A. Jr., *Org. Lett*., **2005**, 7, 1719-1722.

95) Querol M., Chen J.W., Bogdanov A. Jr., Org. Biomol Chem, **2006**, 4, 1887-1895.

96) Tannous B., Grimm J., Perry K., Chen J., Weissleder R., Breakefield X., *Nat. Methods*, **2006**, 3, 291-396.

97) Jastrzębska B., Lebel R., Therriault, McIntyre J.O., Escher E., Guérin B., Paquette B., Neugebauer W.A., Lepage M., *J. Med. Chem*., **2009**, 52, 1576-1581.

98) Bogoyevitch M.A., *DNA and Cell Biology*, **2002**, 21, 855-856.

99) Zhang Y., Yu L.-C., *Curr. Opinion in Biotechn.*, **2008**, 19, 506-510.

100) Lu Y., *Stem cells and Development*, **2004**, 13, 133-145.

101) Templeton N.S., *DNA and Cell Biol.*, **2002**, 21, 857-867.

102) Zelphati O., Szoka F.C. Jr, *J. Controlled Released* 41, **1996**, 99-119.

103) Samad A., Sultana Y., Aqil M., *Curr. Drug Delivery*, **2007**, 4, 297-305.

104) Deshayes S., Morris M.C., Divita G., Heitz F., *Cell. Mol. Life Sci.*, **2005**, 1839-1849.

105) Simeoni F., Morris M.C., Heitz F., Divita G., *Nucleic Acids Res.*, **2003**, 31, 2717–2724.

106) Muratovska, A. and Eccles M.R., *FEBS Lett.*, **2004**, 558, 63-68.

107) Brooks H., Lebleu B., Vives E., *Advanced Drug Delivery Rev.*, **2005**, 57, 559-577.

108) Elliott G., O'Hare P., *Cell*, **1997**, 88, 223-233.

109) Jha, D., Mishra R., Ugurbil K., Engelmann J., Wiesmüller K.-H., *30th European Peptide Symposium (30EPS),* **2008**, *30, 157.*

110) Derossi D., Joliot A.H., Chassaing G., Prochiantz A., *J. Biol. Chem*., **1994**, 269, 10444-10450.

111) Fernandez-Carneado J., Kogan M.J., Castel S., Giralt E., *Angew. Chem. Int. Ed. Engl*., **2004**, 43, 1811-1814.

112) Rothbard J.B., Garlington S., Lin Q., Kirschberg T., Kreider E., McGrane P.L., *Nat. Med.*, **2000**, 1253-1257.

113) Mitchell D.J., Kim D., Steinmann L., Fathman C.G., Rotbard J.B., *J. Pept. Res*., **2000**, 56, 318-325.

114) June C.H., *J. Clin. Invest*., **2007**, 117, 1466-1476.

115) Reya T., Morrison S.J., Clarke M.F., Weissman I.L., *Nature*, **2001**, 414, 105-11.

116) Rosser A. E., Zietlow Rike., Dunnett S.B., *Cur. Opin. Neurol.*, **2007**, 20, 688-92.

117) Walczak P., Bulte J.W.M., *Neurodegenerative Dis*., **2007**, 4, 306-313.

118) Perin E. C., *Tex Heart Inst J.*, **2006**, 33, 204–208,

119) Leri A., Anversa P., Frishman W. H., *Cardiovascular Regeneration and Stem Cell Therapy*, **2007**, Wiley-Blackwell.

120) Scott C. T., *Stem Cell Now: From the Experiment That Shook the World to the New Politics of Life, Penguin Group (USA),* **2005**.

121) Kiessling F., *Molecular Imaging II, Handbook of Experimental Pharmacology, Springer-Verlag Berlin Heidelberg*, **2008**, 185/II, 305-321,.

122) McAfee J.G., Subramanian G., Gagne G., *Semin. Nucl. Med*, **1984**, 2, 83-106

123) Mateos J. J., Velasco, M., Lomeńa, F., Horcajada J. P., Setoain F. J., Martín F., Ortega, *Nuc. Med. Commun.*, **2002**, 23, 1137-1142.

124) Aicher A., Brenner W., Zuhayra M., Badorff C., Massoudi S., Assmus B., Eckey T., Henze E., Zeiher A. M., Dimmeler S., *Circulation*, **2003**, 107, 2134-2139.

124) K. J. Fotherby, E. P. Wraight, H. Garforth, and J. O. Hunter, *Postgrad Med J*., **1986**, 62, 457–462.

125) Giaffer M.H, *Gut*, **1996**, 38, 1–5.

126) Pelosi E., Baiocco C., Pennone M., Migliaretti G., MD3; Varetto T., Maiello A., Bello M., Bisi Gianni, *J. Nucl. Med.*, **2004**, 45, 438–444.

127) Uslu, H., Varoglu E., Kadanali S., Yildirim M., Bayrakdar R., Kadanali A., *Nucl.Med. Commun.*, **2006**, 27, 179-183.

128) Askensay N., Farkas D.L., *Stem Cells*, **2002**, 20, 501-513.

129) Fox D., Kouris G.J., Blumofe K.A., Helize T.J., Husak V., Greisler H.P., *J. Surg. Res.*, **1999**, 86, 9-16.

130) Voura E.B., Jaiswal J.K., Mattoussi H., Simon S.M., *Nat. Med*., **2004**, 10, 993-998.

131) Mothe A.J., Kulbatski I., van Bendegem R.L.,. Lee L., Kobayashi E., Keating A., Tator C. H., *J. Histochem. Cytochem*., **2005**, 53, 1215-1226.

132) Shichinone H., Kuroda S., Lee J.B., *Brain Res. Prot*., **2004**, 13, 166-175.

133) Yamauchi K., Yang M., Jiang P., Yamamoto N., Xu M., Amoh Y., Tsuji K., Bouvet Michael., Tsuchiya H., Tomita K., Moossa A.R., Hoffman R. M., *Can. Res*., **2005**, 65, 4246-4252.

134) Inoue H., Ohsawa I., Murakami T., Kimura A.,Hakamata Y., Sato Y., Kaneko T., Takahashi M.,Okada T., Ozawa K., Francis J., Leone P., Kobayashi E., *Bioch. Biophys. Res. Commun.*, **2005**, 329, 288–295.,

135) Takahashi M., Hakamata Y., Murakami T., Takeda S.-i.,Kaneko T., Takeuchi K., Takahashi R.-i., Uda M., Kobayashi E., *Bioch. Biophys. Res. Commun*., **2003**, 305, 904–908.

136) Kim D.-E., Schellingerhout D., Ishii K., Shah K., Weissleder R., *Stroke*, **2004**, 35, 952-957.

137) Tang Y., Shah K., Messerli S.M., Synder E., Breakfield X., Weissleder R., *Hum. Gene Therapy*, **2003**, 14, 1247-1254.

138) Bolus N. E., *J. Nucl. Med. Technol*., **2008**, 36, 11–17.

139) Hoehn M., Wiedermann D., Justicia C., Ramos-Caber P., Kruttwig K., Farr T., Himmelreich U., *J. Physiol*., **2007**, 584, 25-30.

140) Jacobs R.E., Fraser S.E., *Science*, **1994**, 263, 681-684.

141) Jacobs R.E., Ahrens E.T., Meade T.J., Frasewr S.E., *Trends Cell Biol.*, **1999**, 9, 73-76.

142) Modo M., Cash D., Mellodew K., Williams S.C., Fraser S.E., Meade T.J., Price J., Hodges H., *Neuroimage*, **2002**, 17, 803-811,

143) Modo M., Mellodew , Cash D., Fraser S.E., Meade T.J., Price J., Williams S.C., *Neuroimage*, **2004**, 21, 311-317.

144) Hoehn M., Kustermann E., Blunk J., Wiedermann Dirk., Thorsten T., Wecker S., Föcking M., Heinz A., Hescheler J., Fleischmann B. K., Schwindt W., Bührle C., *Proc. Natl. Acad. Sci. U.S.A.*, **2002**, 99, 16267-16272.

145) Arbab A.S., Pandit S.D., Anderson S.A., Yocum G. T., Bur M., Frenkel V.,[b] Khuu H.M., Read E. J., Franka J. A., *Stem Cells*, **2006**, 24, 671-678.

146) Hansen M.D. , Filipovich A. H., Davies S. M. , Mehta P., Bleesing J., Jodele S., Hayash R., Barnes Y., Shenoy S., *Bone Marrow Transpl.*, **2008**, 41, 349–353.

147) Endres P.J., MacRenaris K.W., Vogt S., Meade T.J., *Bioconjugate Chem*., **2008**, 19, 2049-2059.

148) Merrifield B., *Bioscience Reports,* **1985**, 5, *353-376.*

149) Terrett N.K., Gardner M., Gordon D.W., Kobylecki R.J., Steele J., *Tetrahedron*, **1995**, 51, 8135-8173.

150) Morrow S.J., *J. Macromol. Sci. Chem*., **1976**, A10, 259-288.

151) Chang C.-D., Meienhofer J., *Int. J. Pep. Prot. Res*., **2009**, 11, 246-249.

152) Whitfield D.M., Douglas S.P., Glycoconjugate J., **1996**, 13, 5-17.

153) Demchenk A. V., *Handbook of Chemical Glycosylation: Advances in Stereoselectivity and Therapeutic Relevance, WILEY-VCH Verlag GmbH & Co. KGaA*, **2008**.

154) Janczuk A.J., Zhang W., Andreana P. R., Warrick J., Wang P. G., *Carbohydr. Res*., **2007**, 337, 1247-1259.

155) Qin Z-H, Li H., Cai M.-S., Li Z.-J., *Carbohydr. Res*., **2002**, 337, 31-36.

156) Shirley A., Sgarbi-Wacowich D.R., Bundle, *J. Org. Chem*., **1999**, 64, 9080-9089.

157) M. Izumi, S. Kaneko, H. Yuasa, H. Hashimoto, *Org. Biom. Chem*., **2006**, 4, 681-690.

158) Wei W.-H., Tomohiro T., Kodaka M., Okuno H., *J. Org. Chem.* **2000**, *65*, 8979-8987.

159) Kunz H., Uverzagt C., *Angew. Chem. Int. Ed. Engl*., **1988**, 27, 1697-1699.

160) Yan L, Kahne D., *Synlett*, **1995**, 523-524.

161) Oikawa Y., Yoshioka T., Yonemitsu O., *Tetrahedron Lett*., **1982**, 23, 885-888.

162) Kent, S.B., Alewood, D., Alewood, P., Baca, M., Jones, A.,Schnolzer, M. *Innovations and Perspectives in Solid Phase Synthesis, R. Epton, (Ed.), Intercept. Ltd., Andover, UK*, **1992**, l-22.

163) Bedford J., Hyde C., Johnson T., Jun W., Owen D., Quibell M., Sheppard R.C., *Int. J. Pept. Prot. Res.*, 1992, 40, 300- 307.

164) Kaiser E., Colescott R. L., Bossinger C. D., Cook P. I., *Analytical Biochem.*, **1970**, 34, 595-598.

165) Mizukami S., Takikawa R., Sugihara F., Hori Y., Tochio H., Wälchli M., Shirakawa M., Kikuchi K., *J. Am. Chem. Soc.*, **2008**, 130, 794-795.

166) Kienle S., Nollert Peter., Wiesmüller K.-H., *Lett. Pept. Sci.*, **1999**, 6, 143–149.

167) Lin H., Thayer D. A., Wong C.-H., Walsh C. T., *Chem. & Biol*., **2004**, 11, 1635–1642.

168) Meinjohanns E., Meldal M., Paulsen H., Dwek R. A., Bock K., *J. Chem. Soc., Perkin Trans. 1*, **1998**, 549-560.

169) Ziegler T., Röseling D., Subramanian L. R., *Tetrahedron Asymmetry*, **2002**, 13, 911–914.

170) Buskas T., Ingale S., Boons G.-J., *Glycobiology*, **2006**, 16, 113R–136R.

171) Dziadek S., Kunz H., *Synlett*, **2003**, 11, 1623-1626.

172) Brocke C., Kunz H., *Synthesis*, **2004**, 4, 525-542.

173) P. Sjölin, M. Elofsson, J. Kihlberg, *J. Org. Chem*., **1996**, 61, 560-565.

174) Allen M.J., Meade T.J., *J. Biol. Inorg. Chem*., **2003**, 8, 746-750.

175) Barge A., Cravotto G., Gianolio E., Fedeli F., *Contrast Med. Mol. Imaging*, **2006**, 1, 184–188.

176) Wender Paul A., Mitchell D. J., Pattabiraman K., Pelkey E. T., Steinman L., Rothbard J. B., *Proc. Natl. Acad. Sci. USA*,, **2000**, 21, 13003–13008.

177) El-Andalousss S., Järver P., Johannson H. J., Langel Ü., *Biochem. J*., **2007**, 407, 285–292.

178) Simon MJ, Gao Shan, Hyeun Kang W, Banta S, Morrison III B, *Biotech. Bioengin*., **2009**, 104, 10-19.

179) Larson G.M., Lee K.-D., *Arch. Pharm. Res*., **1998**, 621-628.

178) Gabriel T, *Int. J. Pept. Prot. Res*., 30, 40-43.

179) Cornish J, Callon K, Lin C-X, Xiao C, Mulvey T, Cooper G, Reid I, *Am. J. Phys*., **1999**, 277, E779-E783.

180) Prantner A.M., Sharma V., Garbow J.R., Piwica-Worms D., *Mol. Imaging*, **2003**, 2, 333-341.

181) Wai-Yan Chan K., Wong W.-T, *Coord. Chem. Rev*., **2007,** 251, 2428–2451.

182) De León-Rodríguez L.M., Oritz A., Weiner A.L., Zhang S., Kovacs Z., Kodadek T., Sherry A. D., *J. Am. Chem. Soc*., **2002**, 124, 3514-3515.

183) Abiraj K., Jaccard H., Kretzschmar M, Helm L., Maecke H.R., *Chem. Commun.*, **2008**, 3248-3250.

184) Caravan P., Farrar C., Frullano L., Uppal R., *Contrast Media Mol. Imaging*, **2009**, 4, 89-100.

185) Caravan P., *Acc. Chem. Res*., **2009**, 42, 851-862.

186) Räty J.K., Liimatainen T., Kaikkonen U., Gröhn O., Airenne K.J., Ylä-Herttuala S., *Mol. Therapy*, **2007**, 9, 1579-1586.

187) Aime S, Delli Castelli D, Geninatti Crich S, Gianolio E, Terreno E, *Acc. Chem.Res.*, **2009**, 42, 822-831.

188) Koshland D.E., *Biol. Rev.*, **1953**, 28, 416-436.

189) Stokes T.M., Wilson I.B., *Biochem.*, **1972**, 11, 1061-1064

190) Jacobson R.H., Zhang X.-J., DuBose R.F., Matthews B.W., *Nat.*, **1994**, 369, 761-766.

191) Juers D.H., Heightman T.D., Vasella A., McCarter J.D., Mackenzie L., Withers S.G., Matthews B., *Biochem.*, **2001**, 14781-14794.

192) Huber R.E., Gupta M.N., Khare S.K., *Int. J. Biochem*., **1994**, 26, 309-318.

193) Tenu J.P., Virtalle O.M., Yon J., *Eur. J. Biochem*., **1972**, 112-118,

194) Huber R.E., Parfett C., Woulfe-Flanagan H., Thompson D.J., *Biochem.*, **1979**, 18, 4090-4095.

195) Huber R.E., Gaunt M.T., *Arch. Biochem. Biophys*., **1983**, 220, 263-271,

196) Zarnitz M.L., *Doctoral Dissertation, Freiburg, Ger*., **1958**.

197) Huber R.E., Gaunt M.T., Hurlburt K.L., *Arch. Biochem. Biophys*., **1984**, 234, 151-160.

198) Monod J., Cohen-Bazire G., Cohn M., *Biochim. et Biophys. Acta*, **1951**, 7, 585.

199) Bock K., Adelhorst K., *Carbohydr. Res*., **1990**, 202, 131-149.

200) Huber R.E., Roth N.J., *J. Biol. Chem*., **1996**, 271, 14296-14301.

201) Roth N.J., Rob B., Huber R.E., *Biochem*., **1998**, 37, 10099-10107.

202) Marshall P., Reed C.G., Sinnott M.L., Souchard I.J.L., *J. Chem. Soc. Perkin Trans. 2*, **1977**, 1198-1202.

203) Wallenfels J., lehmann J., Malhorta O.P., *Biochem. Z.*, **1969**, 333, 209.

204) Lehmann J., Reinnshagen H., *Libigs Ann. Chem*., **1979**, 732, 112-120.

205) Lederberg J., *J. Bacteriol*., **1950**, 60, 381-392.

206) Yuan J., Martinez-Bilbaot M., Huber R.E., *Biochem. J*., **1994**, 299, 527-531,

207) Manafi M., Kneifel W., Bascomb S., *Microbiol. Rev*., **2000**, 30, 336-340.

208) Chaudhary S.K., Hernandez O., *Tetrahedron Lett*., **1979**, 2, 95-98.

209) Ekborg G., Vranešić B, Bhattacharjee AK, Kovăč, Glaudemans CPJ, *Carbohydr. Res*., **1985**, 142, 203-211.

210) Marinier A., Martel A., Bachand C., Plamondon S., Turmel B., Daris J.-P., Banville J. , Lapointe P., Carl Ouellet, Dextraze P., Menard M., Wright J. J. K., Alford J., Lee D., Stanley P., Nair X., Todderud G., Tramposch K. M., *Biorg. Biomed. Chem*., **2001**, 9, 1395-1427.

211) Pietrzik N., *Doctoral Dissertation, Tuebingen, Ger*., **2009**.

212) Mishra A.K., Chatal J.-F., *New J. Chem*., **2001**, 25, 336-339.

213) Pocsi I., Taylor S.A., Richardson A.C., Smith B.V., Price R.G., *Biochim. Biophys. Acta*, **1993**, 1163, 54-60,

214) Horwitz J.P., Chua J.P., Curby J., Tomson R.J., DaRooge A.J., Fisher B.E., Mauricio J., Klundt I., *J. Med. Chem*., **1964**, 7, 1142-1147.

215) Skold C.N., Gibbons I., Russell M.E., Juartisti E., Rowley G.L., Ullman E.F., *Biochim. et Biophys. Acta*, **1985**, 830, 64-70.

216) Diepenbrock F., Heckler R., Schickling H., Engelhard T., Bock D., Sander J., *Clin. Biochem.*, **1992**, 25, 37-39.

217) Kuby S.A., Lardy H.A., *J. Am. Chem. Soc*., **1953**, 75, 890.

218) Sinnott M.L., Souchard I.J.L., *Biochem. J*., **1973**, 133, 89-98.

219) Bothner B., Chavez R., Wei J., Strupp C., Phung Q., Schneemann A., Siuzdak G., *J. Biol. Chem.*, **2000**, 275, 13455-13459.

220) Fling S.P., Gregerson D.S., *Anal. Biochem*., **1986**, 155, 83-88.

221) Blim H., Beier H., Gross H.J., *Electrophoresis*, **1987**, 8, 93-99.

222) Moseley M., Donnan G., *Stroke*, **2004**, 35, 2632-2634.

223) Kobayashi H., Koyama Y., Barrett T., Hama Y., Regino C. A. S., Shin I. S., Jang B-S, Le N., Paik C. H., Choyke P. L., Urano Y., *ACS Nano*., **2007**, 1, 258–264.

224) Zhang Z., Achilefu S., *Photochem. Photobiol.*, **2005**, 81, 1499–1504,

225) Pandey S. K, Gryshuk A. L., Sajjad M., Zheng X., Chen Y., Abouzeid M. M., Morgan J., Charamisinau I., Nabi H. A., Oseroff A., Pandey R. K., *J. Med. Chem.*, **2005,** 48, 6286-6295.

226) Huber M.M. Staubli A.B., Kustedjo K., Gray M.H.B., Shih J., Fraser S.E., Jacobs R.E., Meade T.J., *Bioconjugate Chem.*, **1998**, 9, 242-249.

227) Josephson L., Tung C.-H., Moore A., Weissleder R., *Bioconjugate Chem.*, **1999**, 10, 186-191.

228) Lewin M., Carlesso N., Tung C.-H., Tang X.-W., Cory D., Scadden D.T., Weissleder R., *Nat. Biotechn.*, **2000**, 18, 410-414.

229) Kircher M.F., Mahmood U., King R.S., Weissleder R., Josephson L., *Cancer Res*., **2003**, 63, 8122-8125.

230) Moore A, Medarova Z., Potthast A., Dai G., *Cancer Res*., **2004**, 64, 1821-1827.

231) Denis M.C., Mahmood U., Benoist C., Mathis D., Weissleder R., *Prot. Natl. Acad. Sci. U.S.A.*, **2004**, 101, 12634-12639.

232) Quinti L, Weissleder R., Tung C.-H., *Nano Lett.*, **2006**, 6, 488-490.

233) Geninatti Crich S., Biancone L., Cantaluppi V., Duó D., Esposito G., Russo S., Camussi G., Aime S., *Mag. Reson. Med*., **2004**, 51, 938-944.

234) Sabbatini P., Aghajanian C., Dizon D., Anderson S., Dupont J., Brown J.V., Peters W.A., Jacobs A., Mehdi A., Rivkin S., Eisenfeld A.J., Spriggs D. , *J. Clin. Oncol.*, **2004**, 22, 4523–4531.

235) Montgomery C.P, Murray B.S., New E.J., Pal R., Parker D., *Acc. Chem. Res*., **2009**, 42, 925-37.

236) Pandya S., Yu J., Parker D., *Dalton Trans*., **2006**, 2757-2766.

237) Auzenne E., Donato N.J., Li C., Leroux E., Price R.E., Farquhar D., Klostergaard J. , *Clin. Cancer Res.*, **2002**, 8, 573–581.

238) Bhatt R., Vries P., Tulinsky J., Bellamy G., Baker B., Singer J.W., Klein P., *J. Med. Chem*., **2003**, 46, 190–193.

239) Lu Z.-R., Wang X., Parker D. L., Goodrich K. G., Buswell H.R., *Bioconjugate Chem*., **2003**, 14, 715-719.

240) Wen X., Jackson E.F., Price R.E., Kim E., Wu Q., Wallance S., Charnsangavej C., Gelovani J., Li C., *Bioconjugate Chem.*, **2004**, 15, 1408-1415

241) Mohs A.M., Wang X., Goodrich K.G., Zong Y., Parker D.L, Lu Z.-R., *Bioconjugate Chem.*, **2003**, 15, 1424-1430.

242) Jacques V, Desreux JF, *Top. Curr. Chem*., **2002**, 221, Chapter 5, p.131.

243) Davis B.G., Chambers D., Cumpstey I., France R., Gamblin D., *Best Synthetic Methods: Carbohydrates, Elsevier Science Ltd.*, **2003**, p.77-78.]

244) Bukowski R., Morris L. M., Woods R. J., Weimar T., *Eur. J. Org. Chem*., **2001**, 2697-2705].

245) Weng S.-S., Lin Y.-D., Chen C.-T., *Org. Lett.*, **2006**, 8, 5633-5636.

246) Winum J.-Y., Leydet A., Seman M., Montero J.-L., *IL Farmaco*, **2001**, 56, 319–324.

247) Mishra A.K., Chatal J.-F., *New J. Chem*., **2001**, 25, 336-339.

References